

AD-A085 506

ILLINOIS UNIV AT URBANA-CHAMPAIGN COORDINATED SCIENCE LAB F/G 7/4
ENCAPSULATION STUDIES AND PLANAR DEVICE FABRICATION IN GALLIUM --ETC(11)
SEP 79 M J MELIX N00014-79-C-0424

UNCLASSIFIED

R-050

NL

AD-A085 506



LEVEL

TV

82

12

REPORT E-049 SEPTEMBER 1979

ILLI-ENG 78-2251

CSL COORDINATED SCIENCE LABORATORY

ADA085506

**ENCAPSULATION STUDIES AND
PLANAR DEVICE FABRICATION
IN GALLIUM ARSENIDE**

DTIC
ELECT
JUN 12 1980

Unclassified

SECURITY CLASSIFICATION OF THIS PAGE (When Data Entered)

REPORT DOCUMENTATION PAGE		READ INSTRUCTIONS BEFORE COMPLETING FORM
1. REPORT NUMBER	2. GOVT ACCESSION NO.	3. RECIPIENT'S CATALOG NUMBER
	AD-A08550A	9) Doctoral th
4. TITLE (and Subtitle)		5. TYPE OF REPORT & PERIOD COVERED
ENCAPSULATION STUDIES AND PLANAR DEVICE FABRICATION IN GALLIUM ARSENIDE.		TECHNICAL REPORT
7. AUTHOR(s)		6. PERFORMING ORG. REPORT NUMBER
Max John/Helix		R-858, UILU-ENG-78-2251
9. PERFORMING ORGANIZATION NAME AND ADDRESS		8. CONTRACT OR GRANT NUMBER(s)
Coordinated Science Laboratory University of Illinois at Urbana-Champaign, Urbana, Illinois 61801		N00014-79-C-0424, ONR N00014-76-C-0806
11. CONTROLLING OFFICE NAME AND ADDRESS		10. PROGRAM ELEMENT, PROJECT, TASK AREA & WORK UNIT NUMBERS
Joint Services Electronics Program		
14. MONITORING AGENCY NAME & ADDRESS (if different from Controlling Office)		12. REPORT DATE
		September 1979
		13. NUMBER OF PAGES
		86
		15. SECURITY CLASS. (of this report)
		UNCLASSIFIED
		15a. DECLASSIFICATION/DOWNGRADING SCHEDULE
16. DISTRIBUTION STATEMENT (of this Report)		
Approved for public release; distribution unlimited		
17. DISTRIBUTION STATEMENT (of the abstract entered in Block 20, if different from Report)		
18. SUPPLEMENTARY NOTES		
19. KEY WORDS (Continue on reverse side if necessary and identify by block number)		
Ion Implantation GaAs Silicon Nitride		
20. ABSTRACT (Continue on reverse side if necessary and identify by block number)		
<p>Low temperature photoluminescence and Auger electron spectroscopy (AES) are used to study SiO₂ and Si₃N₄ as encapsulants for high temperature annealing of GaAs. These encapsulants are used in the fabrication of planar diodes in GaAs, and the resulting electrical and optical properties of the devices are examined.</p> <p>Silicon dioxide or silicon oxy-nitride layers allow the outdiffusion of Ga when they are used to encapsulate GaAs during high temperature annealing.</p>		

DD FORM 1 JAN 73 1473 EDITION OF 1 NOV 65 IS OBSOLETE

SECURITY CLASSIFICATION OF THIS PAGE (When Data Entered)

September 1979

SECURITY CLASSIFICATION OF THIS PAGE(When Data Entered)

In contrast, silicon nitride layers which are essentially free of oxygen can be used to anneal GaAs with negligible Ga outdiffusion. A versatile rf plasma deposition system capable of depositing high quality Si_3N_4 films at low temperatures is described. In this system, reacting gases are introduced into the reaction chamber separately, and great care is taken to reduce residual oxygen in the system. Composition (ratio of silicon to nitrogen), index of refraction, etch rate, and deposition rate are reported for films deposited under various conditions. Electrical characterization of the Si_3N_4 films is also presented.

Ion implantation of Be is used to fabricate planar GaAs p-n junctions. The most critical processing step is the use of an essentially oxygen-free Si_3N_4 layer as an encapsulant during the post implantation anneal. Current-voltage characteristics are presented for Be-implanted devices fabricated with SiO_2 , $\text{Si}_x\text{O}_y\text{N}_z$, or Si_3N_4 as the encapsulant. Leakage currents as low as 10^{-10}A at 80V and breakdown voltages $>200\text{V}$ for $250\mu\text{m}$ diameter devices have been obtained using "oxygen-free" Si_3N_4 encapsulation. Diodes fabricated with SiO_2 or $\text{Si}_x\text{O}_y\text{N}_z$ encapsulants exhibit significantly higher reverse leakage currents. Planar avalanche photodiodes fabricated with Be implantation and Si_3N_4 encapsulation demonstrate quantum efficiencies of 75% at 8750 \AA for devices with junction depths of $1.2\mu\text{m}$, p-type doping levels of 10^{18}cm^{-3} , and no intentional antireflection coating. Avalanche gains of 10-15 have been measured.

Current-voltage characteristics for devices fabricated by Be implantation into LPE and VPE GaAs are compared, as well as characteristics of Zn-implanted and Zn-diffused devices. Also, preliminary studies are presented which indicate negligible lateral diffusion of Be when proper fabrication procedures are followed.

SECURITY CLASSIFICATION OF THIS PAGE(When Data Entered)

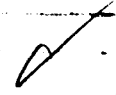
ENCAPSULATION STUDIES AND PLANAR DEVICE
FABRICATION IN GALLIUM ARSENIDE

by

Max John Helix

This work was supported in part by the Joint Services Electronics
Program (U.S. Army, U.S. Navy and U.S. Air Force) under Contract N00014-
79-C-0424 and the Office of Naval Research under Contract N00014-76-C-0806.

Reproduction in whole or in part is permitted for any purpose
of the United State Government.

APPROVED FOR RELEASE	
DATE	
BY	
REASON	
REMARKS	
A	

Approved for public release. Distribution unlimited.

ENCAPSULATION STUDIES AND PLANAR DEVICE
FABRICATION IN GALLIUM ARSENIDE

BY

MAX JOHN HELIX

B.S., University of Illinois, 1975
M.S., University of Illinois, 1976

THESIS

Submitted in partial fulfillment of the requirements
for the degree of Doctor of Philosophy in Electrical Engineering
in the Graduate College of the
University of Illinois at Urbana-Champaign, 1979

Thesis Advisor: B. G. Streetman

Urbana, Illinois

ENCAPSULATION STUDIES AND PLANAR DEVICE
FABRICATION IN GALLIUM ARSENIDE

by

Max John Helix

Edited by B. G. Streetman

This work was supported in part by the Joint Services Electronics
Program (U.S. Army, U.S. Navy and U.S. Air Force) under Contract N00014-
79-C-0424; Office of Naval Research under Contract N000-14-76-C-0806.

ENCAPSULATION STUDIES AND PLANAR DEVICE
FABRICATION IN GALLIUM ARSENIDE

Max John Helix, Ph.D.
Coordinated Science Laboratory and
Department of Electrical Engineering
University of Illinois at Urbana-Champaign, 1979

Low temperature photoluminescence and Auger electron spectroscopy (AES) are used to study SiO_2 and Si_3N_4 as encapsulants for high temperature annealing of GaAs. These encapsulants are used in the fabrication of planar diodes in GaAs, and the resulting electrical and optical properties of the devices are examined.

Silicon dioxide or silicon oxy-nitride layers allow the outdiffusion of Ga when they are used to encapsulate GaAs during high temperature annealing. In contrast, silicon nitride layers which are essentially free of oxygen can be used to anneal GaAs with negligible Ga outdiffusion. A versatile rf plasma deposition system capable of depositing high quality Si_3N_4 films at low temperatures is described. In this system, reacting gases are introduced into the reaction chamber separately, and great care is taken to reduce residual oxygen in the system. Composition (ratio of silicon to nitrogen), index of refraction, etch rate, and deposition rate are reported for films deposited under various conditions. Electrical characterization of the Si_3N_4 films is also presented.

Ion implantation of Be is used to fabricate planar GaAs p-n junctions. The most critical processing step is the use of an essentially oxygen-free Si_3N_4 layer as an encapsulant during the post implantation anneal. Current-voltage characteristics are presented for Be-implanted devices fabricated with SiO_2 , $\text{Si}_x\text{O}_y\text{N}_z$, or Si_3N_4 as the encapsulant. Leakage currents as low as 10^{-10} A at 80V and breakdown voltages >200 V for $250\mu\text{m}$

diameter devices have been obtained using "oxygen-free" Si_3N_4 encapsulation. Diodes fabricated with SiO_2 or $\text{Si}_x\text{O}_y\text{N}_z$ encapsulants exhibit significantly higher reverse leakage currents. Planar avalanche photodiodes fabricated with Be implantation and Si_3N_4 encapsulation demonstrate quantum efficiencies of 75% at 8750\AA for devices with junction depths of $1.2\mu\text{m}$, p-type doping levels of 10^{18}cm^{-3} , and no intentional antireflection coating. Avalanche gains of 10-15 have been measured.

Current-voltage characteristics for devices fabricated by Be implantation into LPE and VPE GaAs are compared, as well as characteristics of Zn-implanted and Zn-diffused devices. Also, preliminary studies are presented which indicate negligible lateral diffusion of Be when proper fabrication procedures are followed.

ACKNOWLEDGMENTS

The author wishes to express his deepest appreciation to many individuals who have helped him in the course of his work. First he wishes to thank Professors B. G. Streetman and G. E. Stillman for their direction, encouragement, and support.

Secondly, the author is grateful to the following people: to Dr. P. K. Chatterjee of Texas Instruments for ellipsometry measurements and electron beam lithography work; to R. J. Blattner and Dr. C. A. Evans, Jr. for Auger electron spectroscopy measurements; to Dr. H. B. Dietrich of Naval Research Laboratory for Rutherford backscattering studies; to Dr. G. Y. Robinson and T. R. Ohnstein of the University of Minnesota for electrical characterization of silicon nitride films; to Dr. D. L. Keune and Dr. W. O. Groves of Monsanto for donating VPE gallium arsenide used for part of this work; and to Professors J. T. Verdeyen and B. Cherrington for their advice and guidance in earlier graduate work.

He also appreciates the assistance and friendship of his colleagues Dr. W. V. McLevige, J. D. Oberstar, K. J. Soda, Dr. G. T. Marcyk, Dr. R. A. Milano, Dr. M. Y. Tsai, T. H. Yu, S. S. Chan, D. S. Day, T. H. Windhorn, Dr. S. Modesti, Dr. K. Hess, J. Kang, Dr. D. R. Myers, B. S. Seymour, D. J. Wolford, and Dr. K. V. Vaidyanathan. He wishes to thank the many members of the professional staff of the Coordinated Science Laboratory for their invaluable help throughout the course of his work.

Most of all, the author wishes to thank his wife Audrey for her love, comfort, and support of many kinds, without which this work would be meaningless.

TABLE OF CONTENTS

CHAPTER	Page
1. INTRODUCTION.....	1
1.1. Ion Implantation.....	3
1.2. Encapsulation.....	6
2. ENCAPSULATION STUDIES.....	10
2.1. Deposition Systems.....	10
2.1.1. Silicon Dioxide Deposition.....	10
2.1.2. RF Plasma Deposited Silicon Nitride.....	12
2.2. Annealing Studies.....	18
2.2.1. Photoluminescence Studies.....	18
2.2.2. Auger Electron Spectroscopy Studies.....	22
2.3. Characteristics of the "Oxygen-Free" System.....	28
2.4. Electrical Properties of RF Plasma Si_3N_4 Layers.....	34
3. PROPERTIES OF PLANAR P-N JUNCTIONS.....	38
3.1. Junction Fabrication.....	42
3.2. Comparison of Be-Implanted, Zn-Implanted, and Zn-Diffused Planar Diodes.....	45
3.3. Effects of the Encapsulant on Planar Be-Implanted Junctions.....	47
3.4. Planar Be-Implanted Avalanche Photodiodes.....	55
3.4.1. Electrical Characteristics.....	55
3.4.2. Optical Characteristics.....	62
3.5. Lateral Diffusion Studies.....	70
4. SUMMARY AND CONCLUSIONS.....	72
4.1. Encapsulation Studies.....	72
4.2. Planar P-N Junction Studies.....	74
REFERENCES.....	79
VITA.....	86

1. INTRODUCTION

Present and projected requirements for high speed digital devices in signal processing [1-4], microwave devices, and opto-electronic elements [5] have created considerable interest in GaAs planar device fabrication. The higher electron mobility and saturation velocity of GaAs and the availability of semi-insulating GaAs substrate material make this material very attractive for high speed integrated circuits with low speed-power products. While early work in GaAs integrated circuits used etched mesas and epitaxial or single implant fabrication [6-10], the development of a planar GaAs IC technology is necessary to reduce the power dissipation to levels compatible with LSI [1-3,11]. The use of selective ion implantation is essential for such a planar technology [1-3]. Ion implantation, with its proven uniformity, reproducibility, and versatility, can be used for multiple localized implants into isolated areas on semi-insulating substrates. This allows one to optimize various circuit elements and increase the packing density.

Most work in GaAs IC's has been centered on using MESFET's as the active circuit element, but studies show that the dissipated power can be decreased considerably with only a slight decrease in speed if JFET's are used instead [3]. This reduced power would allow higher packing densities and higher levels of integration. Currently Zn diffusions are used for the p-type regions in these studies, but because of problems with Zn [12-14], the size and performance of these devices are limited. An attractive alternative to Zn is Be introduced by ion implantation.

For integrated circuit applications, planar junctions must be introduced using some form of selective masking, with lateral diffusion under the mask tolerable on the scale of device dimensions. A versatile IC technology also requires junctions which exhibit low reverse leakage

current, high breakdown voltage, and low forward resistance. It has been shown that junctions meeting these criteria can be fabricated in GaAs by ion implantation of Be [13,15,16]. Selective beryllium implantation into various III-V compounds has also been used to make high quality optical waveguides [17], varactors [18], detectors [16,19], FET's [20], and light-emitting diodes [21].

While ion implantation seems to be the best method by far for fabricating GaAs integrated circuits, there are certain problems associated with ion implantation which have not been fully solved. Considerable lattice damage is introduced during the implantation process, especially for high dose or heavy-ion implants. To reorder the crystal and activate the implanted impurity, the sample must be annealed at a high temperature. This high temperature anneal is relatively straightforward for silicon, but problems are encountered when annealing the III-V semiconductors. In GaAs, for example, the high vapor pressure of As results in considerable surface degradation at temperatures as low as 600°C [22]. It is therefore necessary to encapsulate the sample with a suitable dielectric layer [15,23-31] or to perform the anneal in a carefully controlled ambient [32-35].

In this work we have used photoluminescence and Auger depth profiles to study the encapsulating properties of silicon dioxide, silicon nitride, and oxy-nitride. A system capable of depositing high quality oxygen-free silicon nitride layers using an rf plasma is described. Properties of both the system and the resulting deposited films are presented. Finally, these encapsulants are used in conjunction with ion implantation and photolithographic procedures to form planar p-n junctions in GaAs. The electrical properties of these junctions are presented, along with some optical properties of Be-implanted GaAs avalanche photodiodes.

In the remainder of this section some background information on ion implantation and encapsulation of III-V compounds is presented as an introduction.

1.1. Ion Implantation

Ion implantation is now a standard technique of doping semiconductors and has been extensively reviewed in the literature [36-40]. Basically, ion implantation consists of energetic ions entering the substrate and losing energy through collisions with the lattice until they come to rest in the substrate. The distribution of ions in the substrate is a function of the incident ion species and its energy, along with properties of the substrate material. The two major forms of energy loss for the incoming ion are interactions with the electrons of the substrate atoms and collisions with the nuclei. While only approximately true, these two loss mechanisms can be assumed to be independent of one another. Under this assumption we can write

$$\frac{-dE}{dx} = N[S_n(E) + S_e(E)] \quad (1.1)$$

where E is the energy of the ion at a point x along its path, $S_n(E)$ is the nuclear stopping power, $S_e(E)$ is the electronic stopping power, and N is the average number of target atoms per unit volume.

To a fairly good approximation, the nuclear stopping power can be assumed to be elastic scattering processes, independent of one another. In the context of these assumptions, the collisions can be treated with classical mechanics. When a potential which takes into account the screening of electrons is used, fairly accurate values of the nuclear stopping power can be obtained.

The electronic stopping power is more difficult to compute

theoretically. There are basically two different models that have been used to calculate this quantity. The first method approximates the electrons in the target by a free electron gas. In this approximation the ion loses energy by collisions with the electrons and excitation of plasma resonances. For ion velocities less than that of an electron having an energy below the Fermi energy of the gas, Lendhard and Winther [41] have shown that $S_e(E)$ can be given by

$$S_e(E) = CV = kE^{\frac{1}{2}} \quad (1.2)$$

where the parameter k is a function of the ion and substrate involved.

The other model, proposed by Firsov [42], is based on the electronic interactions in a two-body collision. The process may be visualized by the two atoms forming a "quasi-molecule" as they approach each other. The atoms will exchange outer electrons as they attempt to form a molecule. These electrons will take on the net momentum of the "quasi-molecule". When the atoms separate again, the incoming ion will have lost energy to the stationary one. While the Firsov model assumes participation of all the electrons, it is more appropriate to assume some screening from the inner electrons. Electronic stopping power is more important for high energies and light ions, while nuclear stopping is the major force for low energies and heavy ions.

Once S_n and S_e are known, they can be substituted into equation 1.1, and the total distance or range (R) the ion travels on its winding path in the substrate can be found. Experimentally, we can only observe the distance travelled perpendicular to the surface, the projected range (R_p). Also, since the ions suffer collisions in a random fashion, the ions will come to rest in some type of distribution about the projected range. The spread of the distribution is defined by the standard deviation (ΔR), and

the spread perpendicular to the surface is described by the projected standard deviation (ΔR_p).

Differential equations for computing R_p and ΔR_p have been derived by Lindhard, Scharff, and Schiott [43]. This theory, henceforth referred to as LSS, describes the basic features of the implanted profile. The implanted profile can usually be approximated by a gaussian function given by

$$N(x) = N_p \exp \left[\frac{-(x - R_p)^2}{2\Delta R_p^2} \right] \quad (1.3)$$

where $N(x)$ is the concentration of atoms (cm^{-3}) at a point x and N_p is the peak concentration. This peak concentration is expressed by

$$N_p = \frac{0.4}{\Delta R_p} N_D \quad (1.4)$$

where N_D is the fluence or dose of the implant expressed in atoms/ cm^2 .

Values of R_p , ΔR_p , and related quantities have been tabulated for various ions and substrates [44]. Distortion of the profile when higher order moments are considered has also been described [44].

While the LSS theory gives fairly accurate impurity profiles for unannealed samples, the distribution can change drastically after the annealing process necessary to restructure the crystal and activate the impurities. Considerable work has been done to study how various impurities diffuse during annealing and how well the impurities are electrically and optically activated. Both of these pieces of information are essential in fabricating devices with the desired doping profiles.

The implantation process consists basically of forming a plasma containing the desired ions, accelerating the ions to a predetermined energy, selecting only the appropriate ion species out of the beam by mass separation, and directing the ions uniformly onto the substrate by scanning

the beam in some manner. The charge hitting the sample is countered so that the desired dose of impurities can be obtained. A schematic diagram of the 300 keV Accelerators, Inc. 300-MP ion implanter used in this work is shown in Figure 1.1.

1.2. Encapsulation

One of the major problems with ion implantation of III-V semiconductors is the dissociation of the surface at the temperatures required for annealing. In GaAs, for example, considerable surface degradation occurs at temperatures as low as 600°C [22]. Because of this, the surface must be protected during the anneal by an encapsulating layer of a suitable dielectric or by annealing in a carefully controlled atmosphere [32-35]. Dielectrics used to encapsulate GaAs include SiO_2 [26-30], AlN [31], and Si_3N_4 deposited by chemical vapor deposition [23,24], reactive sputtering [25,26,31], or rf plasma deposition [15,28,29]. Multilayered dielectric structures have been used for encapsulation during anneals at higher temperatures (1100°C) than have been achieved with single layers. However, indiffusion of Si from the encapsulant raises questions about the usefulness of such high temperature anneals [45].

Studies [29,30] have shown that SiO_2 layers allow Ga outdiffusion during high temperature anneals. This Ga outdiffusion greatly decreases the electrical activation of donor impurities which must go on the As sites [46]. While the Ga outdiffusion can improve the electrical activation of dopants which must incorporate on Ga sites [46], the reproducibility of the impurity profile and the junction characteristics [15] are adversely affected.

The most widely used encapsulant for GaAs is Si_3N_4 , which can be deposited by several different methods. The most dense and chemically inert Si_3N_4 layers are deposited by a pyrolytic reaction between SiH_4 and NH_3 [47].

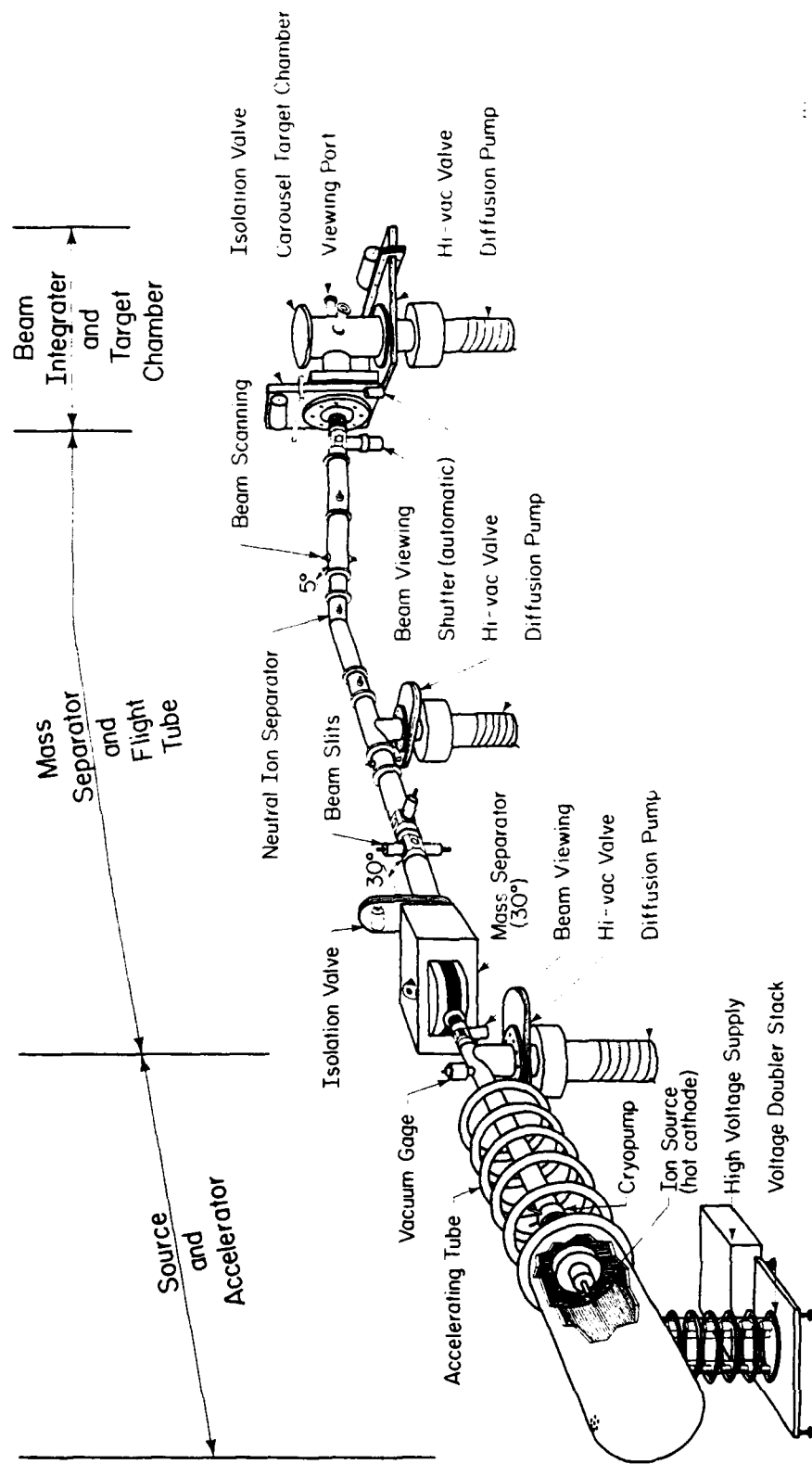


Figure 1.1. Schematic diagram of the ion implantation system.

This process, however, must be carried out at temperatures in excess of 650°C . In order to prevent surface degradation during the encapsulation, the sample must be heated up very quickly (~ 6 sec.), and the film is deposited rapidly (~ 9 sec.) [24]. This process has been used successfully for annealing GaAs samples when the implants are done through this Si_3N_4 layer. This system cannot be used for all types of devices, however, and cannot be extended to other III-V compounds such as InP.

Reactive sputtering and rf plasma deposition can be used to deposit Si_3N_4 at lower temperatures, and both of these methods have been used successfully to anneal ion implanted GaAs. Very little analysis of sputtered Si_3N_4 as an encapsulant has been reported, but considerable work has been done with rf plasma deposited Si_3N_4 [47-55]. Silicon nitride layers can be plasma deposited over a wide range of temperatures (25° - 500°C) and chemical compositions, and these films can be used in the annealing of a variety of III-V compounds, including InP and $\text{In}_x\text{Ga}_{1-x}\text{As}_y\text{P}_{1-y}$ [56]. In this work we have developed a system for depositing high quality Si_3N_4 layers using an inductively coupled plasma to react N_2 and SiH_4 . While many rf plasma systems use NH_3 to increase deposition rates, problems with handling and purification of NH_3 can be avoided by using N_2 , which can be obtained in extremely pure form. A description of the system developed in this work, along with the characteristics of the resulting films, will be presented in section 2. Commercial systems for plasma deposition of Si_3N_4 have generally been designed for use in Si device fabrication and are not necessarily optimized for use with GaAs. In particular, such commercial systems result in nitride films which contain considerable oxygen. The system used in this work is designed specifically to be used for encapsulating III-V compounds with high quality "oxygen-free" Si_3N_4 .

Recently, success with laser and electron beam annealing of Si has generated work on beam annealing of ion implanted GaAs. This work has met with some limited success [57-59], but as with thermal annealing, the problems associated with beam annealing of GaAs are much greater than is the case with silicon.

2. ENCAPSULATION STUDIES

For an encapsulant to be used successfully, it must not only prevent deterioration of the physical appearance of the sample during the anneal, but it must also maintain the chemical composition of the encapsulated surface. In this study, the encapsulating properties of chemical vapor deposited (CVD) SiO_2 and rf plasma deposited Si_3N_4 layers were examined.

Low temperature photoluminescence (PL) and Auger electron spectroscopy (AES) were used to investigate the encapsulating properties of the films during the high temperature anneals. Rutherford backscattering (RBS) and ellipsometry measurements were also used to study some of the chemical and physical properties of the rf plasma deposited Si_3N_4 layers for various deposition conditions.

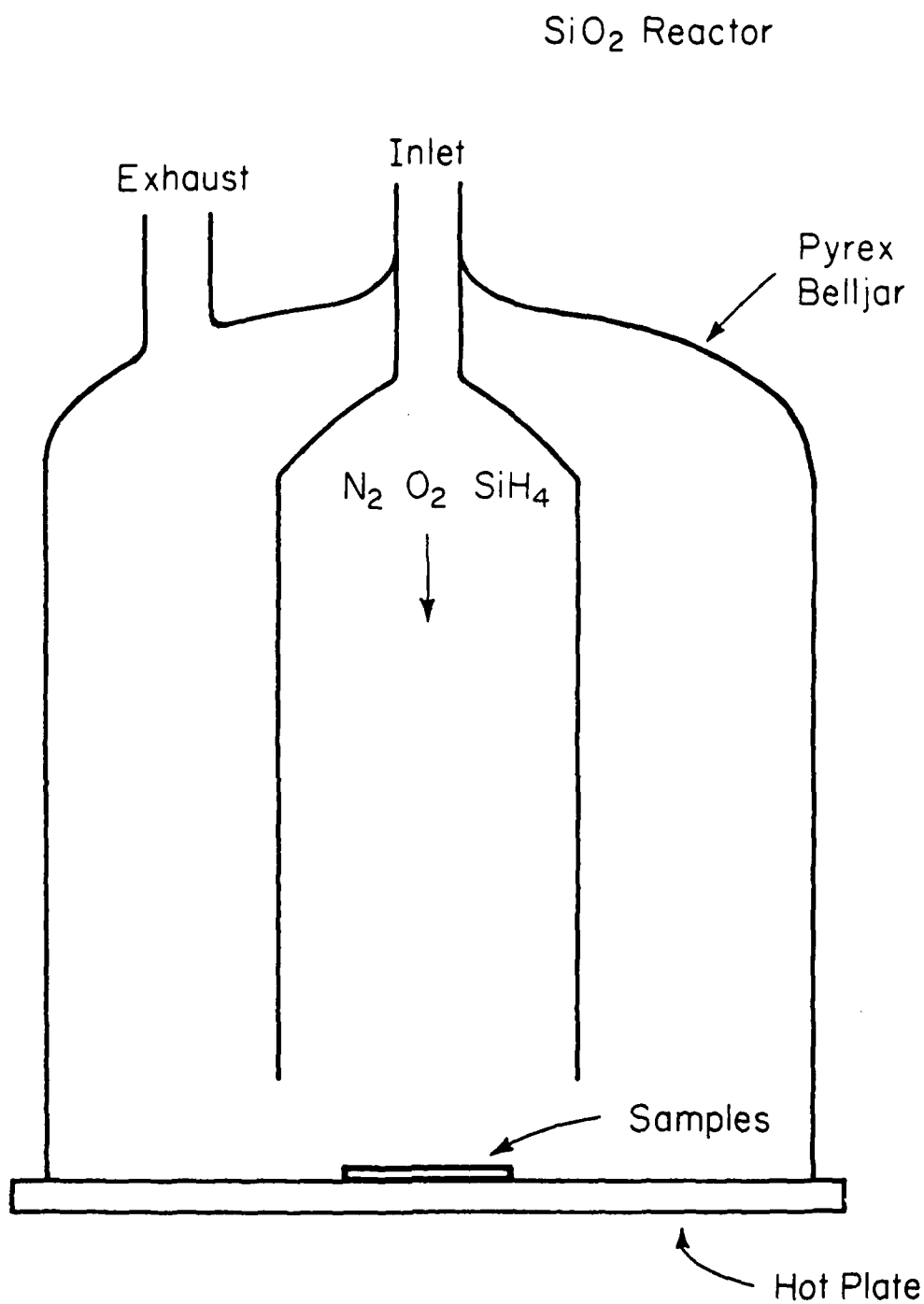
2.1. Deposition Systems

Four different deposition systems were used to deposit the various dielectric films used in the encapsulation studies. One system was used to deposit SiO_2 by the oxidation of silane, and the other three systems were rf plasma deposition systems used for depositing the Si_3N_4 layers.

2.1.1. Silicon Dioxide Deposition

The SiO_2 films were deposited by a CVD reaction involving a mixture of silane, oxygen, and nitrogen flowing over the sample mounted on a heated plate [60] (Figure 2.1).

Before the deposition, the gas lines and chamber are purged with nitrogen while the hot plate comes up to temperature. After the system is up to temperature, the gas lines are switched over from nitrogen to the gases used during the deposition. The three gas lines carry N_2 as a carrier



LP-1463

Figure 2.1. Schematic diagram of silicon dioxide reactor [61].

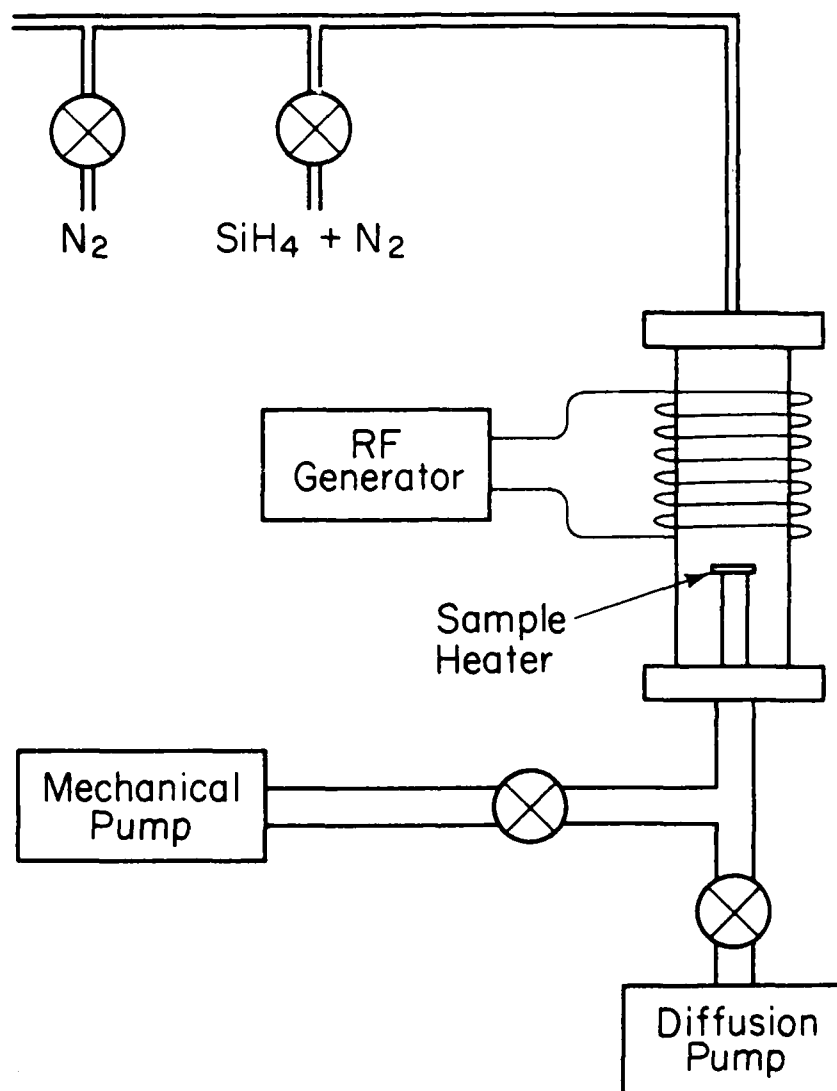
gas, O_2 , and 2% SiH_4 in a nitrogen carrier. The reacting gases are flowed through the chamber for several minutes with no samples present in order to remove the N_2 used for purging the lines. The silane is then shut off and the glass chamber removed from the hot plate. The samples are placed on the heater and the chamber is replaced. After the sample has come to temperature and the flowing N_2 and O_2 have displaced any atmosphere that was introduced while loading the samples, the flow of SiH_4 is resumed and deposition takes place. After the deposition the silane is again turned off and the samples are removed.

The flow of gases is controlled by needle valves and monitored by flowmeters. The approximate flow rates were ~80 standard cubic centimeters per minute (SCCM) of N_2 , ~1.1 SCCM of O_2 , and ~28 SCCM of 2% SiH_4 with 98% N_2 . Films were deposited at ~450°C and were typically 1500 to 2000Å thick.

2.1.2. RF Plasma Deposited Silicon Nitride

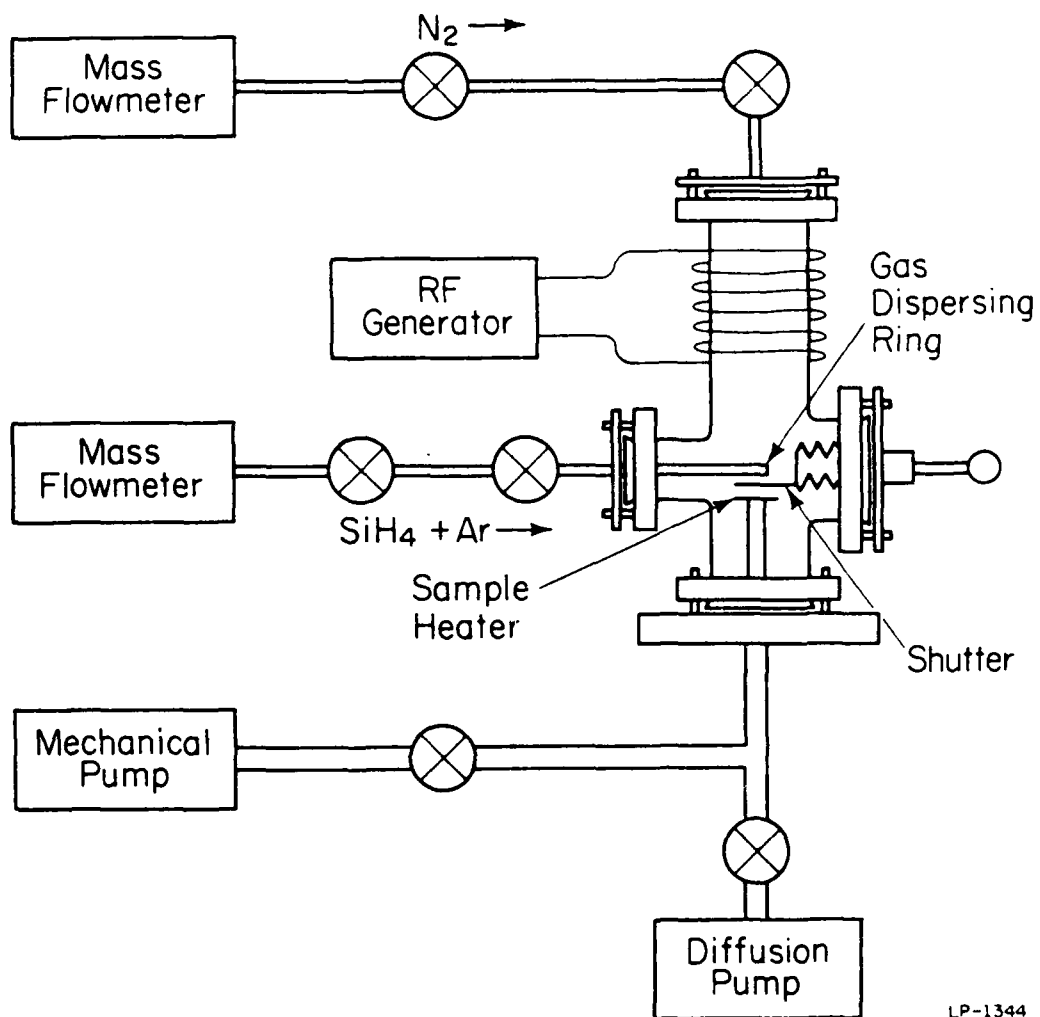
As discussed in section 1.2, there are advantages in using rf plasma deposition instead of other processes for depositing silicon nitride. All of the Si_3N_4 films used in this study were deposited by rf induced plasmas.

There were two types of nitride systems used in this work. Those nitrides labeled A in section 2.2 were deposited in a system where the silane and nitrogen were mixed prior to their introduction to the reaction chamber (Figure 2.2). Those nitrides referred to as type B in section 2.2 and those analyzed in section 2.3 were deposited in a system where the reacting gases were introduced separately [48]. The nitrogen is introduced into the top of the chamber and passes through the inductively coupled rf field. The silane diluted in argon is introduced just above the surface of the sample and below the rf coil (Figure 2.3).



LP-1345

Figure 2.2. Schematic diagram of rf plasma silicon nitride deposition system in which gases are mixed before introduction to the reaction chamber.



LP-1344

Figure 2.3. Schematic diagram of rf plasma silicon nitride deposition system in which gases are introduced into reaction chamber separately [48].

All of the systems used for depositing Si_3N_4 layers employed liquid nitrogen trapped oil diffusion pumps to evacuate the chamber and gas lines before deposition and a mechanical pump for pumping during the actual deposition.

The systems used in the annealing study of section 2.2 both used the same vacuum system and most of the same gas lines. The only difference in the hardware was the reaction chamber. The chamber used for depositing Si_3N_4 (A) was simply a Pyrex cylinder with an rf coil around it. All gases were brought in through the single gas line at the top. Films of type Si_3N_4 (B) were deposited in a chamber which consisted of a Pyrex cylinder with one gas line feeding in just above the sample through a Kovar-glass graded seal. The 2% SiH_4 in Ar entered through this opening, and the N_2 was fed into the top of the chamber.

Deposition procedures for the two systems were essentially the same. After loading the samples into the system, the chamber and the gas lines leading from the chamber to the metering valves were pumped out using the diffusion pump. Typical pressures for these systems were $1-2 \times 10^{-5}$ torr. Next, the valve to the diffusion pump was closed and the SiH_4 and carrier gas were introduced. Then, while pumping with the mechanical pump, the pressure was adjusted to 0.125 torr by the needle valve in the SiH_4 line. For Si_3N_4 (A) layers, the gas used was 15% SiH_4 in N_2 ; for Si_3N_4 (B) layers the gas used was 2% SiH_4 in Ar. As mentioned above, the 2% SiH_4 was introduced into the side of the chamber in system B. After the pressure was stabilized, N_2 was metered into the top of the chamber, bringing the total pressure to 0.4 torr. The samples were then quickly heated to 450°C (<30 sec.) and the discharge was initiated. When the desired film thickness was obtained, the rf power was turned off and the chamber was again evacuated

before venting with nitrogen.

The third system was similar in design to that used for $\text{Si}_3\text{N}_4(\text{B})$ layers, but was considerably upgraded. The vacuum system was improved to increase the pumping speed and decrease the ultimate vacuum obtainable. Mass flowmeters were used in the gas lines to monitor the flow rates. A gas dispersing ring was added to improve the flow of SiH_4 over the sample. Finally, a metal shutter was used to shield the samples from any discharge in the chamber before deposition.

The deposition procedure was slightly different for this upgraded system. After the samples were loaded, the chamber and gas lines were pumped down to $<3 \times 10^{-6}$ torr. The high vacuum valve was then closed and the N_2 flow was set while pumping with the mechanical pump. Typically the flow rate was 50 SCCM at a pressure of ~ 0.3 torr. Then, with the shutter covering the sample, the rf power was turned on and a nitrogen discharge was initiated to help remove remaining oxygen from the system. After running the nitrogen discharge for a few minutes, the rf power was turned off and the shutter was moved away from the sample. The N_2 and $\text{SiH}_4 + \text{Ar}$ flow rates were then set to those desired for the deposition. For most encapsulation work the flow rates were 50 SCCM for N_2 and 11-12.6 SCCM for the 2% SiH_4 in Ar. When the flow rates were set, the sample was quickly heated to 300° - 350°C and the discharge was initiated. When the desired film thickness was obtained, the rf power and gases were turned off and the chamber was evacuated before venting with nitrogen.

Studies [29] presented in section 2.2 show that there was considerable difference between the nitride layers deposited when the gases were mixed before introduction into the chamber ($\text{Si}_3\text{N}_4(\text{A})$) and the layers deposited when the gases were introduced separately ($\text{Si}_3\text{N}_4(\text{B})$). The major

difference between the films was the oxygen level. In the Si_3N_4 (A) films the oxygen content was much higher. It is believed that by introducing the SiH_4 into the chamber below the rf coil, the probability of the silane reacting with oxygen in the system is decreased. A possible reason for this is that by letting only the N_2 pass through the rf coil and not the SiH_4 , some of the oxygen is tied up in nitrogen compounds and cannot react with the SiH_4 . Another possibility is that since the SiH_4 itself is not excited by the plasma, it cannot react with residual oxygen as easily. It is not clear, however, exactly what the mechanism is.

Films deposited by the two systems in which the gases were introduced separately were of comparable quality, with those films deposited in the upgraded system being slightly better. Even though the films deposited in the upgraded system were of slightly better quality and much more reproducible, the films from the older system were used in the study of section 2.2. This was done to eliminate the possibility of the difference between the two types of nitrides being due to a better vacuum system and better control.

It was found that running a nitrogen discharge before the actual deposition also decreases the oxygen content of the films. The degree of improvement obtained varies with the amount of Si_3N_4 deposited on the interior of the chamber. Little is gained by the use of a nitrogen discharge if the inside of the chamber is very clean, but there can be substantial improvement when the chamber is "dirty". This seems to indicate that the nitrogen plasma acts to "scrub" the walls and remove some of the adsorbed oxygen. However, some problems have been observed with running a nitrogen discharge prior to deposition. In all III-V compounds we have coated, exposure of the sample to the nitrogen discharge adversely affected the adhesion of the Si_3N_4 .

film. This problem has been avoided by using the shutter to shield the sample during the discharge. There was, however, never any adhesion problem observed for Si_3N_4 on Si.

2.2. Annealing Studies

It is well known from diffusion experiments in Si that Ga has a very high diffusion coefficient in SiO_2 [62]. Gyulai et al. [30] have used proton backscattering spectrometry to show that SiO_2 layers on GaAs permit outdiffusion of Ga. Previous low temperature photoluminescence studies of GaAs [63] have demonstrated the growth of emission bands from anneals under various conditions. A broad band with a peak near 1.356 eV has been correlated with the outdiffusion of Ga [63]. There is other evidence to suggest that this band is related to the incorporation of Cu on Ga sites [64,65] as Ga atoms are lost due to outdiffusion. In either case, this band can be directly or indirectly attributed to Ga loss.

In this work, the 1.356 eV photoluminescence band was monitored after annealing with three types of encapsulation, and the encapsulant films were examined for Ga outdiffusion using AES. The three encapsulants studied were silicon dioxide, silicon nitride, and oxygen-contaminated silicon nitride. All were deposited on semi-insulating GaAs and annealed at 900°C. The anneals were performed in a 12" Trans Temp furnace with a silica liner. The atmosphere during the anneals was flowing forming gas (4% H_2 in high purity N_2), and the temperature was monitored with a chromel-alumel thermocouple and Fluke 2100A digital thermometer.

2.2.1. Photoluminescence Studies

A schematic diagram of the front-face photoluminescence apparatus used in this study is shown in Figure 2.4. After removing the encapsulating

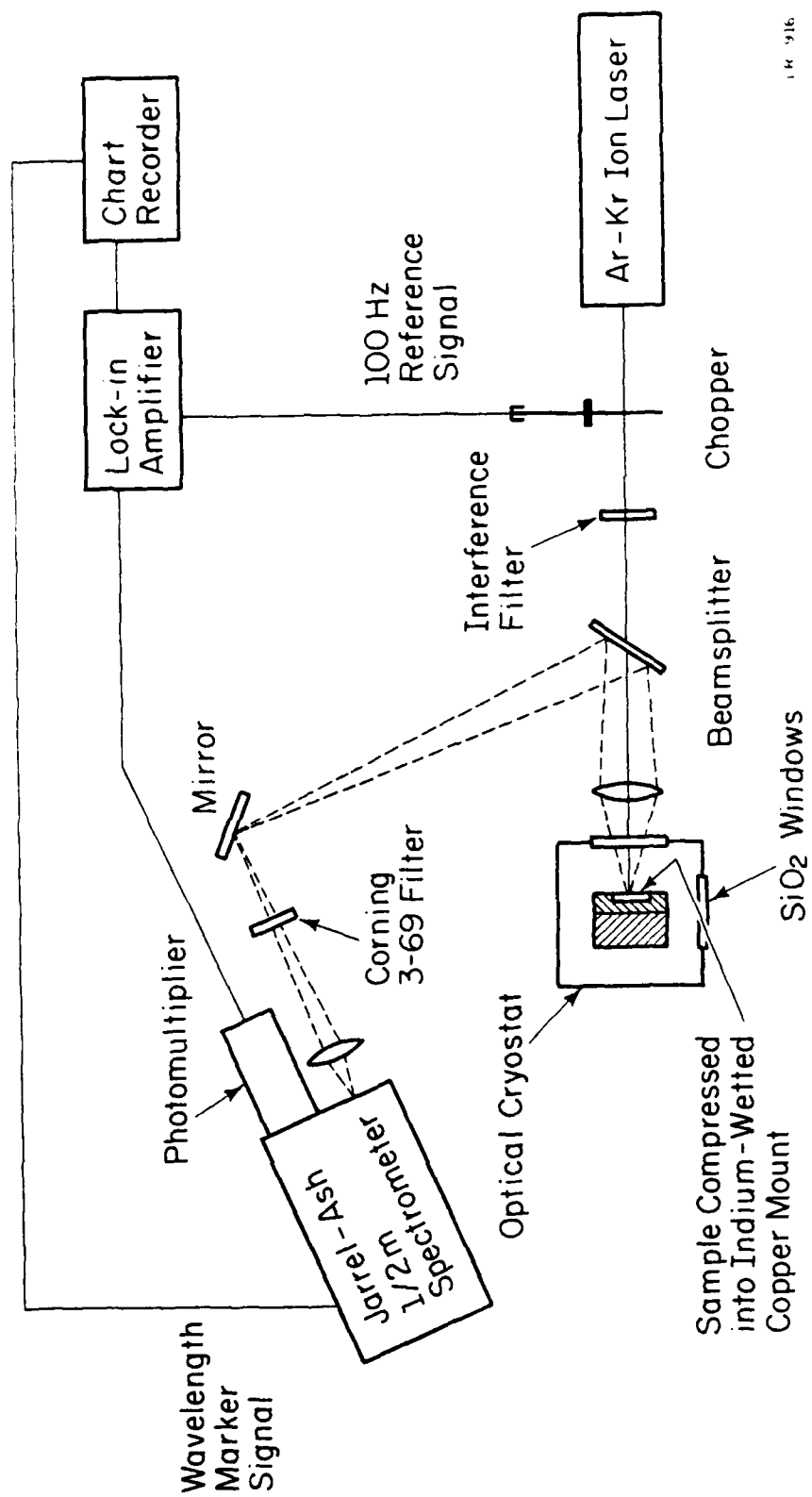


Figure 2.4. Schematic diagram of the front-face photoluminescence apparatus.

layer, the photoluminescence samples were pressed into indium-wetted copper heat sinks [66]. The sample/heat sink assembly was held at 5°K in a Janis Super-Varitemp gas exchange cryostat. Photoluminescence was excited by the 5145Å line from an Ar-Kr ion laser. Spectra were recorded using a 0.5m scanning spectrometer and a cooled (77°K) photomultiplier with S-1 response.

Figure 2.5 shows the 5°K photoluminescence spectra obtained from the GaAs samples annealed at 900°C with various encapsulants. Figure 2.5(a) illustrates that when a sample is annealed with SiO₂ encapsulation, a broad luminescence band is observed with a peak at 1.356 eV. This defect band is related to Ga outdiffusion, as discussed above. Although the SiO₂ films used in this work are considerably better than those studied previously [63], Ga outdiffusion is still quite evident from this peak.

The PL spectrum from a sample annealed with Si₃N₄(A) encapsulation is shown in Figure 2.5(b). This spectrum also clearly indicated Ga loss from the GaAs. The lower energy peaks associated with the 1.356 eV band in Figure 2.5 are phonon replicas of the main zero-phonon peak. These peaks are separated by ~36 meV, the LO phonon energy in GaAs [67]. As discussed in section 2.1, Si₃N₄(A) was prepared by mixing the nitrogen and silane prior to their introduction into the plasma in the reaction chamber. In section 2.2.2, AES studies will show the presence of a uniformly high level of oxygen within the film.

Figure 2.5(c) displays the PL spectrum obtained from a sample with Si₃N₄(B) encapsulation annealed at 900°C for 2 hr. A weak 1.356 eV band is seen. In a sample annealed with such an encapsulant for 1 hr. the intensity of the 1.356 eV band was very weak, similar to the spectrum shown in Figure 2.5(e). The absence of a strong defect PL band even after the 2 hr. anneal suggests that Si₃N₄(B) effectively suppresses Ga outdiffusion. The Si₃N₄(B)

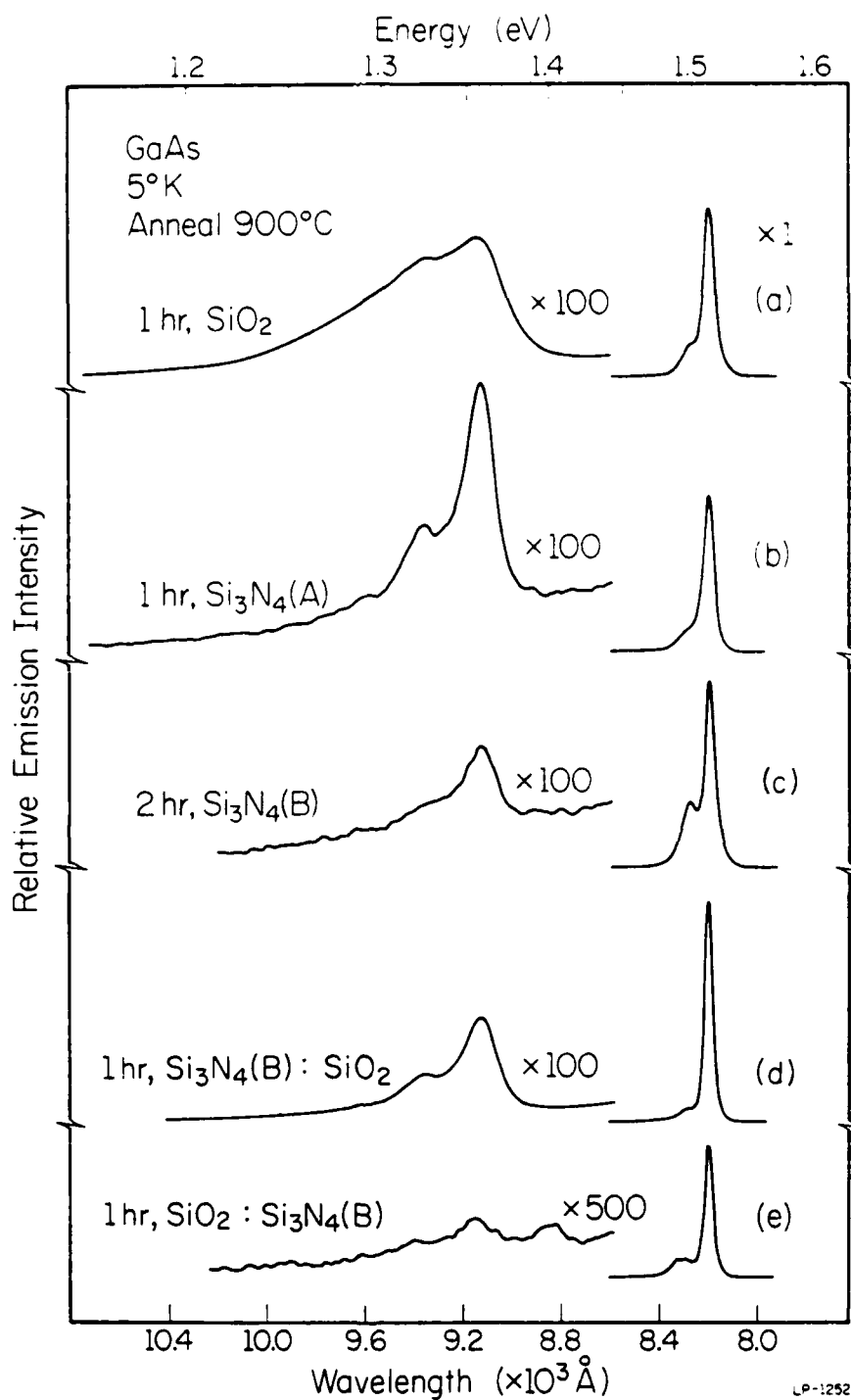


Figure 2.5. Photoluminescence spectra from GaAs samples annealed with various encapsulants. The scale factors are relative to the band-edge peak for each sample [29].

layers were deposited in the system where the nitrogen and silane are introduced into the chamber separately, as discussed in section 2.1. The AES studies show that while the $\text{Si}_3\text{N}_4(\text{A})$ films have a high concentration of oxygen, the oxygen content of the $\text{Si}_3\text{N}_4(\text{B})$ films is barely detectable.

Annealing studies were also carried out using some multilayered dielectrics as the encapsulant. Figure 2.5(d) shows the PL spectrum obtained when a $\text{Si}_3\text{N}_4(\text{B})/\text{SiO}_2$ dielectric layer (SiO_2 in contact with the GaAs) was used as the encapsulant. The 1.356 eV band is observed, although the intensity of this band is weaker than the case where SiO_2 alone is used (Figure 2.5(a)). When the order of layers is reversed ($\text{SiO}_2/\text{Si}_3\text{N}_4(\text{B})$) so that the $\text{Si}_3\text{N}_4(\text{B})$ is in contact with the GaAs, no band is observed at 1.356 eV (Figure 2.5(e)). This spectrum is essentially the same as that of $\text{Si}_3\text{N}_4(\text{B})$ alone after a 1 hr. anneal; no improvement was seen with the addition of the SiO_2 layer.

2.2.2. Auger Electron Spectroscopy Studies

Auger electron spectra (AES) and depth profiles were obtained using either a conventional Physical Electronics Industries Model 545 scanning Auger microprobe (SAM) or a custom-built thin film analyzer (TFA) [68]. Incident electron beam energies were 6 keV (SAM) or 5 keV (TFA) with typical beam currents of 5 and 70 μA respectively. In both systems ion sputtering was performed with 2 keV Ar^+ using either stationary beams from two ion guns in lateral opposition (SAM) or an electrically rastered beam from one ion gun (TFA). Both systems were optimized for maximum depth resolution. Comparative studies on the two instruments gave statistically insignificant differences, and they are therefore considered essentially equivalent. Some of the analysis techniques used in this study have been described in detail elsewhere [68]. First, an Auger spectrum of the sample surface is taken

prior to sputtering. A second complete spectrum is recorded after an "ion dusting", removing $\sim 20\text{\AA}$ for comparison with the unsputtered surface. Finally, conventional multiplexer depth profiling is performed for the specific elements of interest. To avoid charging of the dielectric layers during analysis, samples were mounted at grazing incidence to the electron beam (30°). However, in some cases severe charging was observed and no useful analytical information could be obtained. Subsequent examination of such encapsulants by scanning electron microscopy showed a high degree of surface roughness. Data presented here are from samples which did not exhibit charging phenomena.

An Auger depth profile of a GaAs sample encapsulated with SiO_2 and annealed for 1 hr. at 900°C is shown in Figure 2.6. A detectable Ga signal is observed in the surface Auger spectrum (see Figure 2.6 inset). Since the sample was encapsulated on all sides during the anneal, the presence of Ga at the surface indicates diffusion of Ga from the substrate through the SiO_2 layer. However, no Ga was detected within the SiO_2 layer itself. This is presumably due to the solid solubility of Ga in SiO_2 being below the Auger detection limit of ~ 0.5 atomic percent. The observation of surface Ga together with the photoluminescence results clearly indicate Ga out-diffusion through the SiO_2 layers.

Figure 2.7(a) shows the AES depth profile of a sample annealed with $\text{Si}_3\text{N}_4(\text{A})$ at 900°C for 1 hr. As with the SiO_2 films, a Ga signal is present on the surface of the film. In addition, there is a detectable Ga signal throughout the $\text{Si}_3\text{N}_4(\text{A})$ film. Again, the AES studies of these films are in agreement with the PL data and clearly indicate Ga outdiffusion. The AES depth profile also shows a uniformly high level of oxygen within the film. As discussed in section 2.1, the $\text{Si}_3\text{N}_4(\text{A})$ films were prepared by mixing the silane and nitrogen prior to their introduction into the reaction chamber,

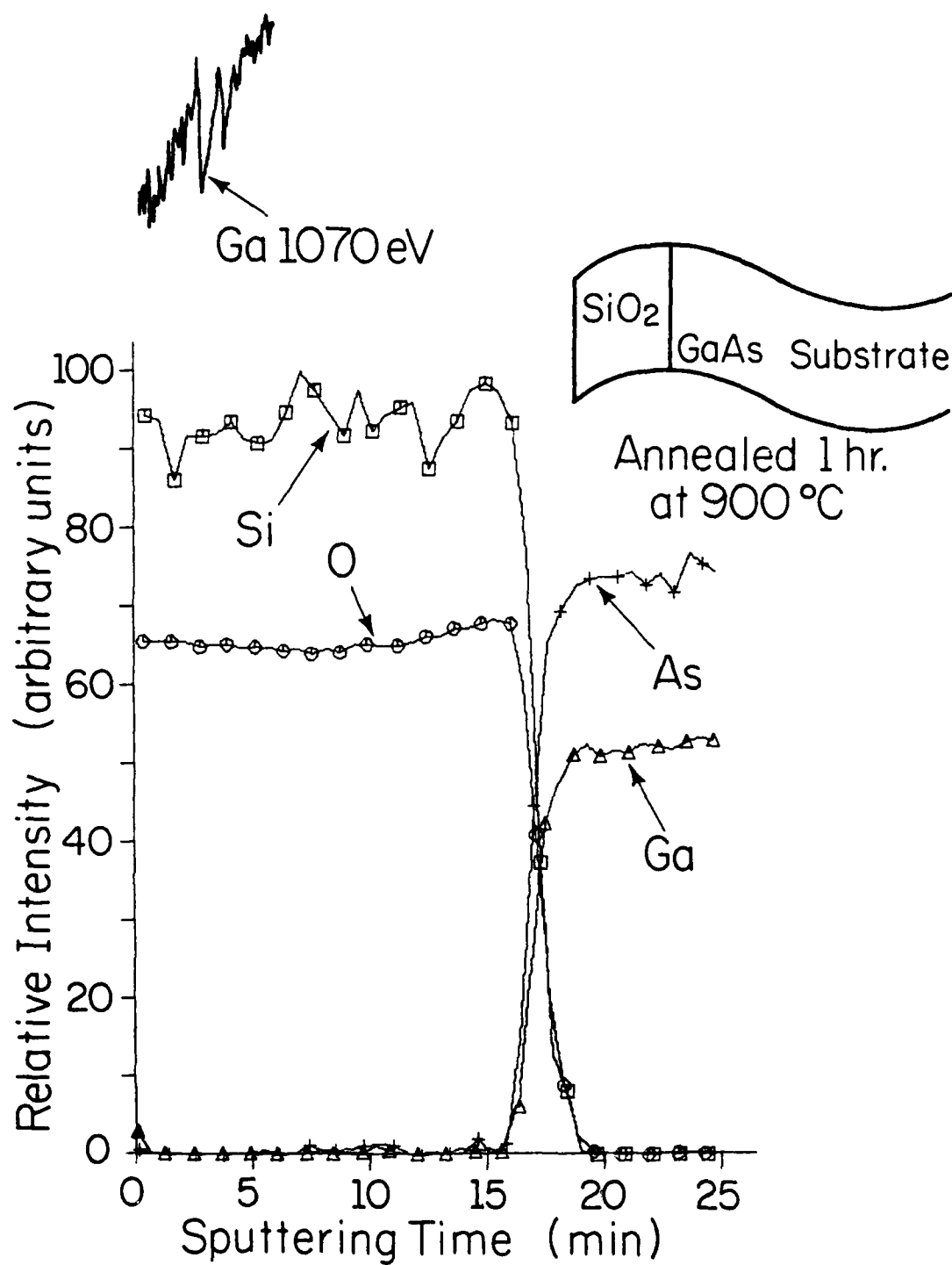


Figure 2.6. Auger depth profile obtained from a GaAs sample annealed at 900°C for 1 hr. The inset illustrates the Ga Auger spectrum observed at the SiO₂ surface prior to sputtering [29].

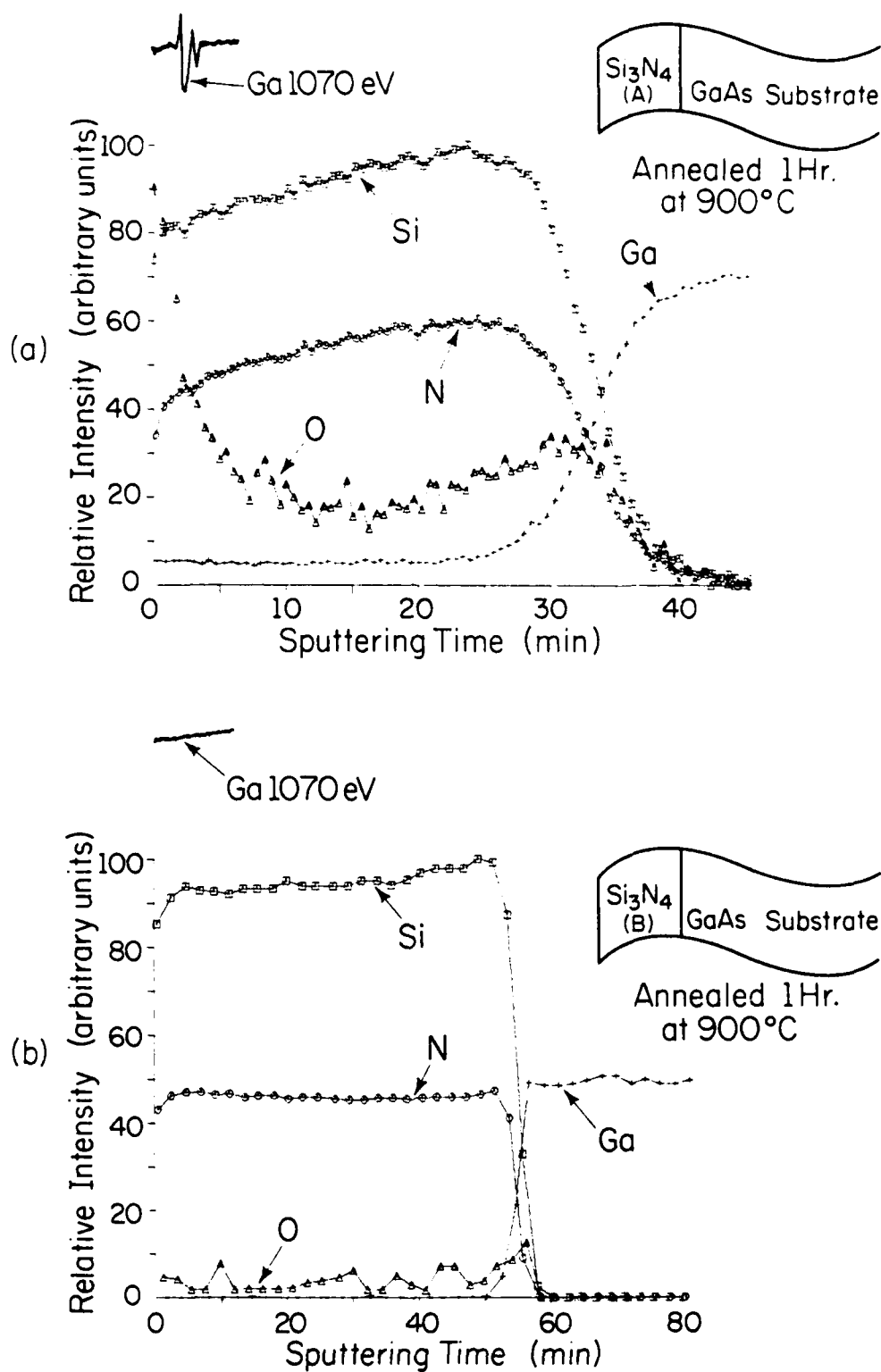


Figure 2.7. Auger depth profiles obtained from GaAs samples encapsulated with (a) Si_3N_4 (A) and (b) Si_3N_4 (B) layers and annealed at 900°C for 1 hr. The insets illustrate the Ga Auger spectra at the Si_3N_4 surfaces prior to sputtering [29].

and both gases were exposed to the rf plasma.

The AES depth profile of samples annealed with $\text{Si}_3\text{N}_4(\text{B})$ for 1 hr. at 900°C (Figure 2.7(b)) shows no Ga signal detectable either in the surface spectrum or within the film itself. The lack of Ga outdiffusion in these films is in agreement with the PL studies. It is important to note the oxygen level in the $\text{Si}_3\text{N}_4(\text{B})$ films. The signal is barely above the detection limit of ~ 0.1 atomic percent. This level is at least an order of magnitude lower than the oxygen level observed in $\text{Si}_3\text{N}_4(\text{A})$. The interface between the GaAs and Si_3N_4 is also much sharper for $\text{Si}_3\text{N}_4(\text{B})$. As discussed in section 2.1, $\text{Si}_3\text{N}_4(\text{B})$ was deposited in a system where the nitrogen and silane are introduced into the chamber separately, with the silane introduced below the rf coil and just above the sample.

Auger depth profiles were also obtained from samples annealed with multiple-layer encapsulants. Figure 2.8 shows the AES depth profiles of samples annealed at 900°C for 1 hr. after being coated first with SiO_2 and then with Si_3N_4 . When the top layer was $\text{Si}_3\text{N}_4(\text{A})$ (Figure 2.8(a)), strong oxygen and gallium signals were present in the nitride layer. The presence of the strong Ga signal is another indication that the Ga diffuses quickly through the SiO_2 layer, even though none is observed within the layer. As expected, no Ga is seen in the $\text{Si}_3\text{N}_4(\text{B})$ layer (Figure 2.8(b)), and very little oxygen is detected. No Ga buildup was observed at the oxide-nitride interfaces in any of the cases studied.

Both the PL and AES studies show that Ga is lost from samples annealed with either SiO_2 or Si_3N_4 with high oxygen content. Silicon nitride which is essentially oxygen-free does serve as a good encapsulant and prevents Ga outdiffusion. Studies of junction characteristics of implanted p-n junctions [15] (presented in section 3.3) also support the suitability of

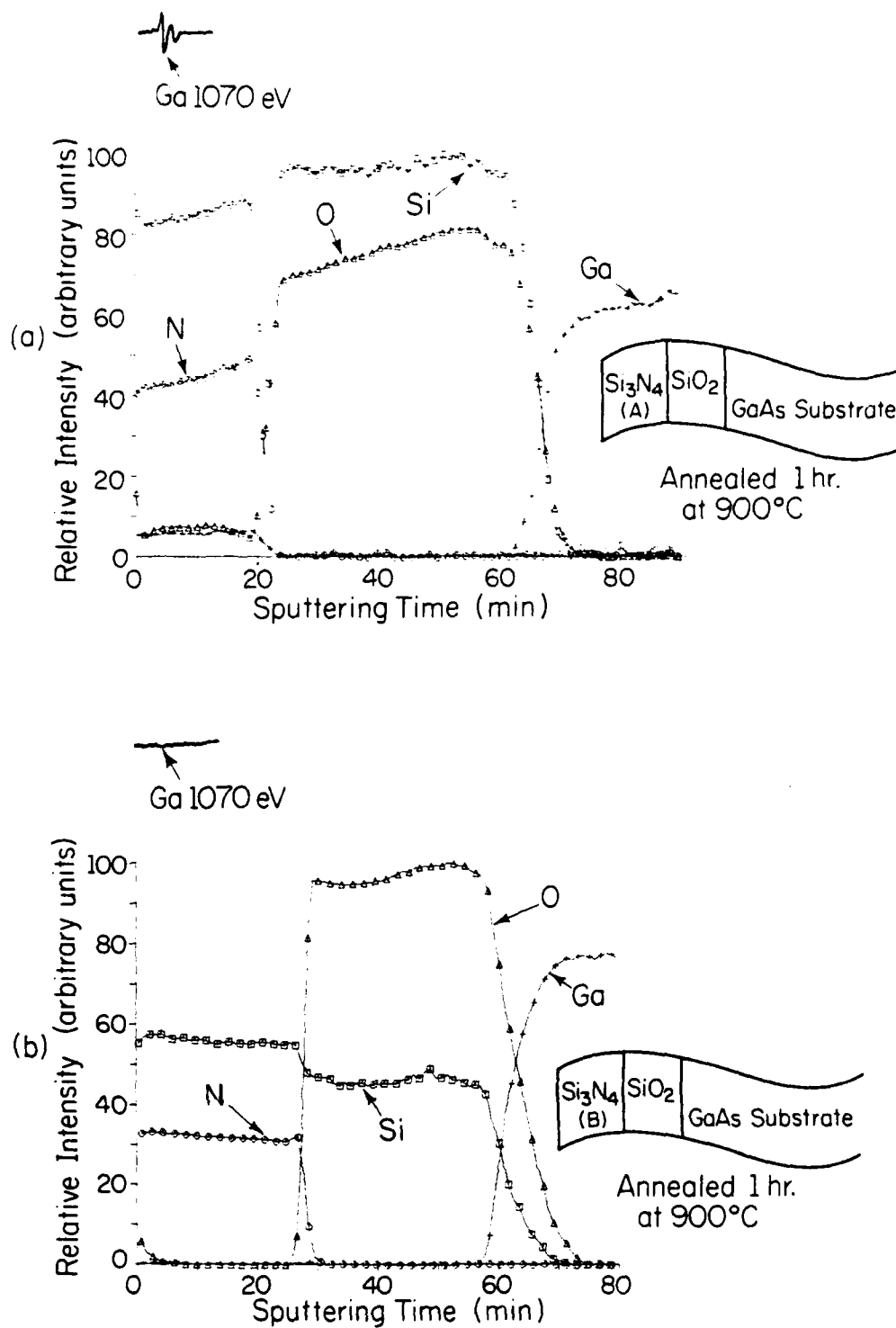


Figure 2.8. Auger depth profiles obtained from GaAs samples encapsulated with (a) $\text{Si}_3\text{N}_4(\text{A})/\text{SiO}_2$ and (b) $\text{Si}_3\text{N}_4(\text{B})/\text{SiO}_2$ layered dielectrics and annealed at 900°C for 1 hr. The insets illustrate the Ga Auger spectra at the Si_3N_4 surfaces prior to sputtering [29].

"oxygen-free" Si_3N_4 as an encapsulant.

2.3. Characteristics of the "Oxygen-Free" System

In order to better characterize the rf plasma Si_3N_4 system and the films deposited in it, depositions were made under varying gas flow conditions, and the resulting films were then analyzed. Film composition, index of refraction, deposition rate, and etch rate were measured for the various films. All Si_3N_4 layers in this study were deposited in the upgraded version of the Si_3N_4 system discussed in section 2.1.2. The films were all deposited at 300°C with the gas pressure in the chamber held at approximately 0.3 torr.

The atomic composition of the deposited nitride layers was measured by Rutherford backscattering (RBS) measurements [69]. To facilitate this measurement, silicon nitride layers were deposited on carbon layers which had been previously deposited on silicon substrates. The index of refraction was obtained from ellipsometry measurements [70] using the 6328\AA line of a He-Ne laser. Index of refraction, deposition rate, and etch rate measurements were made on films deposited on Si substrates. After cleaning with organic solvents, the silicon substrates were cleaned in hot solutions of $5 \text{ H}_2\text{O}:1 \text{ NH}_4\text{OH}:1 \text{ H}_2\text{O}_2$ and $5 \text{ H}_2\text{O}:1 \text{ HCl}:1 \text{ H}_2\text{O}_2$ and then rinsed in deionized water (DI). Finally, they were dipped in HF and again rinsed in DI and blown dry with nitrogen.

Table 2.1 lists the film composition, deposition rate, index of refraction, and etch rate in 20% HF for nitride layers deposited with various nitrogen to silane ($\text{N}_2:\text{SiH}_4$) flow rate ratios. The silane used in the system is diluted to 2% silane, with the balance being argon. This dilution was taken into account in calculating the flow rate ratios. The total flow rate of gases (N_2 , SiH_4 , and Ar) used in this study was 57 to 64 SCCM.

As can be seen from table 2.1, there was considerable excess

Table 2.1. Physical properties of the nitride layers.

Ratio of Flow Rates ^a $N_2:SiH_4$	Composition of Film (RBS Analysis) Si:N	Deposition Rate (\AA min^{-1})	Index of Refraction n	Etch Rate in 20% HF (\AA min^{-1})
357	0.71	51	1.96	800
215	0.78	72	1.98	440
178	0.79	71	2.03	400
143	0.93	77	2.15	300
107	1.14	77	2.24	300
36	1.59	--	2.59	175

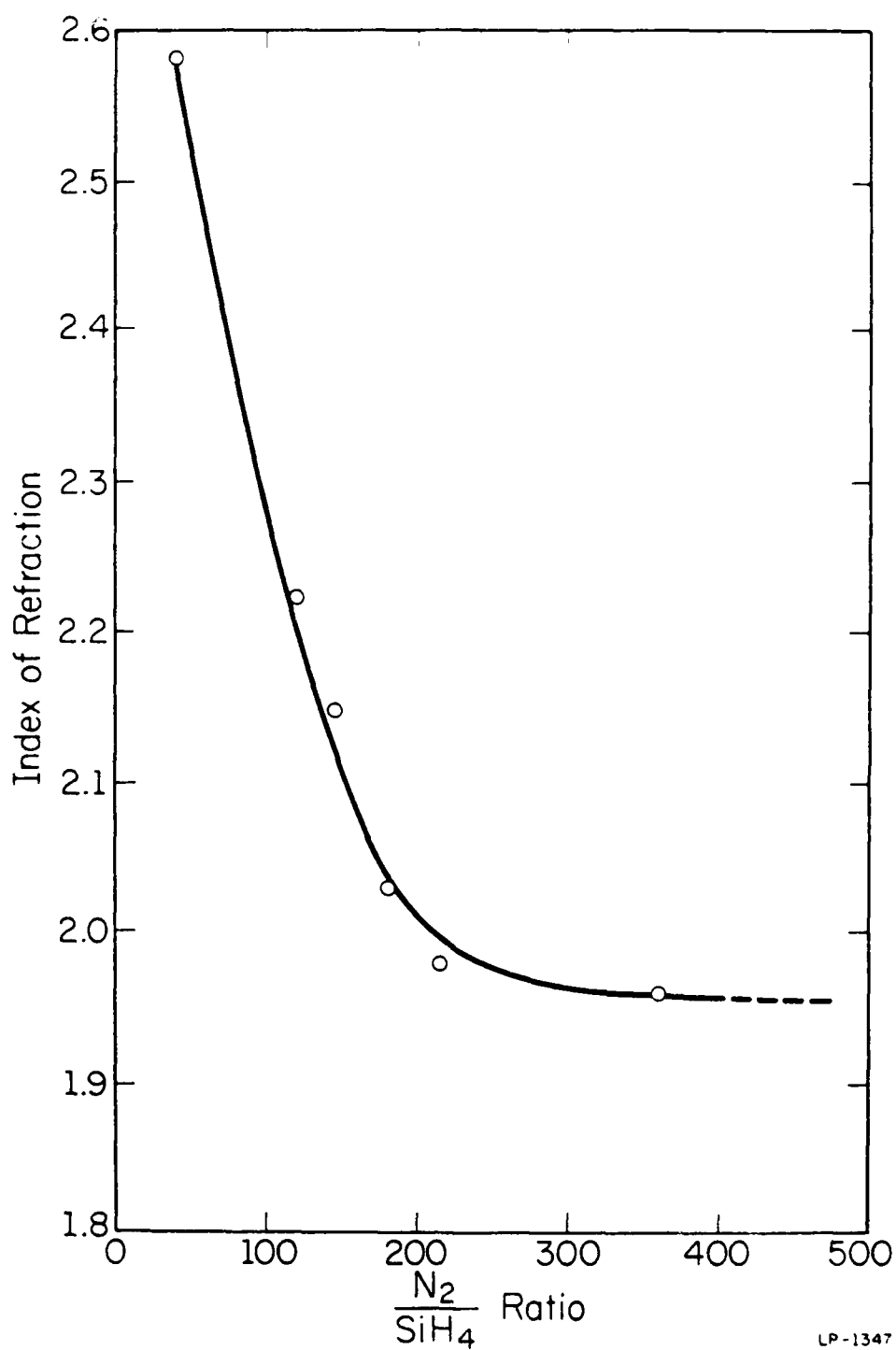
^aThe dilution of the silane in argon has been taken into account in estimating the ratio of flow rates.

silicon in the films deposited with the lower $N_2:SiH_4$ ratios. The stoichiometric ratio of silicon to nitrogen ($Si:N = 0.75$) was obtained for a flow ratio ($N_2:SiH_4$) of about 250. The backscattering data on these films showed the presence of a weak surface oxygen peak but no detectable oxygen signal within the film. The sensitivity of this RBS technique to oxygen was better than about 2 atomic percent.

Figure 2.9 shows the variation of the index of refraction of the films as a function of the ratio of gas flow rates. The index of refraction increases very rapidly as the $N_2:SiH_4$ ratio decreases below 200. For ratios of $N_2:SiH_4$ greater than about 200, the index of refraction tends to level off between 1.9 and 2.0.

The relationship between the index of refraction and the nitride composition is shown in Figure 2.10. The results show that the index of refraction increases linearly with the $Si:N$ ratio. The arrow in this figure shows the point where the $Si:N$ ratio (determined by RBS) is that of stoichiometric Si_3N_4 . At this point the index of refraction is approximately 1.98, a reasonable value for high quality Si_3N_4 . For films with very low oxygen content, this relationship can be conveniently used to determine the composition of the film by measuring the index of refraction. The presence of oxygen in the film lowers the index of refraction towards that of SiO_2 (1.48), and the index of refraction can no longer be used as a measure of film composition.

In Figure 2.11, the nitride deposition rate and etch rate in 20% HF are shown as functions of film composition. The etch rate dramatically decreases as excess silicon is incorporated in the film. Similar studies of plasma deposited nitrides [53,54] report a maximum in the etch rate at the stoichiometric composition and lower etch rates for both nitrogen-rich



LP-1347

Figure 2.9. Variation of the index of refraction with the ratio of flow rates ($N_2:SiH_4$) for silicon nitride layers deposited at $300^\circ C$ and ~ 0.3 torr.

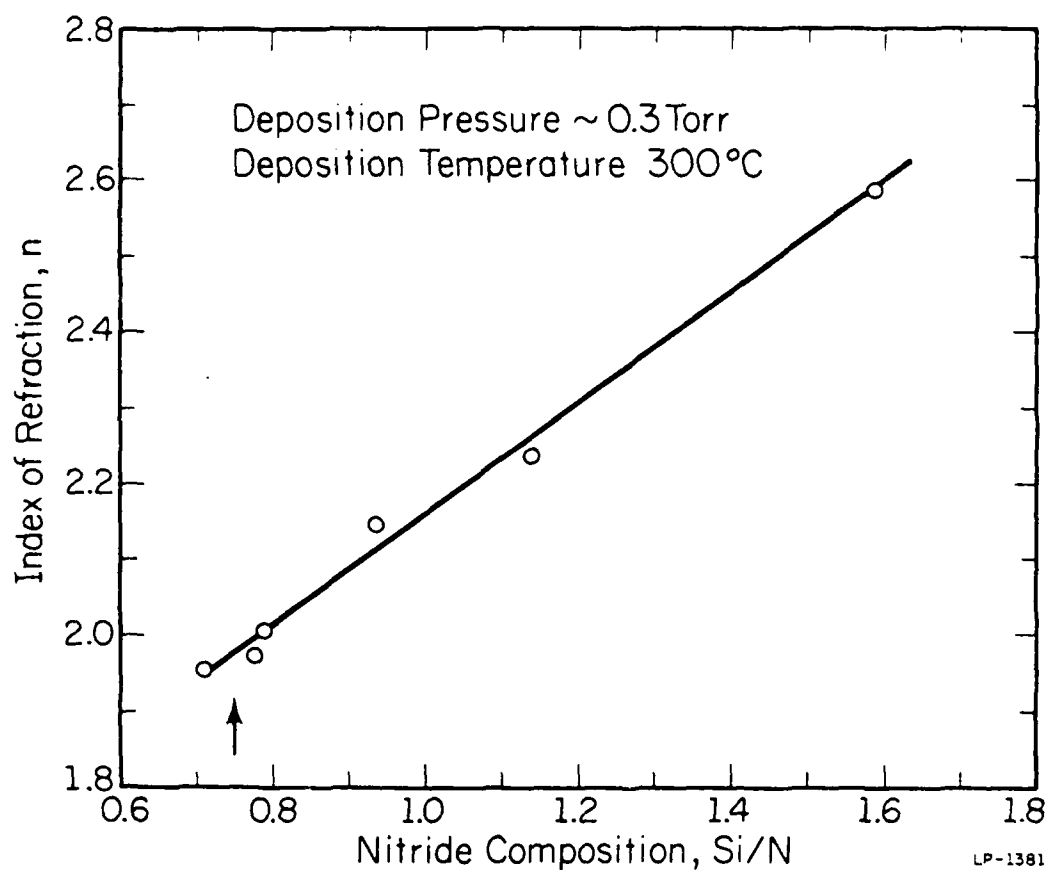


Figure 2.10. Variation of the index of refraction with composition (ratio of silicon to nitrogen) for silicon nitride films deposited at 300°C and ~ 0.3 torr. The stoichiometric ratio ($\text{Si}:\text{N} = 0.75$) is marked with an arrow [48].

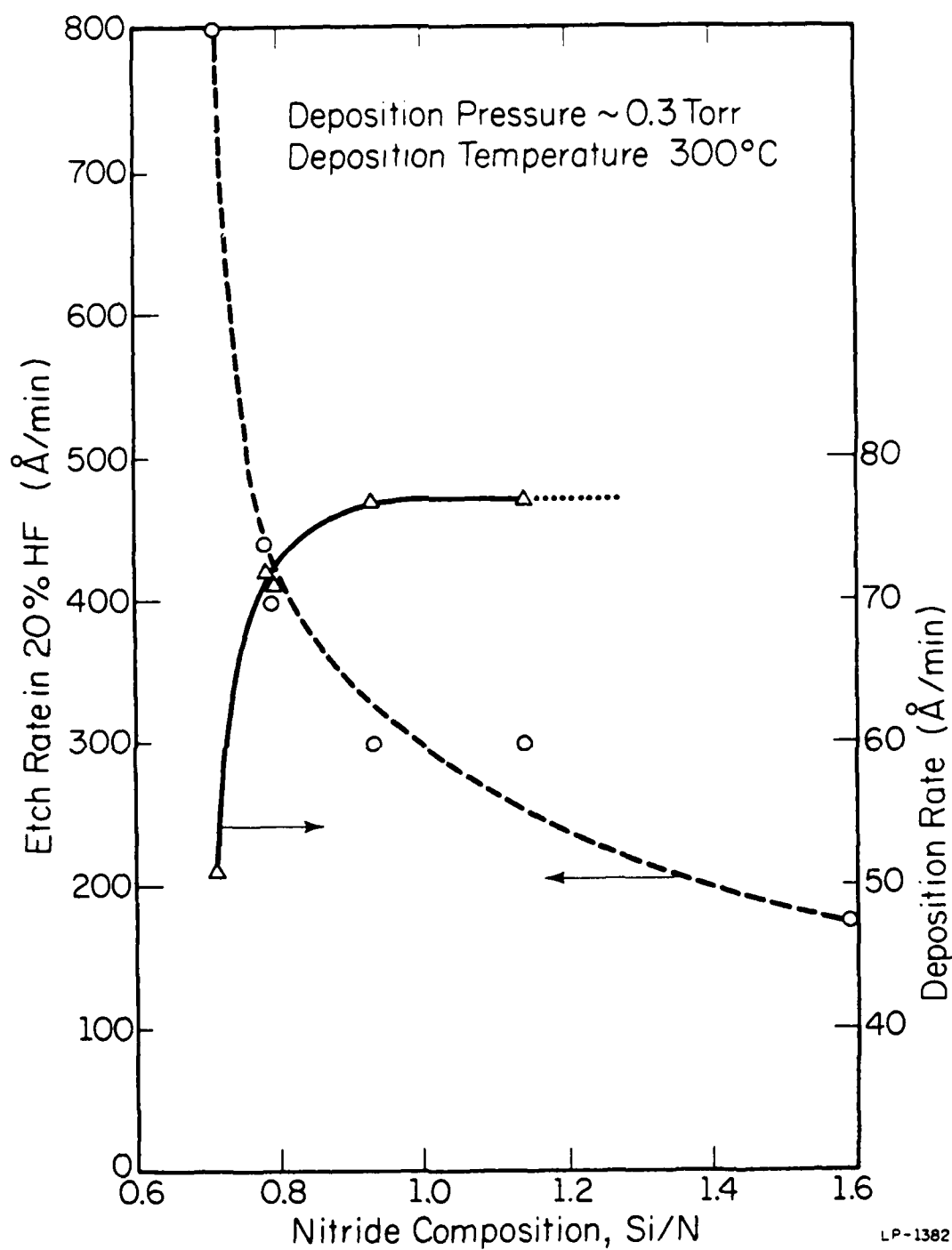
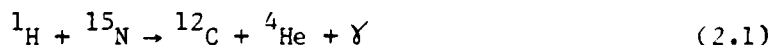


Figure 2.11. Deposition rate (solid line) and etch rate (dashed line) in 20% HF for silicon nitride films deposited at 300°C and ~0.3 torr, shown as a function of the chemical composition of the film [48].

and silicon-rich films. In our films, the etch rate continued to increase with excess nitrogen in the films. This behavior is in agreement with the work of Kuwano [51]. The deposition rate was fairly constant for the silicon-rich films but dropped off rapidly as the films became nitrogen-rich.

The etch rate of the Si_3N_4 films decreased as the deposition temperature increased and also decreased after high temperature anneals. When the films are contaminated with oxygen, the etch rate increases dramatically and the index of refraction decreases.

Preliminary studies [71] of the hydrogen content of these films using the resonant nuclear reaction



have determined that there is on the order of 10% hydrogen. In contrast to this, other studies [72] have shown there to be on the order of 30% hydrogen in plasma deposited Si_3N_4 layers. One possible explanation for the lower hydrogen content is the use of N_2 as the source of N rather than NH_3 . Since there is less hydrogen in the discharge, there should be less in the film. Another possibility is the slower deposition rate used for our films, yielding a denser film with less trapped hydrogen.

In summary, the films deposited from this system had very reproducible properties and very low oxygen content. The studies of sections 2.2 and 3 show that these low oxygen content films serve as excellent encapsulants for GaAs during high temperature anneals.

2.4. Electrical Properties of RF Plasma Si_3N_4 Layers

Recent studies of low oxygen content Si_3N_4 films on GaAs suggest a possible use in MIS-type devices [73,74]. As a part of this study, electrical properties of Si_3N_4 films deposited in the system discussed in section 2.3 have been measured in collaboration with G. Y. Robinson and T. R.

Ohnstein of the University of Minnesota. The films were deposited on both p- and n-type GaAs substrates at a temperature of 325°C. In this study, both capacitance-voltage (C-V) and current-voltage measurements of MIS diodes were made to determine the bulk film properties and to characterize the insulator/GaAs interface. Also, Auger electron spectroscopy was used to determine the Si:N ratio and to detect any contamination present.

The Auger studies showed the Si:N ratio in the films to be between 0.75 and 1.0 and the oxygen contamination level to be 0.1 atomic percent or less. The oxygen level rose slightly at the Si_3N_4 /GaAs interface, but for samples with no intentional oxidation the oxygen level was still less than ~1 atomic percent at the interface.

The results of the electrical measurements for the plasma Si_3N_4 films were also compared to the properties of Si_3N_4 films formed by conventional high temperature chemical vapor deposition and to films formed by anodization of GaAs. The bulk properties of the plasma Si_3N_4 films were found to be superior to the anodic oxides, but slightly inferior to the pyrolytic Si_3N_4 films. The plasma films exhibited a breakdown field of 4.5×10^6 V/cm, a resistivity of $3 \times 10^{15} \Omega\text{-cm}$, a relative dielectric constant of 7.9, and an index of refraction, measured by ellipsometry, of 1.99. The composition of the plasma Si_3N_4 films was found to be very similar to the pyrolytic Si_3N_4 films, but with slightly lower oxygen contamination.

The electrical properties of the plasma Si_3N_4 /GaAs interface, as indicated by the frequency dispersion of the C-V characteristics, differed from those measured for the oxide/GaAs and pyrolytic Si_3N_4 /GaAs structures. On p-type substrates, the plasma Si_3N_4 films showed very high interface state densities across the entire bandgap, unlike anodic films (Figure 2.12). On n-type substrates, a preliminary analysis based on 1 MHz C-V data indicates

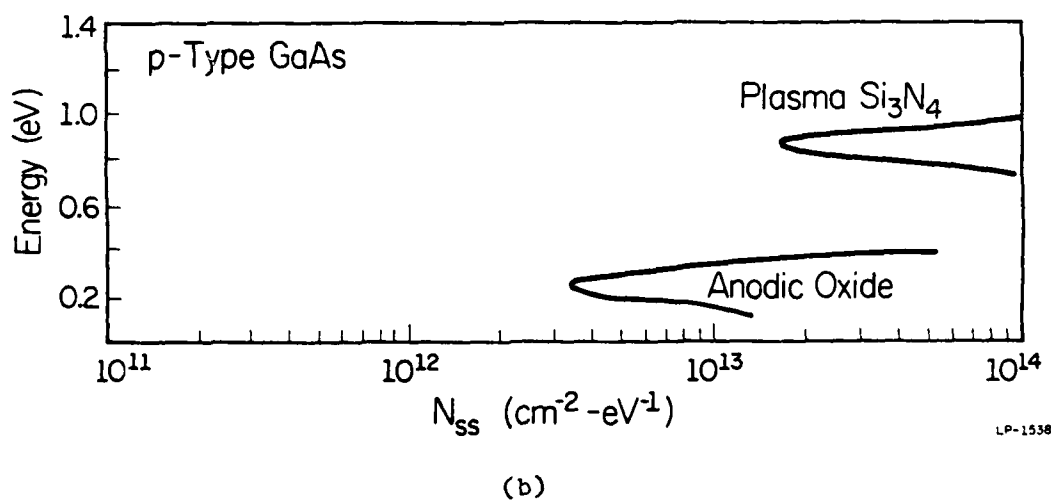
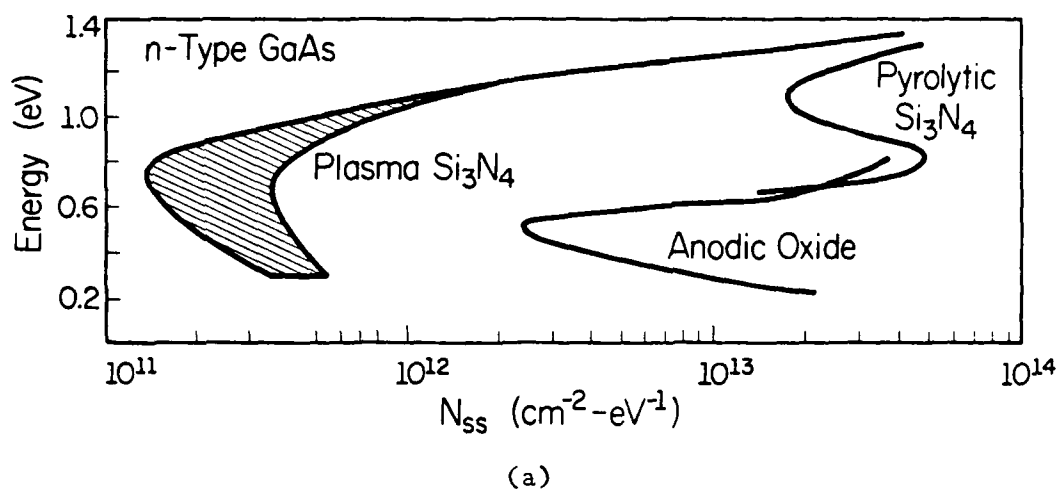


Figure 2.12. Interface state density versus position within the bandgap for various insulators on n-type (a) and p-type (b) GaAs [73].

that the minimum interface state density of the plasma $\text{Si}_3\text{N}_4/\text{GaAs}$ system is approximately $3 \times 10^{11} \text{ cm}^{-2} \text{ eV}^{-1}$, lower than that typical of either the anodic oxide or the pyrolytic Si_3N_4 (Figure 2.12). Other studies [74] have obtained values of $\sim 10^{10} \text{ cm}^{-2} \text{ eV}^{-1}$ near the mid-gap, increasing to $\sim 10^{11} \text{ cm}^{-2} \text{ eV}^{-1}$ towards the conduction band edge.

The results obtained look promising for future work in MIS devices. However, the plasma Si_3N_4 films exhibited significant majority carrier trapping and fixed charge at zero bias, as did the two other types of films studied. Also, the disagreement in N_{ss} between p- and n-type samples is significant and has yet to be resolved.

3. PROPERTIES OF PLANAR P-N JUNCTIONS

In GaAs, the conventional p-type dopant has been Zn. There are, however, problems associated with its rapid diffusion [12,14] which have led to the investigation of alternative acceptors in GaAs. Considerable work has been done using Be as an acceptor [28,75-79]. While Be cannot be introduced conveniently by diffusion, it can be incorporated either by ion implantation or during molecular beam epitaxial growth [80]. Photoluminescence [76] and electrical [81] measurements on Be-implanted layers have shown that this impurity is a shallow acceptor in GaAs with an ionization energy of 28.4 meV.

Since Be is a very light ion, it is ideally suited for fairly deep implantation with less lattice damage than is typical of heavier ions. Studies have been done to investigate the annealing properties of Be-implanted GaAs [28,79,82]. In these studies, photoluminescence has been used to show that Be optical activation and amount of lattice recovery continuously increase as the anneal temperature is increased from 600° to 900°C. This is illustrated in Figure 3.1, where the integrated intensity of the Be-related luminescence band at 1.493 eV is shown for various anneal temperatures.

Effects of high temperature anneals on the Be impurity profiles [82,83] show that while little diffusion occurs for low implant doses, considerable redistribution is observed at high doses. This dependence is summarized in Figure 3.2, where both electrical and atomic (SIMS) profiles are shown for various doses. Diffusion is minimal for the lowest dose of $5 \times 10^{13} \text{ cm}^{-2}$, which corresponds to a peak implanted Be concentration before annealing of $1 \times 10^{18} \text{ cm}^{-3}$. As the dose is increased, the distribution begins to flatten out as Be diffuses toward the surface and deeper into the substrate

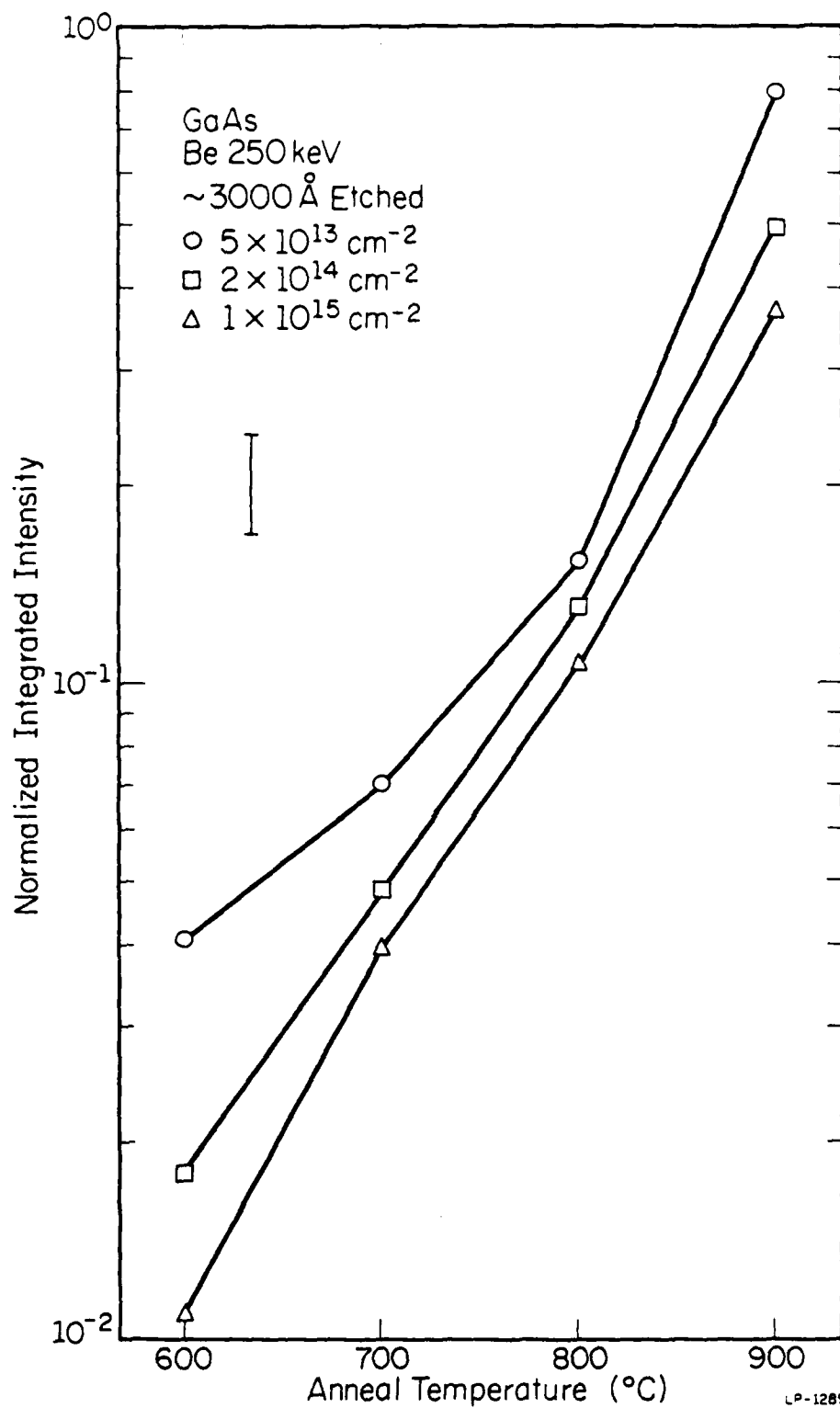


Figure 3.1. Normalized integrated intensity of Be-related luminescence as a function of temperature for $\frac{1}{2}$ hr. anneals for the doses shown [82].

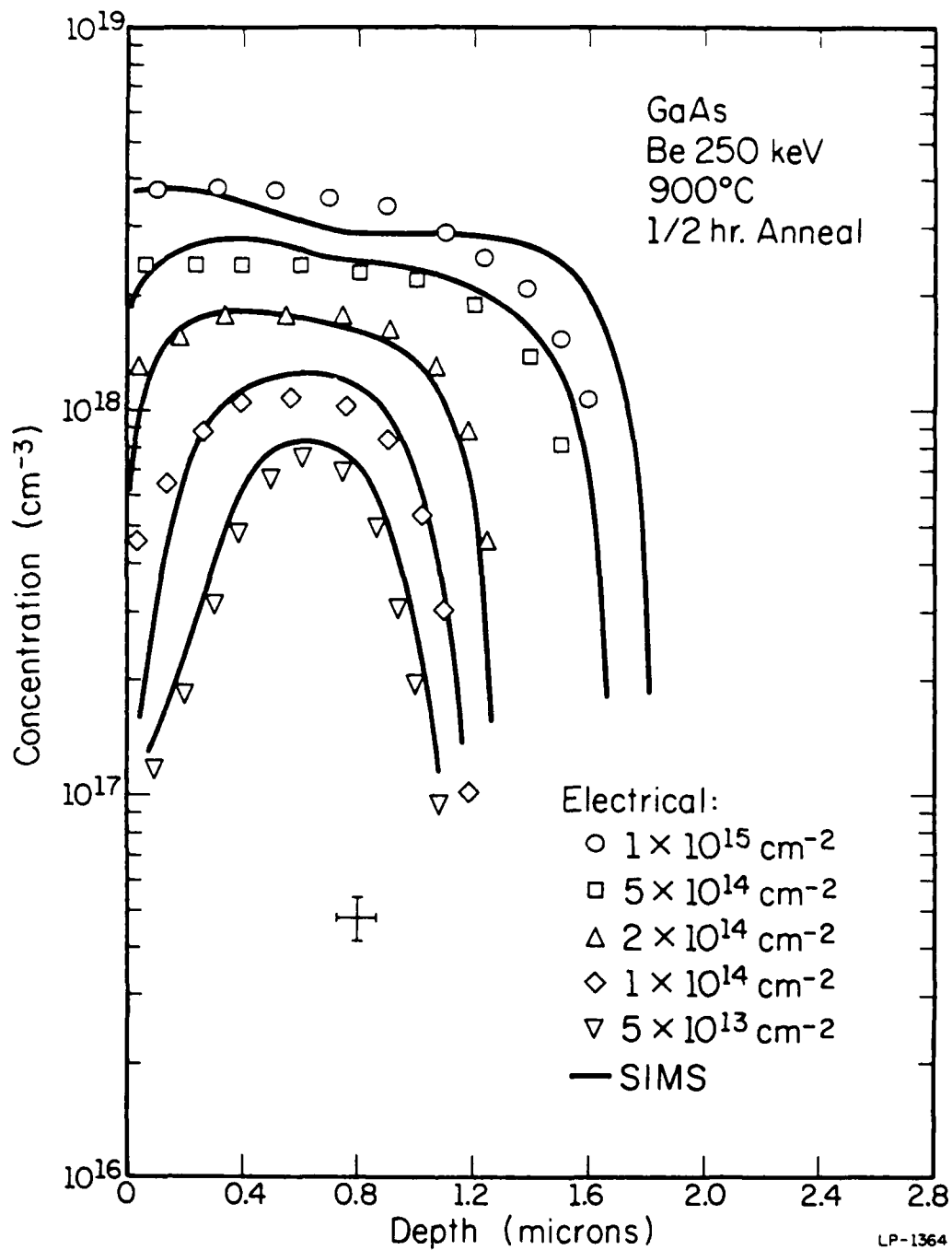


Figure 3.2. Comparison of atomic (SIMS) and net acceptor concentration profiles for the 250 keV Be implants of the indicated doses after an anneal at 900°C for $\frac{1}{2}$ hr. [83].

during the anneal. The three lower doses of 5×10^{13} to 2×10^{14} result in electrical activations of 90-100% of the implanted dose. For higher doses, substantial outdiffusion of Be is observed as well as diffusion into the substrate. The measured electrical activation decreases to 65% of the implanted dose for a $5 \times 10^{14} \text{ cm}^{-2}$ dose and 50% for a $1 \times 10^{15} \text{ cm}^{-2}$ dose. However, the close agreement between the SIMS Be atomic distribution and the electrical data for these doses indicate 85-100% of the Be present after annealing is electrically active. The outdiffusion at the surface is first observed when the Be concentration at the surface reaches $\sim 1 \times 10^{18} \text{ cm}^{-3}$.

It is possible to obtain higher peak concentrations and less diffusion for the higher doses by annealing at lower temperatures. For example, while the peak concentration is $4 \times 10^{18} \text{ cm}^{-3}$ for the dose of $1 \times 10^{15} \text{ cm}^{-2}$ and an anneal at 900°C , a peak concentration of $\sim 1.2 \times 10^{19} \text{ cm}^{-3}$ can be obtained with a 700°C anneal. The electrical activation after such an anneal is 75%, as opposed to 50% after the 900°C anneal. As mentioned above, the low activation of the 900°C anneal is due to the outdiffusion of Be. However, the photoluminescence studies show there is still considerable unannealed lattice damage at the lower anneal temperatures.

The high electrical activation and good lattice recovery of the Be-implanted layers make it an attractive alternative to Zn diffusion. Even though there is considerable diffusion of the Be for high doses after anneals at 900°C , the estimated diffusion coefficient is still approximately two orders of magnitude lower than that for Zn diffused in GaAs at the same temperature [79]. Be-implanted layers have also been shown to have high hole mobilities [79,82], and p-n junctions formed this way have very good characteristics [13,15].

The remainder of this section will deal with the fabrication and

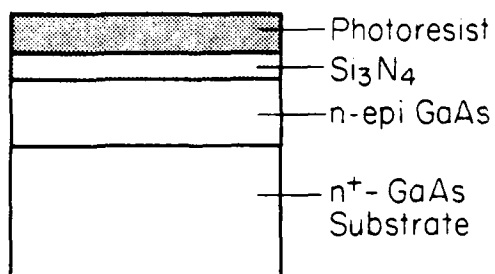
properties of planar p-n junctions formed by Be ion implantation.

3.1. Junction Fabrication

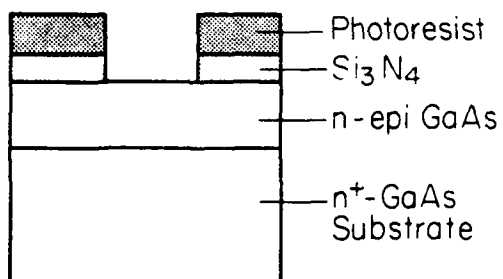
The diodes discussed in sections 3.2-3.4 were fabricated in epitaxially grown n-type GaAs on n^+ substrates. With the exception of some of the diodes in section 3.4, which were grown by liquid phase epitaxy (LPE), all n-type layers were grown by vapor phase epitaxy (VPE).

After cleaning with organic solvents and deionized water, the samples were coated with a dielectric layer 800-1000 \AA thick. The majority of diodes were fabricated using Si_3N_4 deposited in the rf plasma deposition system described in section 2.1, but some were fabricated using SiO_2 for comparison. Next, to define the areas to be implanted, a thick (4-6 μm) layer of AZ1350J photoresist was deposited using multiple spinning applications with intermediate baking at 80°C. (A schematic cross section of the sample at this point and others in the fabrication procedure is shown in Figure 3.3) Then, 10 mil diameter circular areas were opened in the photoresist using standard photolithographic techniques, and the dielectric layer in these circular areas was etched away. For the diodes discussed in sections 3.2 and 3.3, the dielectric layers were etched using a buffered etch consisting of five parts of 40% NH_4F solution and one part HF. The diodes in section 3.4 were fabricated using a CF_4 (Freon-14) plasma to etch the Si_3N_4 layers. Characteristics of diodes formed by these two methods had similar characteristics; however, the yield of good devices was considerably higher when the CF_4 plasma was used. In addition, since the times necessary to etch through the Si_3N_4 layers with buffered HF were quite long (20-45 min.), problems with the photoresist lifting off were often encountered. Therefore, use of the CF_4 plasma was much preferred.

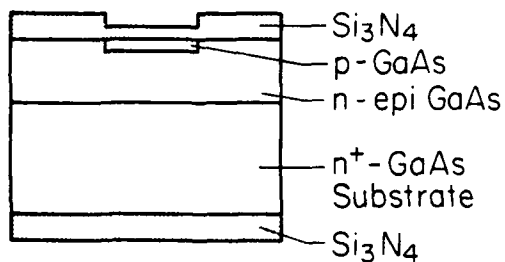
After the holes were opened in the dielectric layer, Be implantation



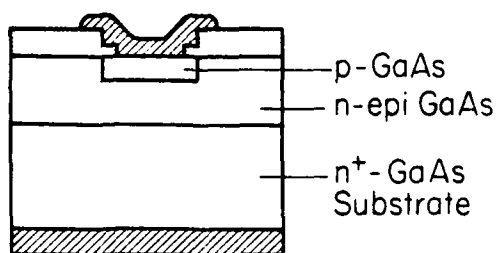
Encapsulate sample with Si₃N₄ and apply photoresist.



Expose PR with a suitable mask, develop and open windows in Si₃N₄.
Ion implant Be or Zn.



Strip photoresist, encapsulate with Si₃N₄ and anneal.



Open contact windows, evaporate and define Ag-Mn for top contact and Ag-Sn for back contact.

LS-1380

Figure 3.3. Schematic cross section of planar diodes at various points in fabrication procedure. Au-Zn and Au-Sn were sometimes substituted for Ag based contacts.

was performed with the thick photoresist layer serving as a mask. For most of the work, the p-type layers were formed by Be-implanted at 250 keV to a dose of $1 \times 10^{14} \text{ cm}^{-2}$ or $1 \times 10^{15} \text{ cm}^{-2}$. Some Zn implants and diffusions were also performed to compare the characteristics. The Zn diffusions were carried out in a sealed ampoule with a ZnAs_2 source at 800°C for 15 min. The photoresist was removed before such diffusions.

The photoresist was removed after the implantation and an $\sim 1000\text{\AA}$ layer of a dielectric was deposited on both the front and back of the samples. This layer together with the original dielectric layer serve as the encapsulant to protect the GaAs during the anneal. The samples were annealed for 30 min. at 800° or 900°C in flowing forming gas (4% H_2 in N_2). After annealing, the dielectric was removed from the back of the wafer and from 5 mil circular areas on the front. These 5 mil areas were defined using photolithography within the 10 mil implanted regions. As before, either a buffered HF etch or CF_4 plasma was used to remove the dielectric layers.

Ohmic contacts were formed to the n^+ backside, using either evaporated Ag-Sn or Au-Sn, or electroplated Au-Sn. Contacts to the p^+ regions were made by evaporating Ag-Mn or Au-Zn, or electroplating Au-Zn. All methods used yielded good ohmic contacts, but the Ag based contacts, while easier to evaporate, were prone to oxidation and more rapid degradation. Some problems were also encountered evaporating the Au-Zn because of the extreme difference in vapor pressures. All contacts were annealed in flowing H_2 . The Ag contacts were annealed at 330° - 350°C for ~ 1 min., and the Au contacts were annealed at 360° - 400°C for similar times.

Most of the device testing was done while the diodes were on the wafer, but for some tests the diodes were cleaved apart and mounted on T0-18 headers. Some of the electrical and optical properties of these diodes will

presented in the following sections.

3.2. Comparison of Be-Implanted, Zn-Implanted, and Zn-Diffused Planar Diodes

To investigate the quality of planar Be-implanted junctions, we have used the procedure described in the preceding section to fabricate planar p-n junctions by Be implantation, Zn implantation, and Zn diffusion. These diodes were fabricated in VPE n-type GaAs grown on n⁺ substrate material. The donor concentration of the n-type layer was $\sim 2 \times 10^{16} \text{ cm}^{-3}$. The ion implantation was performed at room temperature for both the Be and Zn implants. The Be implants were done at 250 keV to a dose of $1 \times 10^{15} \text{ cm}^{-2}$, and the Zn implants were done at 100 keV to a dose of $1 \times 10^{15} \text{ cm}^{-2}$. For both dopants rf plasma deposited Si_3N_4 was used as the encapsulant for the post implantation anneal. The samples were all annealed at 900°C for 30 min. Ag-Mn and Ag-Sn were used to contact the p and n regions respectively.

The Zn diffusions were carried out in a sealed evacuated silica ampoule with a ZnAs_2 source. Silicon nitride was used as the diffusion mask during the 15 min. diffusion at 800°C.

Figure 3.4 shows typical current-voltage characteristics obtained from point-by-point measurements made on Be-implanted junctions. The forward characteristics can be described by

$$I_f = I_o \exp(qV/nkT) \quad (3.1)$$

where the ideality factor $n=2$ and $I_o \approx 10^{-12} \text{ A}$. As seen from the figure, the reverse leakage current is less than $\sim 10^{-10} \text{ A}$ for reverse bias voltages up to -60V. The breakdown is abrupt at -68V. This breakdown voltage is comparable to those reported by Miller and Casey [84] for junctions grown by LPE on n-GaAs with similar doping levels. Leakage currents from other Be-implanted devices in this material ranged from $< 0.1 \text{ nA}$ to $\sim 1 \text{ nA}$. The Be

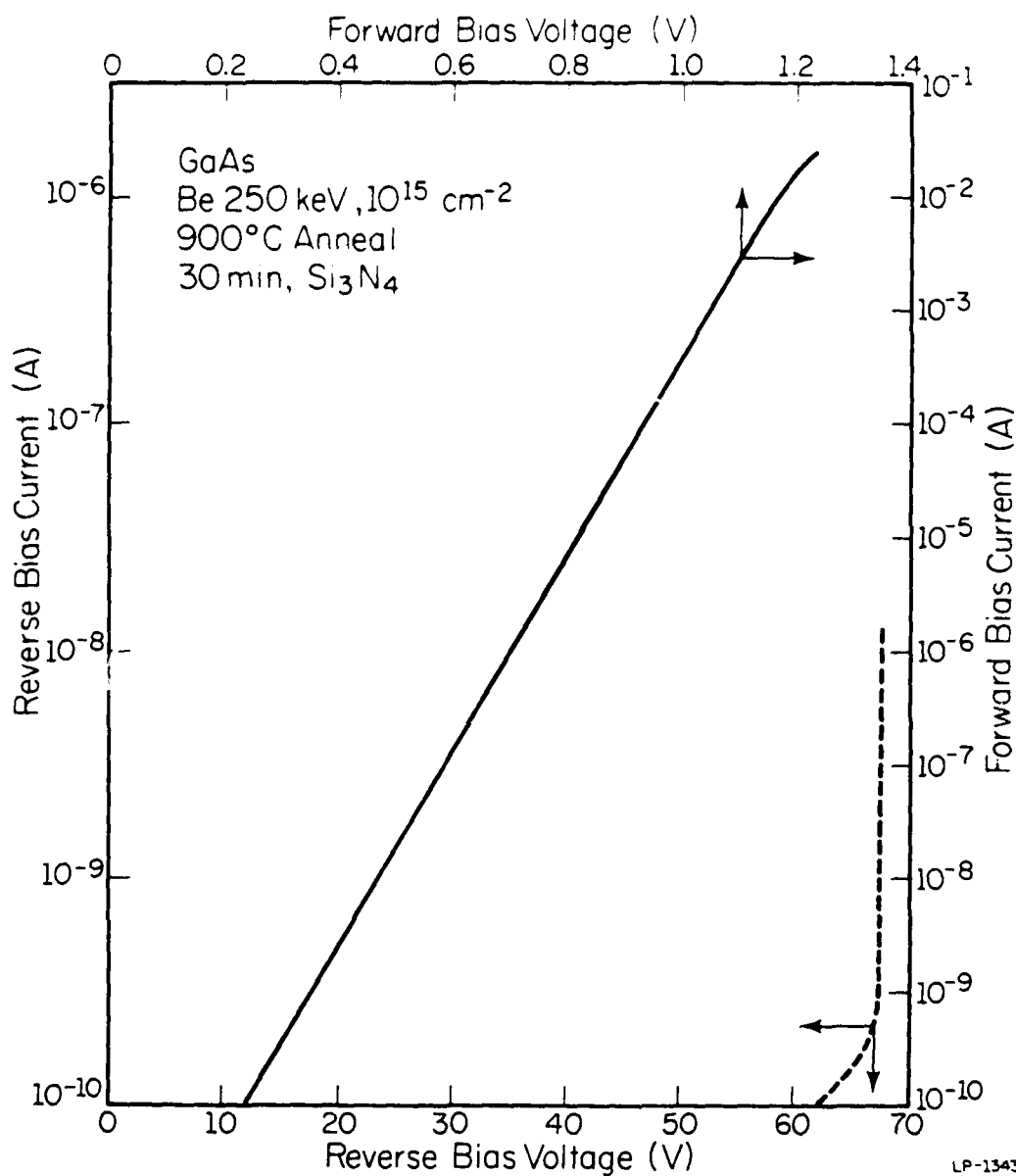


Figure 3.4. Typical I-V characteristics of planar Be-implanted junctions in GaAs. The implant was performed at 250 keV to a dose of 10^{15} cm^{-2} . Samples were annealed at 900°C for $\frac{1}{2}$ hr. [13].

impurity profile for the junction of Figure 3.4 is expected to be essentially flat at $4 \times 10^{18} \text{ cm}^{-3}$, with an abrupt junction at $\sim 1.8 \mu\text{m}$ [82].

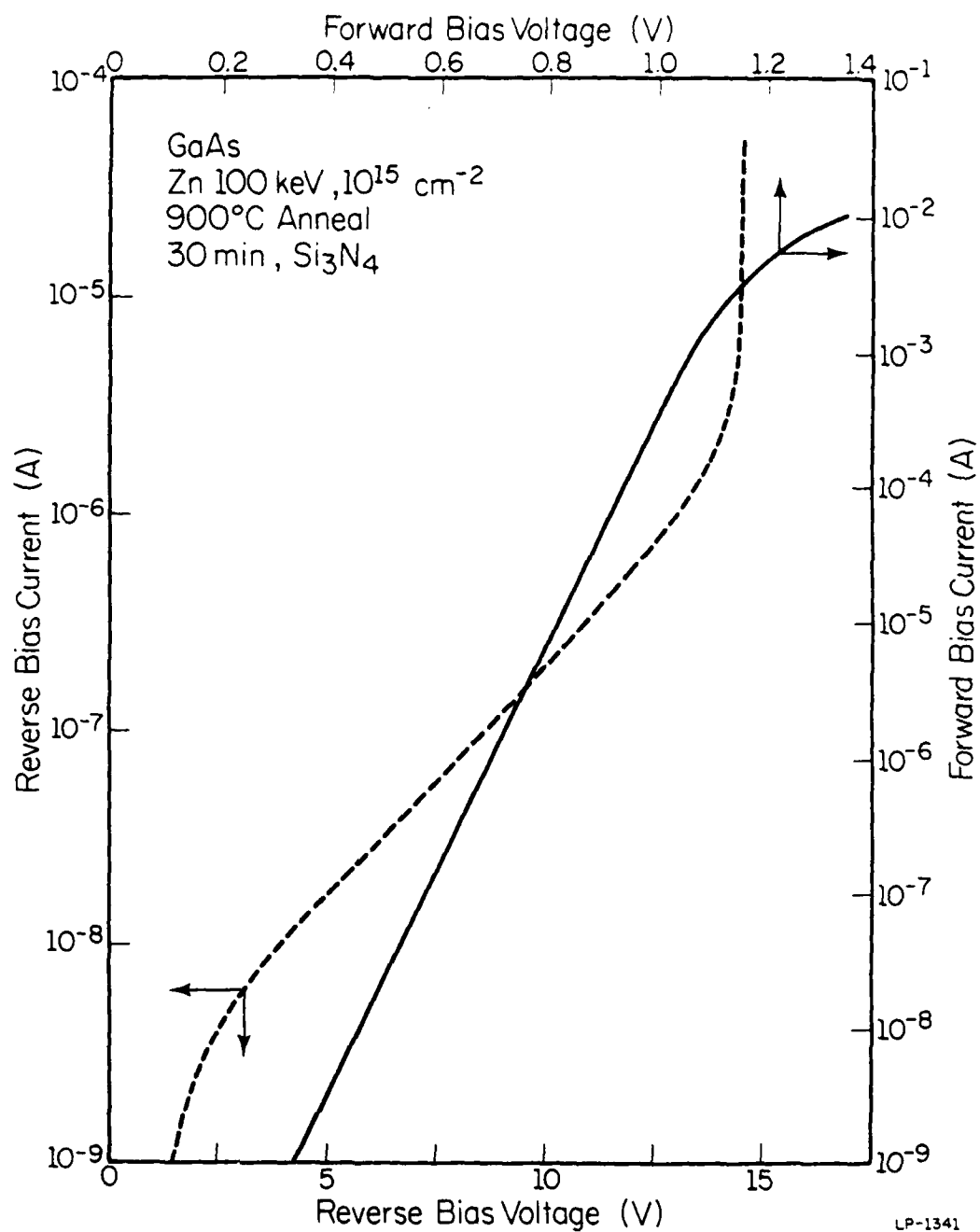
For comparison with the Be-implanted junctions, typical I-V characteristics obtained from Zn-implanted p-n junctions are shown in Figure 3.5. The forward characteristics ($n \sim 1.9$) are similar to the Be-implanted devices. The reverse characteristics, however, are considerably different. The reverse leakage current is excessively high, $\sim 10^{-7} \text{ A}$ at only -10 V . The breakdown voltage is quite low ($\sim 12 \text{ V}$) and relatively soft. While the implant was shallower for the Zn-implanted diodes, the junction depth is actually slightly deeper than that of the Be-implanted junctions because of the much higher diffusion coefficient of Zn at the annealing temperature.

A typical I-V characteristic of a Zn-diffused device is shown in Figure 3.6. The forward characteristics differ somewhat from the implanted diodes, with $n \sim 1.4$. The reverse leakage current is considerably lower than the Zn-implanted devices, but not quite as low as the Be-implanted diodes. The reverse breakdown voltage ($\sim 25 \text{ V}$) is, however, considerably lower than for the Be-implanted diodes.

It is clear that the I-V characteristics of the Be-implanted junctions are far superior to those of the Zn-implanted junctions or the Zn-diffused junctions.

3.3. Effects of the Encapsulant on Planar Be-Implanted Junctions

To study the effects of different encapsulants on the current-voltage characteristics of planar GaAs diodes, devices were fabricated using SiO_2 , oxygen-contaminated silicon nitride ($\text{Si}_x\text{O}_y\text{N}_z$), or "oxygen-free" Si_3N_4 as the encapsulant during the post implantation anneal. As discussed in section 2.2, both SiO_2 and $\text{Si}_x\text{O}_y\text{N}_z$ allow Ga outdiffusion, while "oxygen-free" Si_3N_4 layers do not. The effect of this on the I-V characteristics of planar



LP-1341

Figure 3.5. Typical I-V characteristics of planar Zn-implanted GaAs diode. Implantation was performed at 100 keV to a dose of 10^{15} cm^{-2} . Anneal was at 900°C for $\frac{1}{2}$ hr. [13].

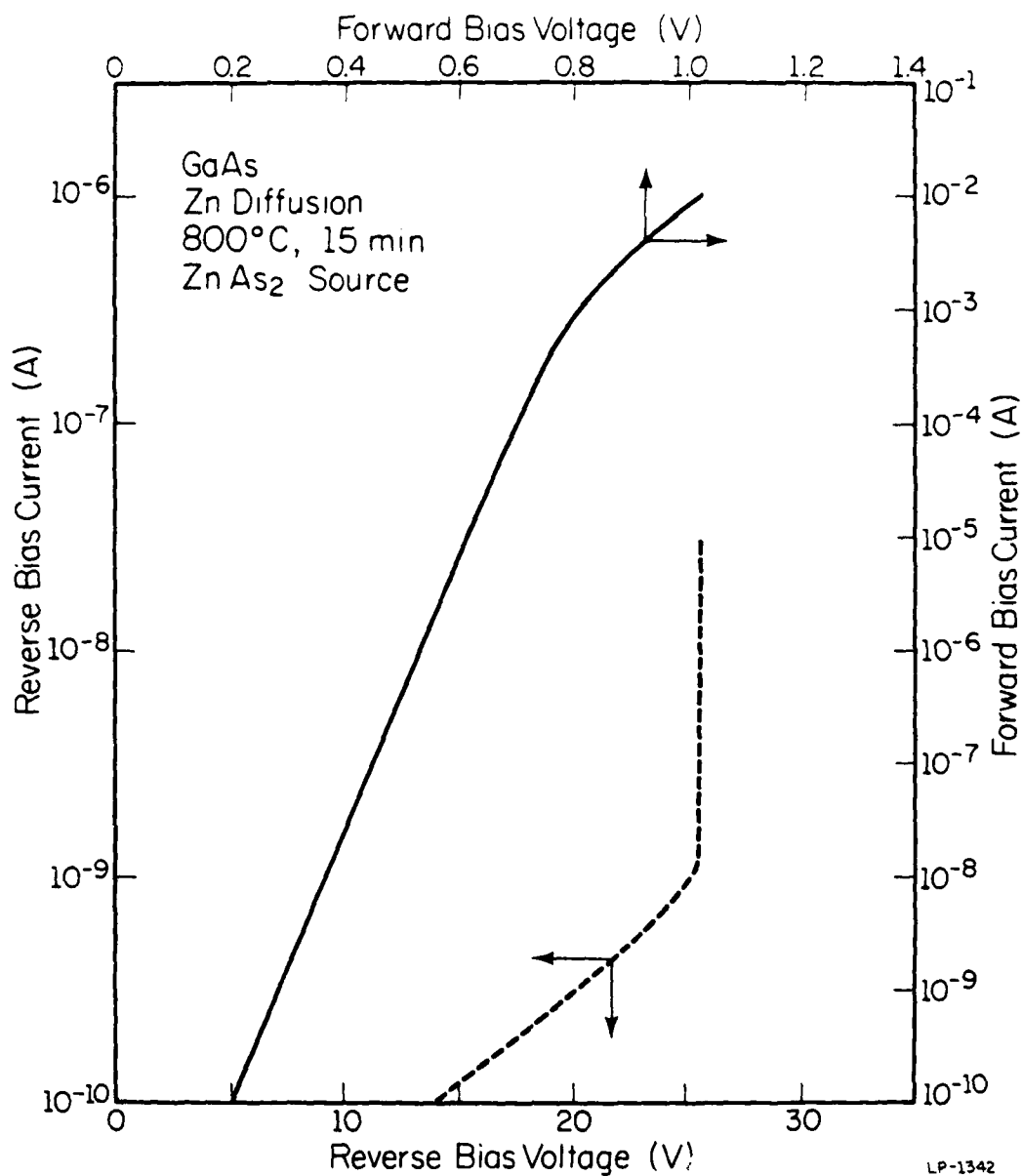


Figure 3.6. Typical I-V characteristic of Zn-diffused diode in GaAs. The Zn diffusion was carried out in a sealed ampoule with a ZnAs₂ source at 800°C for 15 min. [13].

GaAs diodes is examined in this section.

All diodes for this work were fabricated in VPE grown n-type GaAs with a donor concentration of $1-2 \times 10^{15} \text{ cm}^{-3}$. The epitaxial layers were grown on n^+ GaAs substrates. The fabrication procedure discussed in section 3.1 was employed with the three different dielectrics used as the encapsulants. All samples were implanted with Be at an energy of 250 keV to a dose of $1 \times 10^{14} \text{ cm}^{-2}$. The anneals were all carried out at 900°C for 30 min. in flowing forming gas. The contacts used for these diodes were Ag-Mn for the p-type regions and Ag-Sn for the n^+ backside.

Typical I-V characteristics obtained from Be-implanted junctions annealed with SiO_2 encapsulation are illustrated in Figure 3.7. The reverse leakage current is quite high, and these diodes exhibit relatively soft breakdown characteristics. The voltage at breakdown is $\sim 55\text{V}$, which is low for the lightly doped epitaxial layer. The forward characteristic is highly nonlinear on the semilog plot of Figure 3.7 and cannot be described by the usual diode equation. The inset in this figure shows the forward I-V characteristic on a log-log plot, with a slope of unity for low values of current. This linear I-V relationship indicates an ohmic leakage component of current, which is also present in reverse bias.

Figure 3.8 shows typical current-voltage characteristics obtained from Be-implanted junctions annealed with $\text{Si}_x\text{O}_y\text{N}_z$ encapsulation. The presence and effects of oxygen in these films have been discussed in section 2.2. Such films can easily be deposited inadvertently unless great care is taken to eliminate oxygen from the deposition system [48]. The reverse leakage current for these diodes is at least an order of magnitude lower than those shown in Figure 3.7, which were annealed with SiO_2 encapsulation. However, the leakage current is still quite high, and there is an ohmic component

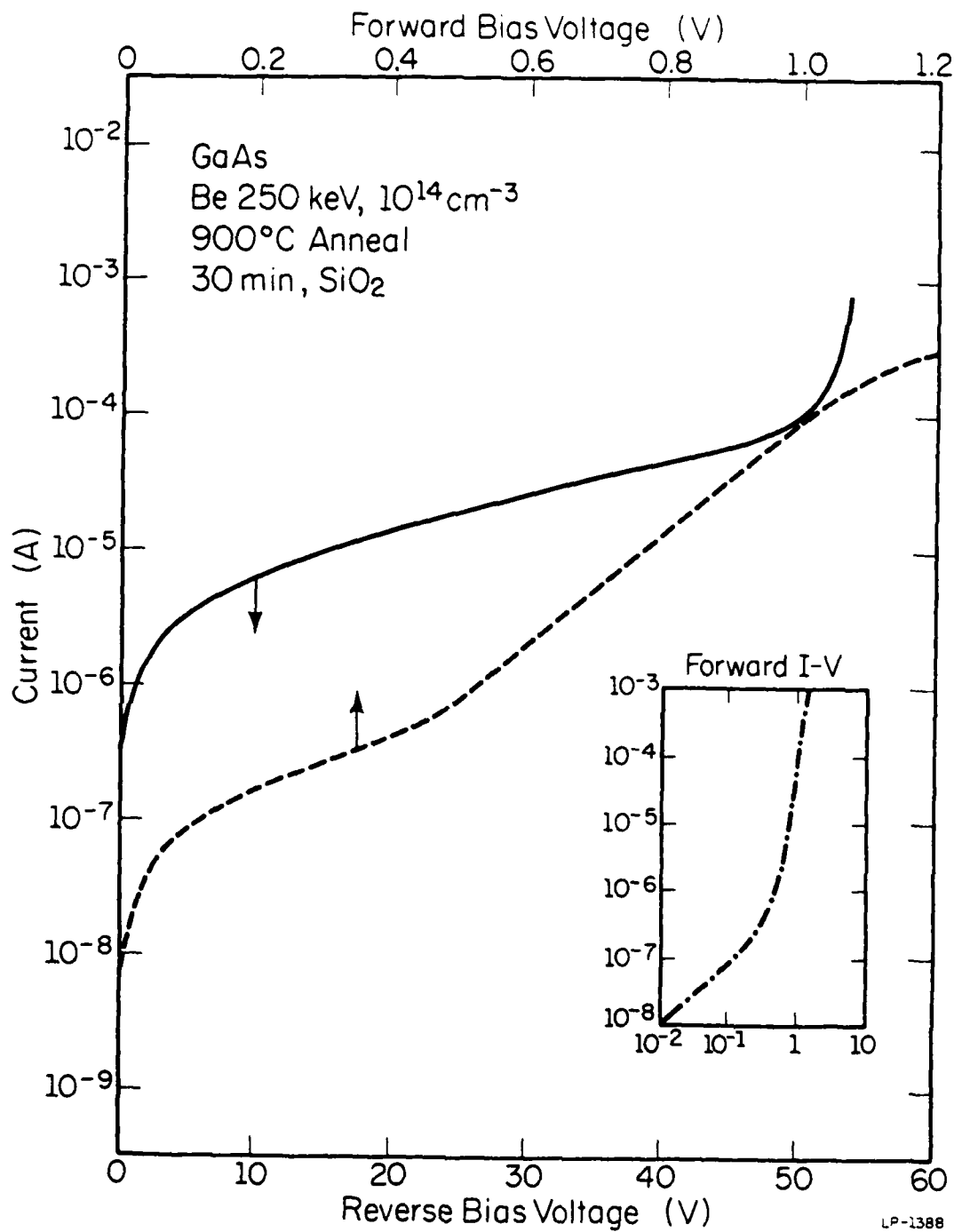


Figure 3.7. I-V characteristics of a typical planar Be-implanted p-n junction annealed with SiO₂ encapsulation. The inset shows the forward characteristics on a log-log plot [15].

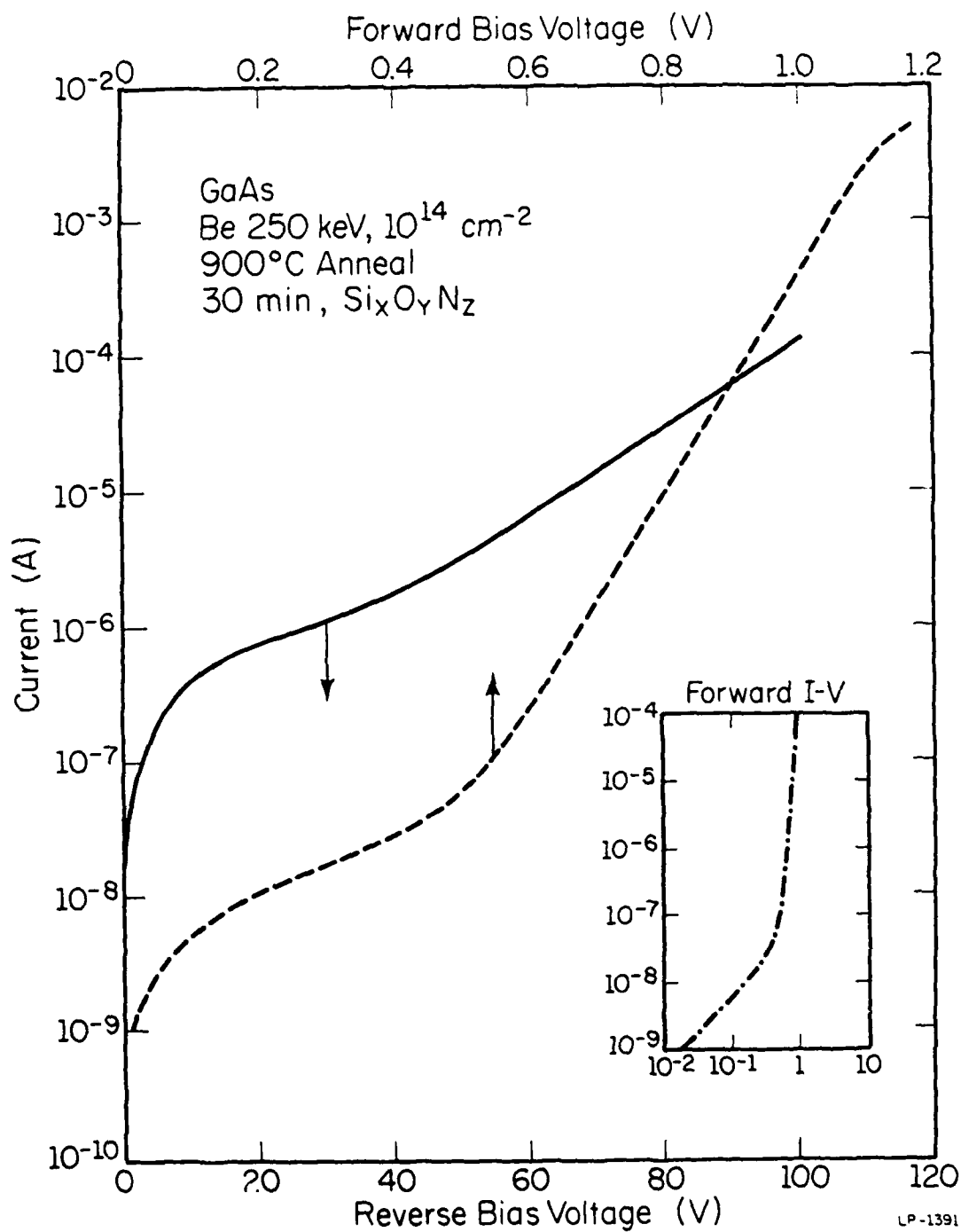


Figure 3.8. I-V characteristic of a planar Be-implanted junction annealed with silicon oxy-nitride encapsulation. The inset is a log-log plot of the forward characteristic [15].

evident in both the forward and reverse characteristics. The inset of Figure 3.8 shows this component clearly on a log-log plot of the forward characteristic.

By reducing the oxygen content in the deposition system, high quality Si_3N_4 films which contain less than about one atomic percent oxygen can be deposited [48]. The upgraded system of section 2.1.2 was used to deposit these Si_3N_4 films with approximately stoichiometric composition, as measured by Rutherford backscattering (RBS), and any oxygen contamination is below the ~ 1 atomic percent RBS detection limit. Current-voltage characteristics obtained from a junction which was encapsulated with such Si_3N_4 films during annealing are shown in Figure 3.9. The leakage current is orders of magnitude lower than for the other encapsulants. Up to a reverse bias of $\sim 80\text{V}$ the leakage current is less than 10^{-10}A . The breakdown occurs at a voltage of $\sim 240\text{V}$. The forward characteristics can be expressed by the conventional diode equation given in equation 3.1 where $n \approx 2$ for $I_f \leq 10^{-9}\text{A}$ and $n \approx 1.6$ for $I_f > 10^{-9}\text{A}$. The reverse leakage and breakdown properties are very good for unguarded planar diodes. The breakdown may actually be occurring as the depletion region reaches the n^+ substrate. For a background doping of $2 \times 10^{15}\text{cm}^{-3}$ and a reverse bias of 240V , the depletion width is approximately $13\mu\text{m}$. The thickness of the epitaxial layer is $12\text{--}15\mu\text{m}$. Measurements performed on ~ 50 such diodes reveal a distribution of breakdown voltages over the range of $170\text{--}250\text{V}$. The inset of Figure 3.9 shows the predicted carrier profile from previous studies [82].

The results of this study clearly demonstrate that when dielectric layers which allow considerable outdiffusion of Ga, such as SiO_2 and $\text{Si}_x\text{O}_y\text{N}_z$ [29], are used as encapsulants during annealing, the resultant Be-implanted GaAs p-n junctions exhibit excessively high leakage currents. By

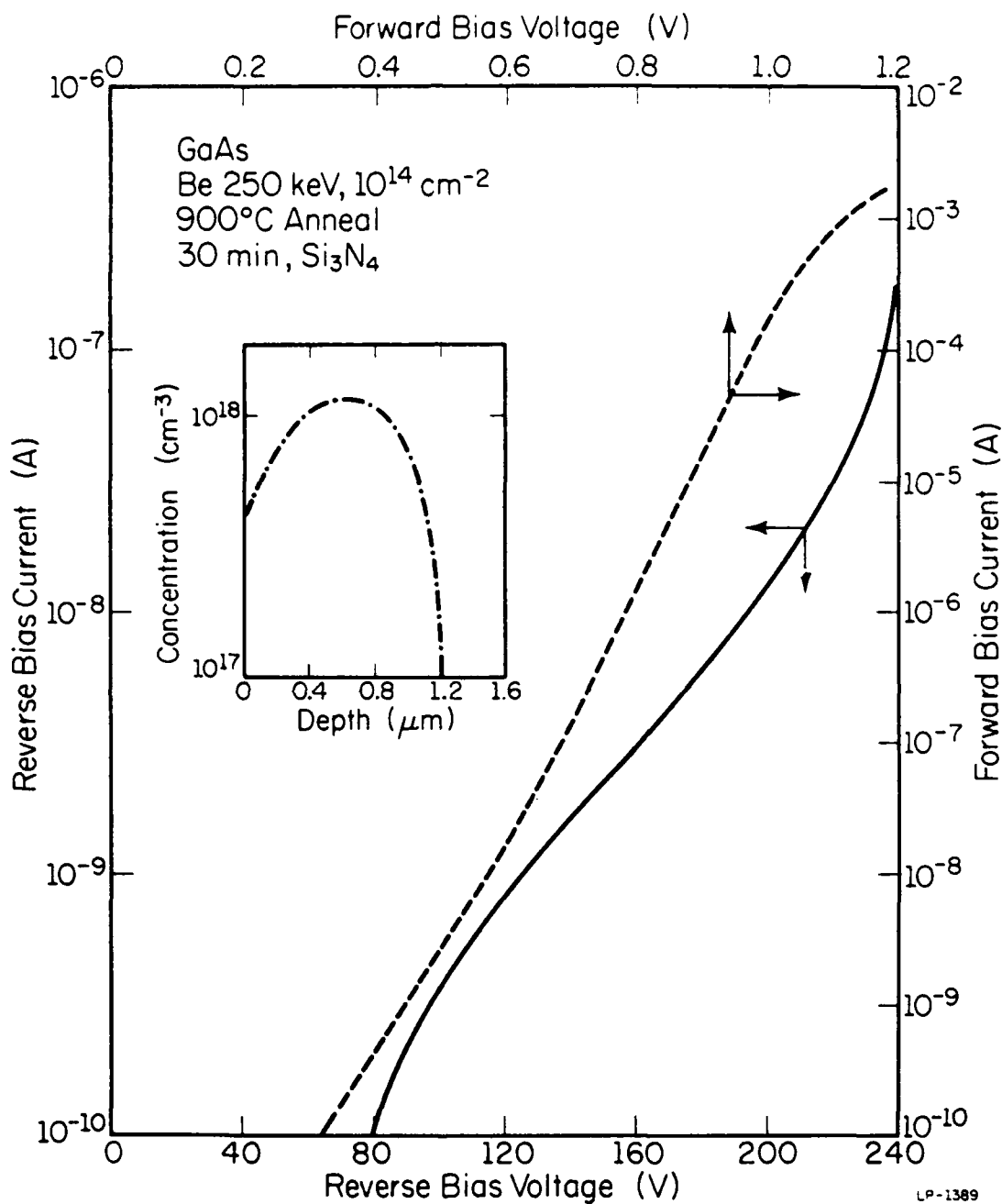


Figure 3.9. Typical I-V characteristics for an unguarded planar Be-implanted junction annealed with Si_3N_4 encapsulation. Inset shows the impurity profile as measured by differential Hall effect and chemical stripping method [15,82].

minimizing such outdiffusion through the use of high quality Si_3N_4 layers, extremely low leakage junctions with good breakdown characteristics can be fabricated.

3.4. Planar Be-Implanted Avalanche Photodiodes

Using the fabrication procedure of section 3.1, planar p-n junctions were formed in two types of GaAs material, and the performance of these junctions as photodiodes was investigated. Both types of GaAs material used were n on n^+ epitaxial material, one grown by liquid phase epitaxy (LPE) and the other by vapor phase epitaxy (VPE). The LPE material had a uniform carrier concentration of $\sim 2 \times 10^{15} \text{ cm}^{-3}$, and the background carrier concentration of the VPE material was $\sim 8 \times 10^{14} \text{ cm}^{-3}$. The Be implants were done at an energy of 250 keV to a dose of $1 \times 10^{14} \text{ cm}^{-2}$. These conditions result in a peak net carrier concentration of $1 \times 10^{18} \text{ cm}^{-3}$ and a junction depth of $\sim 1.2 \mu\text{m}$ [82]. For this study, all anneals were carried out at 800°C for 30 min. The contacts were formed by electroplating Au-Zn and Au-Sn to the p and n regions respectively and then alloying in a H_2 atmosphere. Electrical and optical measurements on these diodes were done in cooperation with Professor G. E. Stillman and R. A. Milano of the University of Illinois.

3.4.1. Electrical Characteristics

The reverse I-V characteristics of diodes fabricated from the two types of epitaxial material are shown in Figures 3.10 and 3.11. The lower curve in Figure 3.10 is representative of devices fabricated in the LPE material. The upper curve represents one type of characteristic observed for devices in VPE material. Other types of characteristics for devices in VPE material with lower values of leakage current are shown in Figure 3.11. For reverse bias voltages less than $\sim 100\text{V}$, the shapes of the curves in

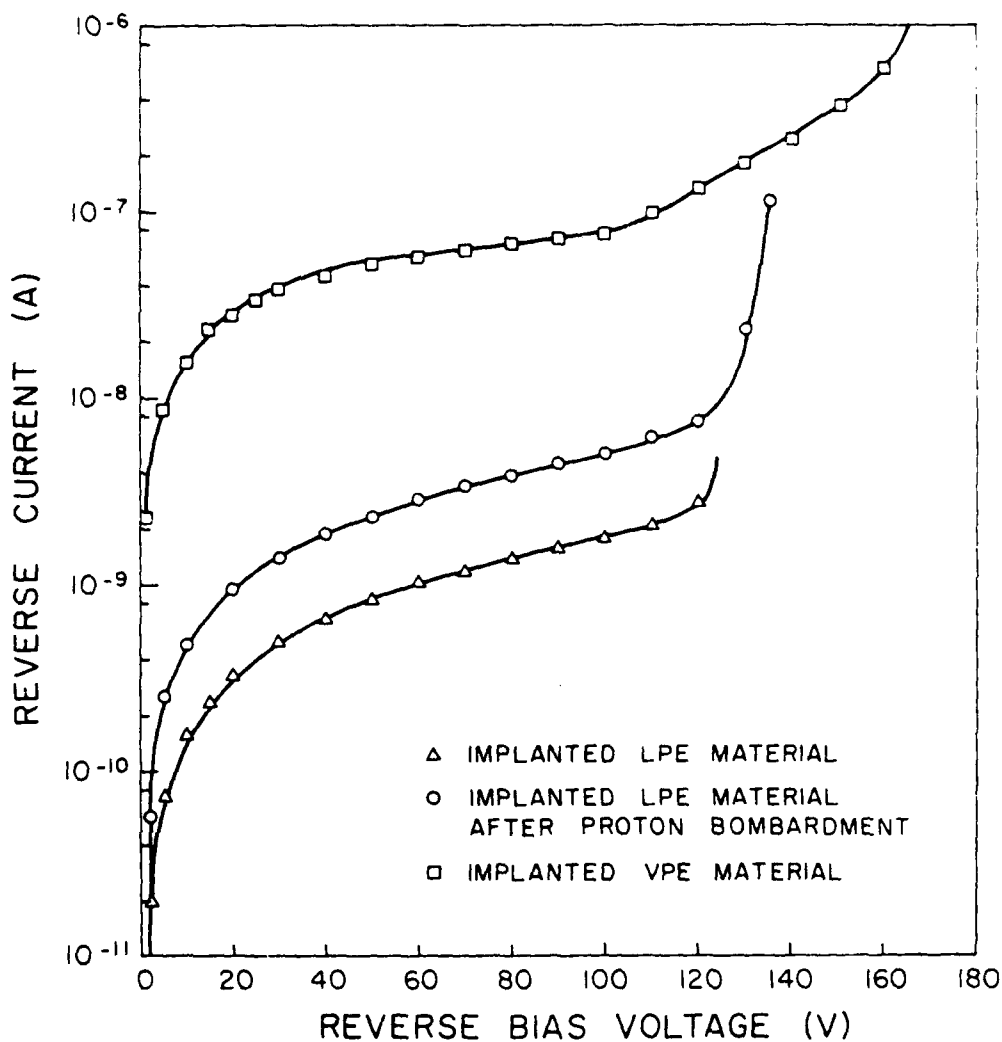


Figure 3.10. Reverse I-V characteristics of Be-implanted GaAs photo-diodes. \square Implanted VPE material; \circ implanted LPE material after proton bombardment; \triangle implanted LPE material. All implants were at 250 keV to a dose of 10^{14} cm^{-2} . Anneals were for $\frac{1}{2}$ hr. at 800°C with Si_3N_4 encapsulation [16].

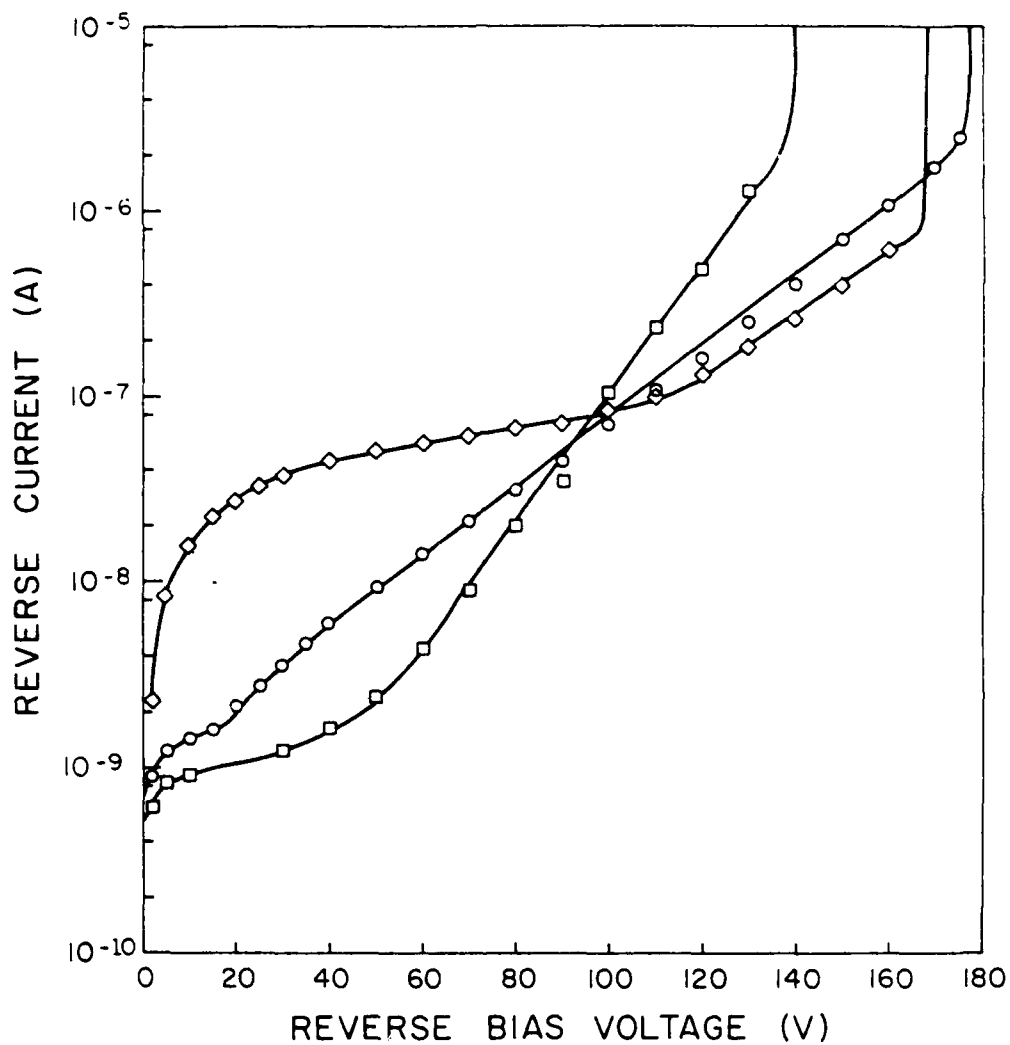


Figure 3.11. Reverse I-V characteristics of three different Be-implanted VPE GaAs photodiodes. Implants were at 250 keV to a dose of 10^{14} cm^{-2} . Anneals were at 800°C for $\frac{1}{2}$ hr. with Si_3N_4 encapsulation [16].

Figure 3.10 are very similar. However, the magnitude of the leakage current for the devices on the VPE material is more than an order of magnitude higher than for the devices on the LPE material. There is also a significant difference in the shape of the I-V characteristic of the VPE device for reverse bias voltages greater than $\sim 100V$. Such changes occurring at different voltages on different devices were commonly observed in the implanted VPE junctions.

Also shown in Figure 3.10 is the reverse I-V characteristic for the same LPE diode after a proton-bombarded [85] high-resistance guard ring was fabricated around the device. The guard ring was formed by masking a circular region about 8 mil in diameter located within the implanted region with thick photoresist. The device then received two damaging implant, first a $2 \times 10^{14} \text{ cm}^{-2}$ dose of 250 keV protons and then a $5 \times 10^{13} \text{ cm}^{-2}$ dose of 150 keV protons. This guarding procedure increased the breakdown voltage only slightly (from about 124V to about 136V). It also caused a slight increase in the leakage current, but no significant change in the shape of the curve. Such an increase in leakage current has also been observed after the formation of proton-bombarded guard rings on Schottky-barrier devices. Presumably the increased leakage current results from the collection of carriers generated in the depleted high-resistivity bombarded material. It should be mentioned, however, that no attempt was made to optimize the proton bombardment procedure in this work.

Reverse I-V characteristics for diffused GaAs devices have generally been ascribed to generation current in the depletion region [86-88]. However, this mechanism should result in a reverse current proportional to $V^{\frac{1}{2}}$. None of the diodes studied exhibited this behavior.

An examination of Figures 3.10 and 3.11 indicates that a difference exists between the functional form of the reverse I-V characteristics for

the diodes fabricated from LPE and VPE material. At very low biases (0 to -10V) all of the devices have an ohmic component of leakage current. Near breakdown, the current increases very rapidly due to the rapid increase in multiplication with small changes in bias. For intermediate bias voltages, however, the leakage current for the LPE diodes varies as $I \propto V^a$, where $a \approx 1$, while the diodes in the VPE material are described over some part of their range by an exponential variation of current with voltage, $I \propto e^{\mu V}$.

Figure 3.12 is a log-log plot of the reverse I-V characteristics of three Be-implanted LPE GaAs diodes for reverse bias voltages between 10 and 100V. This plot clearly shows the form $I \propto V^a$. The two lower curves represent data taken on the three diodes before guard rings were formed. The lower curve is best described by a straight line with unity slope, while the middle curve has a slope of ~ 0.7 . After proton bombardment, the data for all three devices can be described by a line of unity slope, as shown by the uppermost curve in Figure 3.12. The reason for the existence of this ohmic type of characteristic is not understood, although it may be related to bulk and surface leakage paths in shunt with the device.

Figure 3.11 is a semi-logarithmic plot of the reverse I-V characteristics for three Be-implanted VPE GaAs diodes. All of the devices show an exponential dependence over a portion of the range of bias voltages. In particular, two of the devices have a very small ohmic component and exhibit an essentially exponential dependence over almost the entire range of bias voltages. Behavior similar to this was seen in the work of section 3.3. A similar exponential increase of reverse current with voltage was observed in early work on diffused GaAs p-n junctions and was attributed to the generation of microplasmas [89]. In the present work, however, there is no indication of the microplasma noise characteristic of this process, and there is

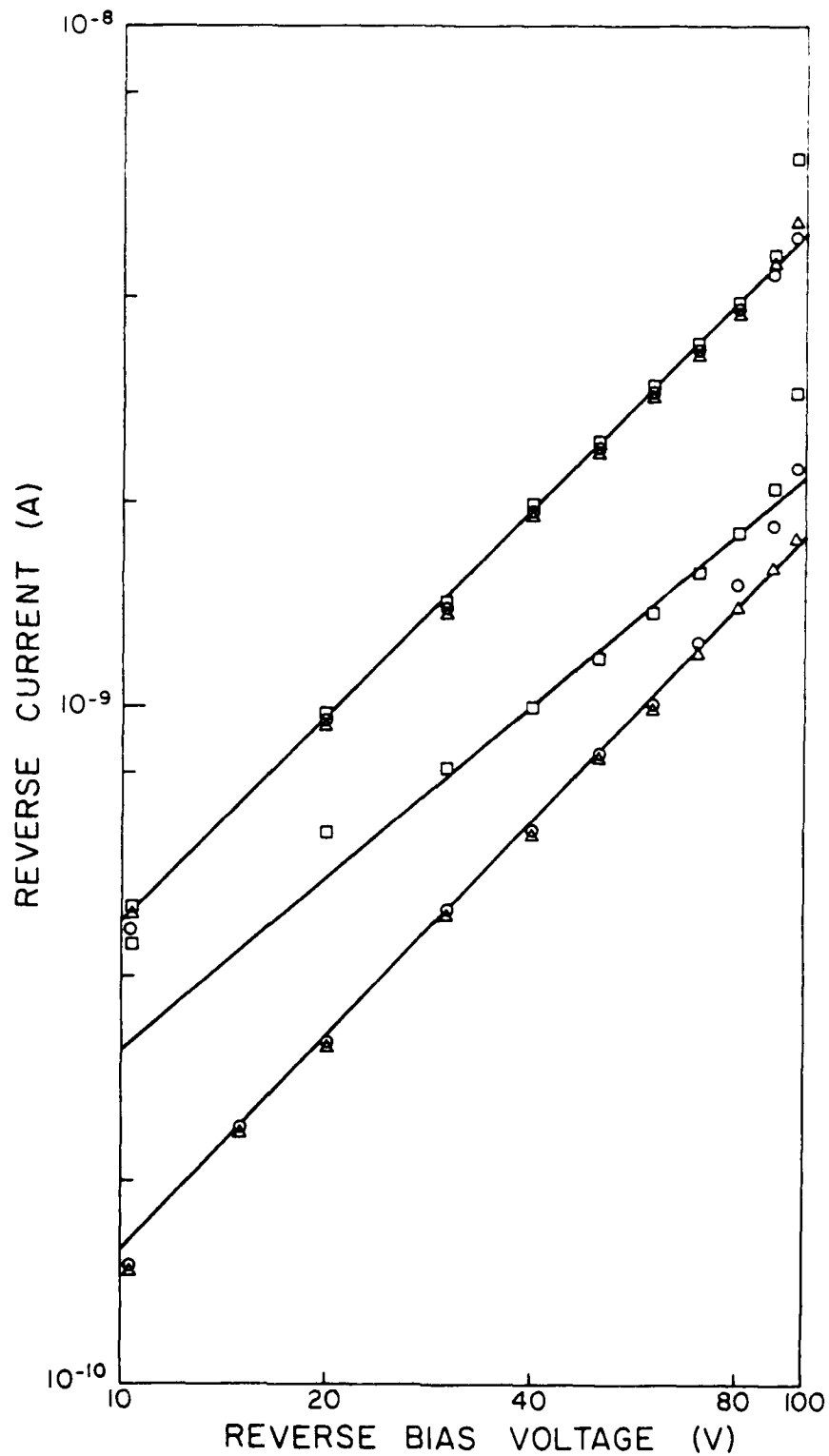


Figure 3.12. Reverse I-V characteristics of three different Be-implanted LPE GaAs photodiodes before (lower curves) and after (upper curve) proton bombardment. Implants were at 250 keV to a dose of 10^{14} cm^{-2} . Anneals were at 800°C for $\frac{1}{2}$ hr. with Si_3N_4 encapsulation [16].

no indication of local areas of high multiplication in optical scans of these devices. It therefore seems unlikely that microplasmas can explain the shape of the I-V characteristics of these VPE diodes. The exponential increase may be due to a voltage-dependent emptying of traps.

The shapes of the reverse I-V characteristics are not understood and need to be studied further. The ohmic component present to some extent on the VPE samples may be related to problems with the encapsulant, as mentioned in section 3.3. The fact that not all devices have the same amount of ohmic leakage may be due to localized problems such as pinholes in the dielectric. The ohmic dependence of the LPE diodes may be caused by some other mechanism, since they all have essentially the same form and magnitude. Also, the magnitude of the leakage is considerably smaller than that of the ohmic components of devices on VPE material.

The exponential dependence of the reverse bias current for the VPE diodes also requires more study. The presence of the exponential dependence seems at least partially related to the epitaxial material. This dependence was not observed in any of the LPE material, nor was it seen in the Be-implanted VPE material discussed in section 3.2. Although it is not shown in Figure 3.4, devices with higher leakage currents (10^{-10} to 2×10^{-9} A) exhibited a saturation of leakage current up to near breakdown and no exponential behavior.

Preliminary studies have shown considerable difference between Schottky-barrier devices formed on this VPE material before and after anneals at 800° and 900° C. While this change may be related to problems with the encapsulating layer, other tests of the Si_3N_4 encapsulant do not indicate such problems.

Some Deep Level Transient Spectroscopy (DLTS) measurements have

been made on Be-implanted diodes in VPE material, but the results are inconclusive at present. There does appear to be a band of traps which may be related to unannealed radiation damage. Photoluminescence studies [28,82] have shown continued improvement as annealing temperature increases, and since these devices were annealed at 800°C , there is undoubtedly some damage remaining. Problems with excessively high leakage currents for devices annealed at 900°C prevented analysis of the higher temperature anneals. Again, this problem may be related to the material and not just the encapsulant, as one might first suspect. Point contact breakdown voltage measurements on this material yield considerably lower breakdown voltages than would be expected for the measured carrier concentration.

Some problems have been encountered with contacts which may suggest some type of barrier affecting the characteristics, but the exponential behavior is also observed in devices showing no signs of contact problems. More work must be done before the nature of the characteristics can be understood.

3.4.2. Optical Characteristics

In order to characterize the (optical) detection properties of these devices, the spectral response, response time of the diode to a pulse from a GaAs DH laser, and the noise were measured. In addition, a laser scanner was used to examine the uniformity of the photoresponse and avalanche gain.

The spectral response of a Be-implanted LPE diode is shown in Figure 3.13 for low (lower curve) and high (upper curve) bias voltages. At low bias the external quantum efficiency is about 75% at 8750\AA , and it decreases rapidly to a value of only about 3% at 6328\AA . The absorption edge shifts to longer wavelengths for high bias voltages due to the Franz-Keldysh

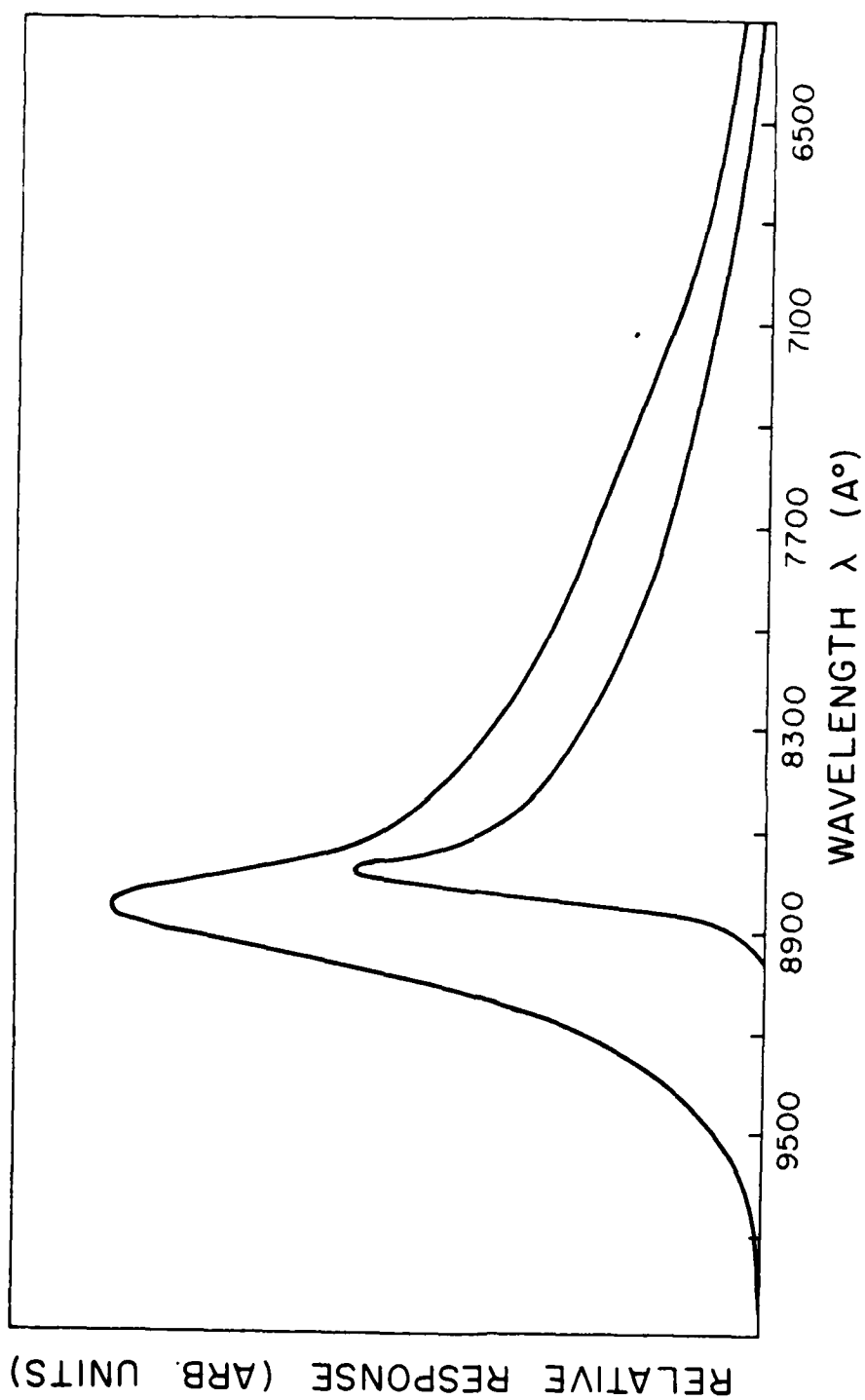


Figure 3.13. Experimental spectral response of Be-implanted LPE GaAs photodiodes biased at -5V (lower curve) and -135V (upper curve) [16].

effect, and the peak response occurs at about 3900Å.

To investigate the reason for the rapid decrease in quantum efficiency at short wavelengths, an expression for the short-circuit current as a function of illumination wavelength for a p^+-n GaAs junction has been derived by Milano [16]. The diffusion equation was solved in the undepleted p^+ and n regions and, including the photocurrent generated in the space charge region, subject to the appropriate boundary conditions. The result [16] is

$$J_{SC} = q\eta I_0 \left(\frac{\alpha L_n}{1 - \alpha^2 L_n^2} \right. \\ \left. \left\{ \frac{[(SL_n/D_n) \cosh(X_1/L_n) + \sinh(X_1/L_n)] \exp(-\alpha X_1) - [\alpha L_n + (SL_n/D_n)]}{\cosh(X_1/L_n) + (SL_n/D_n) \sinh(X_1/L_n)} \right. \right. \\ \left. \left. + \alpha L_n \exp(-\alpha X_1) \right\} - \frac{\alpha L_p \exp(-\alpha X_2)}{1 + \alpha L_p} - [\exp(-\alpha X_1) - \exp(-\alpha X_2)] \right) \quad (3.2)$$

where η is the quantum efficiency, I_0 is the incident photon flux, X_1 is the junction depth, $X_2 - X_1$ is the depletion layer width, and the other symbols have their usual meanings. In deriving this equation, recombination in the depletion region and at the layer-substrate interface was neglected, but front surface recombination was taken into account by the surface recombination velocity S .

The experimental data (broken curve) and spectral response curves (solid curves) calculated using equation 3.2 for $S=10^3$ cm/sec. and $S=10^6$ cm/sec. over a range of photon energies from 1.41 to 2.1 eV are shown in Figure 3.14. The value of X_1 (1.2μm) is consistent with measured impurity profiles [82] for the implant procedure employed here; the $X_2 - X_1$ (3.2μm) corresponds to the depletion layer width measured by C-V analysis. The surface recombination velocity has only a secondary effect on the spectral response in Figure

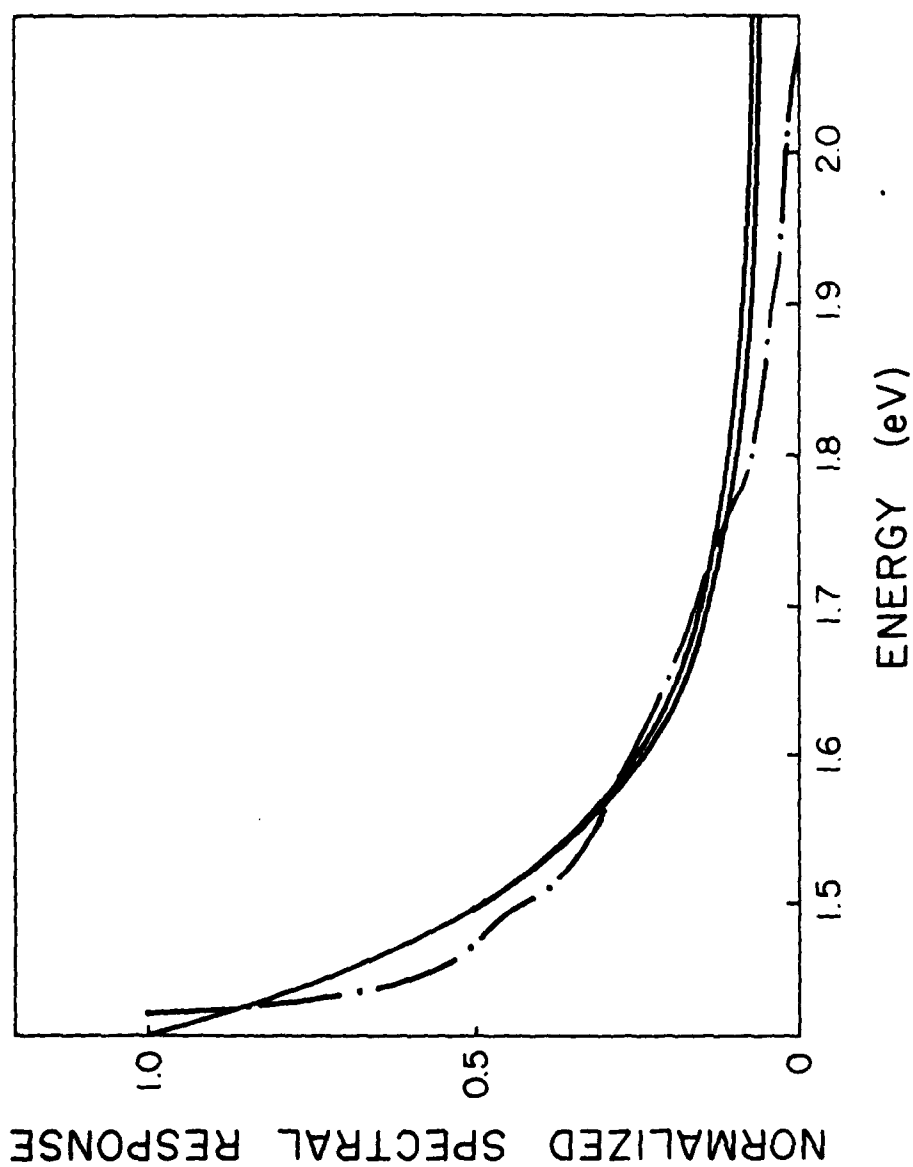
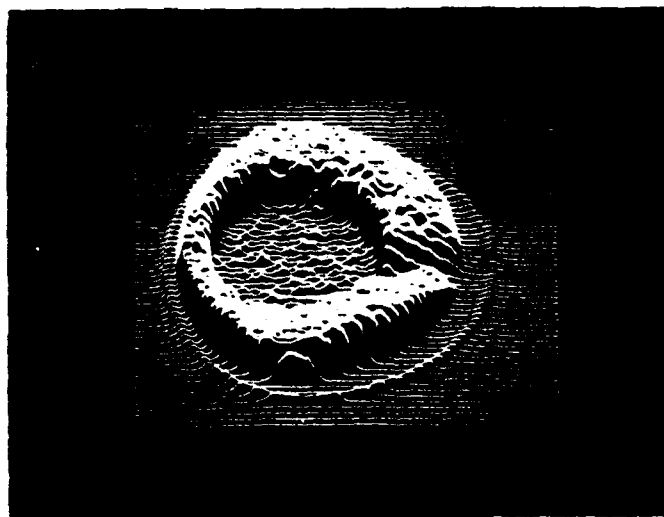


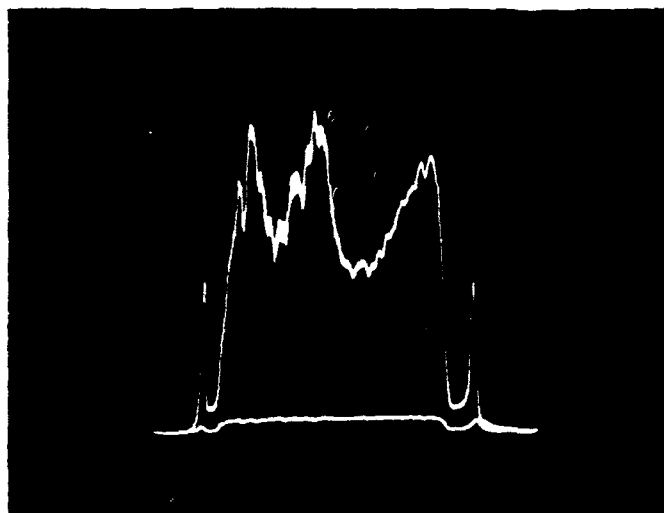
Figure 3.14. Experimental (broken curve) and theoretical (solid curves) spectral response of a p^+-n GaAs photodiode. The theoretical response was calculated for $X_1=1.2\mu\text{m}$, $X_2=3.2\mu\text{m}$, $L_n=0.25\mu\text{m}$, $L_p=1.0\mu\text{m}$, $D_n=90\text{cm}^2/\text{sec}$, and $S=10^3\text{cm/sec}$. (upper curve) or $S=10^6\text{cm/sec}$. (lower curve) [16].

3.14. The parameter of primary importance in determining this fit is the electron diffusion length in the heavily doped implanted region. When larger values of L_n were used, it was impossible to adjust S or the other parameters to obtain the rapid decrease in spectral response at short wavelengths. An electron lifetime $\tau_e = L_n^2 / D_n$ of approximately 6 psec. is calculated from the curve fitting parameters. This rather short lifetime suggests that not all of the damage introduced by the implant has been removed by the 800°C anneal. Another factor which may make this lifetime appear to be so short is the doping profile. In the calculations a uniform doping profile was assumed, whereas the actual profile dips at the surface. This dip produces an essentially "dead layer" at the surface and would make the overall lifetime appear shorter than it actually is.

The photoresponse of a planar diode, obtained with a laser scanner using 6328Å radiation, is shown in Figures 3.15(a) and (b) [16]. Figure 3.15(a) shows the spatial variation of the photoresponse at low bias after the formation of a proton bombarded guard ring. The position of the Au-Zn ohmic contact and the shadowing of the 1 mil Au wire is evident in this figure. The small response at the perimeter of the device indicates the location of the original Be-implanted 10 mil diameter region. A comparison of the two line scans across the active part of the device at low and high bias in Figure 3.15(b) shows that this diode has an average gain greater than 10. Diodes fabricated by this process have typically exhibited gains of 10-15. The response and gain at the periphery of the unguarded junction apparently result from imperfect guarding and a high-field region at the edge of the device. However, there is never any indication of microplasmas that could be limiting the avalanche gain. It is possible that there are microplasmas or leakage breakdown regions under the ohmic contact which are shielded from



(a)



(b)

Figure 3.15. (a) Photoresponse as a function of position across the photodiode using 6328\AA laser emission; (b) Photoresponse at -70V bias ($M=1$) lower curve and -135V ($M\sim 10$) upper curve [16].

the laser scanner. At still higher bias voltages, the avalanche gain saturates and the dark current increases very rapidly. Scans of devices without proton bombarded guard rings show considerable response at the edge of the junction. It is believed that this is due to poor sensitivity of the relatively deep ($1.2\mu\text{m}$) junction to the 6328\AA light. The edge of the junction comes up to the surface and is much more sensitive to the laser light.

The response of a Be-implanted LPE detector to 8300\AA radiation from a pulsed GaAs DH laser is shown in Figures 3.16(a)-(c) for three different bias levels. At the lowest bias level there is a slow component due to diffusion ($\tau \leq 7\text{ns}$) and a fast component ($\tau \leq 1\text{ns}$) due to generation in the depletion region. For bias voltages in excess of $\sim 100\text{V}$ the risetime is independent of bias voltage and is about 500 psec. This is approximately the RC-limited risetime for this detector because of the capacitance of the relatively large-area device ($A = 5 \times 10^{-4} \text{cm}^2$) and the stray capacitance of the T0-18 header and leads. The ringing observed in Figure 3.16 is from the laser itself, and is not caused by the detector.

Noise measurements have also been performed on these devices [16]. For bias voltages up to 0.8 of the breakdown voltage, the measurement was limited by the noise of the detection amplifier. At voltages greater than this, the noise increased monotonically because of the avalanche multiplication. The noise is larger than the ideal shot noise for such a device, $L_n^2 = 2qIB$, but less than the ideal multiplied shot noise $2qIBM^2$. This is probably due to the contribution of amplifier noise and the low values of multiplication used in these measurements.

In general, the properties of the avalanche photodiodes look promising, considering the fact that doping levels and junction depths were not

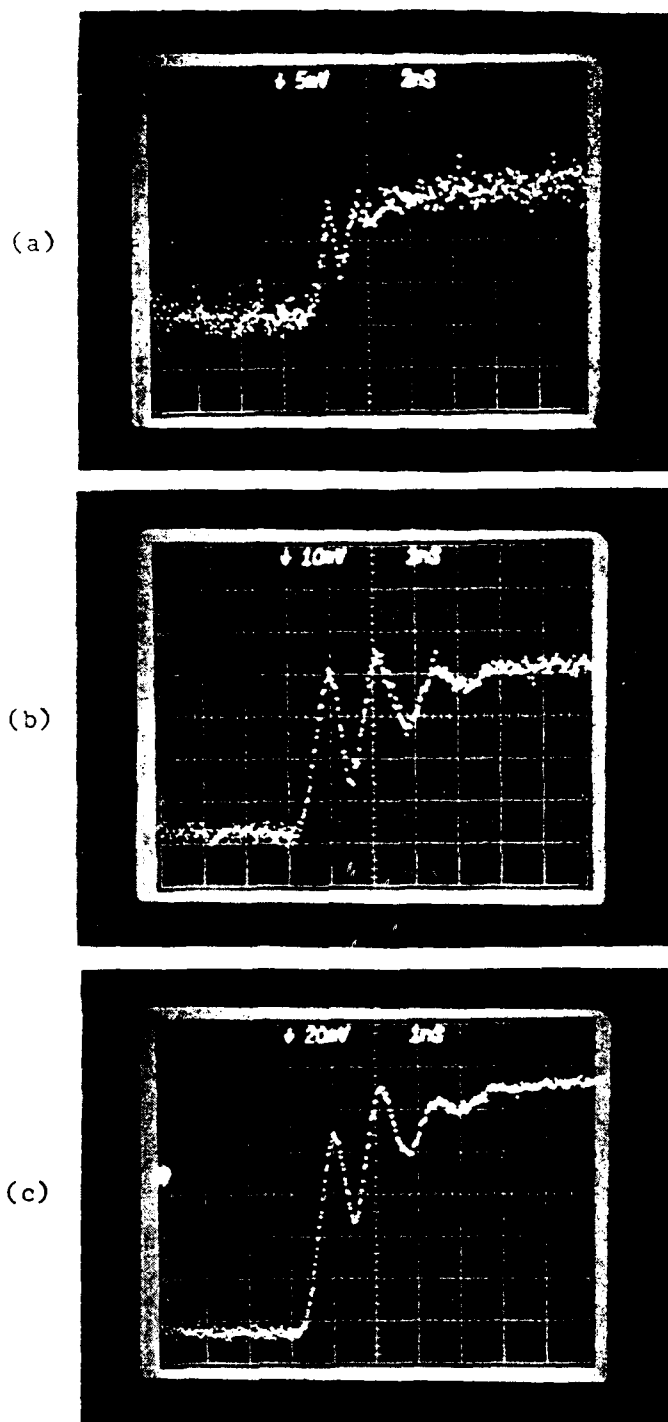


Figure 3.16. Response of a Be-implanted LPE GaAs photodiode to a pulse from a GaAs DH laser operating at 8300 Å. (a) $V_{\text{bias}} = -5\text{V}$; (b) $V_{\text{bias}} = -135\text{V}$; (c) $V_{\text{bias}} = -150\text{V}$ [16].

optimized. There is some question as to the rapid decrease in spectral response at short wavelengths, which must be investigated further.

3.5. Lateral Diffusion Studies

An extremely important consideration when fabricating integrated circuits with fine linewidths is lateral diffusion under the mask. It has been shown that when Zn is diffused in III-V compounds with either SiO_2 [12] or Si_3N_4 [14] as a mask, considerable lateral diffusion occurs. It is likely that this is due in part to strains present at the semiconductor-dielectric interface. To investigate the lateral diffusion effects in Be-implanted GaAs, we have fabricated junctions with various spacings. Stripes of $10\mu\text{m}$ width with spacings between stripes of $1\mu\text{m}$, $2.5\mu\text{m}$, $5\mu\text{m}$, $10\mu\text{m}$, and $20\mu\text{m}$ were opened in the Si_3N_4 using electron beam lithography [13,90]. Be was implanted in the $10\mu\text{m}$ stripes at 100 keV. After annealing at 900°C for 30 min. with Si_3N_4 encapsulation, the encapsulant was removed and the surface p and n regions were delineated by a selective etch (3 parts HNO_3 , 4 parts H_2O , and 1 part HF). A micrograph of the resulting structure is shown in Figure 3.17. The p and n regions are clearly visible and the integrity of the n regions are maintained, including the $1\mu\text{m}$ wide region. This suggests there may be very little lateral diffusion in Be-implanted GaAs junctions. The procedure used to delineate the regions in Figure 3.17 is not definitive, however. Currently, other types of measurements are being attempted to further investigate the lateral diffusion properties. One such measurement uses a scanning SIMS system to compare thin Be-implanted regions before and after high temperature anneals.

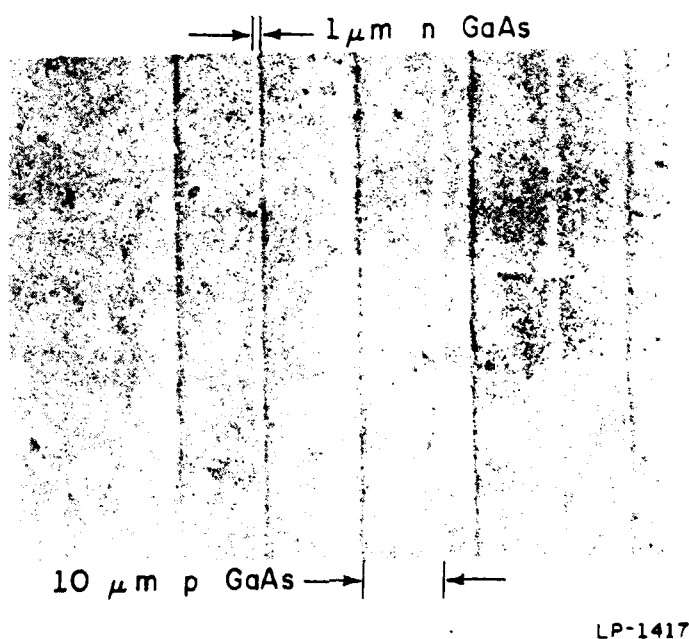


Figure 3.17. Micrograph of a Be-implanted GaAs surface with various spacings between $10\mu\text{m}$ wide implanted stripes. The width of the interspersed n-type regions are $1\mu\text{m}$, $2.5\mu\text{m}$, $5\mu\text{m}$, $10\mu\text{m}$, and $20\mu\text{m}$ [13].

4. SUMMARY AND CONCLUSIONS

In this work, photoluminescence and Auger electron spectroscopy (AES) have been used to study the encapsulating properties of SiO_2 , oxygen-contaminated Si_3N_4 , and "oxygen-free" Si_3N_4 on GaAs. Properties of the "oxygen-free" Si_3N_4 films and the rf plasma deposition system used to deposit them have been presented. Current-voltage measurements were used to evaluate the quality of planar p-n junctions in GaAs formed by ion implantation of Be. The effects of various encapsulants on the I-V characteristics were also studied. Finally, various optical measurements were performed to characterize the detection properties of the Be-implanted planar p-n junctions. In the following sections the results and conclusions of these studies are summarized and suggestions for further investigations are presented.

4.1. Encapsulation Studies

Earlier work by Gyulai et al. [30] using proton backscattering found that when GaAs is annealed with SiO_2 as an encapsulant there is considerable outdiffusion of Ga through the encapsulant. This work further substantiates that result by using photoluminescence and AES to study the outdiffusion. In addition, both photoluminescence and AES indicate that when Si_3N_4 having a very low oxygen content (≤ 1 atomic percent) is used as an encapsulant, negligible Ga outdiffusion occurs. The studies also show that if the nitride contains higher levels of oxygen, the resulting $\text{Si}_x\text{O}_y\text{N}_z$ no longer serves as a good encapsulant, but allows considerable outdiffusion of Ga, as observed for SiO_2 . It is not known if there is a threshold of oxygen content in Si_3N_4 above which Ga outdiffusion occurs or if the Ga outdiffusion simply decreases with the oxygen content of the film. The latter

case seems more likely, but further studies with Si_3N_4 layers deposited with various levels of oxygen content would be needed to resolve this question and the mechanism for the Ga outdiffusion.

In addition to the photoluminescence and AES work, studies of the planar Be-implanted p-n junctions illustrated that the encapsulants exhibiting Ga loss during annealing yield a much higher reverse leakage current than the "oxygen-free" Si_3N_4 . A large ohmic component is evident in both the forward and reverse I-V characteristics of devices which employed SiO_2 or oxygen-contaminated Si_3N_4 as the encapsulant for the post implant anneals. Leakage currents for devices fabricated using "oxygen-free" Si_3N_4 are many orders of magnitude lower than for those fabricated using SiO_2 or oxygen-contaminated Si_3N_4 . It is therefore important to use Si_3N_4 deposited in a manner which yields an essentially oxygen-free film for encapsulating GaAs during high temperature annealing.

The importance of having "oxygen-free" Si_3N_4 is not restricted to applications where it is used as an encapsulant for annealing. It has been shown in this and other studies [73,74] that Si_3N_4 films used in MIS structures must also be "oxygen-free" to obtain the best results.

It is possible to deposit Si_3N_4 layers with negligible oxygen content by rf plasma deposition if proper care is taken. Since the affinity of SiH_4 for oxygen is orders of magnitude higher than for nitrogen, it is imperative that oxygen be kept from the system and that the silane be introduced outside the rf excitation region. Such a system was developed and used in this work.

The rf plasma deposition system used here is leak-tight and employs a nitrogen trapped oil diffusion pump to evacuate the system before a nitrogen discharge is used prior to the deposition to "scrub"

the walls and help remove oxygen from the system. The gases (N_2 and 2% SiH_4 in Ar) are introduced separately. The SiH_4 is brought in below the rf coil and just above the sample. This configuration is used to reduce the oxygen in the film by not passing the SiH_4 through the rf coil, thus decreasing the probability of silane reacting with residual oxygen in the chamber. A similar system, in which the gases are all brought into the top of the chamber and are passed through the rf coil, deposits Si_3N_4 layers with considerably higher oxygen levels. Finally, ultra high purity N_2 is used as a source of nitrogen rather than NH_3 since it can be obtained in a more purified form and is easier to handle than NH_3 .

Films can be deposited over a wide range of temperatures (25° - $400^\circ C$) and flow conditions. By varying the flow rates of the gases, films with Si:N ratios of 0.71 to 1.59 and refractive indices from 1.96 to 2.59 are obtained. The index of refraction varies linearly with composition and for "oxygen-free" films can be used as a simple measurement of composition. A stoichiometric ratio of Si:N (0.75) is obtained in our system when the ratio of the flow rates ($N_2:SiH_4$) is 250. The exact flow rates necessary to obtain this ratio will vary for different systems, but the dependence of properties on flow rates is expected to be similar for all systems with this configuration. It is evident that this type of system is very versatile and can be used to deposit "oxygen-free" Si_3N_4 layers for use in encapsulation of GaAs and other III-V compounds and for use in MIS devices.

4.2. Planar P-N Junction Studies

High quality planar p-n junctions have been fabricated in GaAs by Be implantation. Junctions with reverse leakage currents less than 10^{-10} A at 60-80V have been obtained in VPE grown GaAs for 10 mil diameter diodes. High breakdown voltages, comparable to those reported for LPE grown junctions

[84] and theoretically calculated for abrupt junctions [91], have been achieved.

Planar junctions fabricated using Zn implantation and Zn diffusion yield devices with much lower breakdown voltages (15 to 20V) than Be-implanted junctions in similar material. The Zn-implanted devices exhibit reverse leakage currents many orders of magnitude higher than the Be-implanted devices, and leakage currents for Zn-diffused devices are comparable or slightly higher than the Be-implanted case.

The quality of the devices obtained is very sensitive to the encapsulant used during annealing. Diodes fabricated identically except for the encapsulant exhibit leakage currents orders of magnitude higher when encapsulants permitting Ga outdiffusion are used (SiO_2 and oxygen-contaminated Si_3N_4). These junctions contain a large ohmic component in both the forward and reverse directions for low currents. It seems likely that this component could be related to surface leakage paths introduced by the loss of gallium from the surface. Devices with "oxygen-free" Si_3N_4 used as an encapsulant exhibit little or no ohmic leakage.

Ion implantation of Be has been used to fabricate planar avalanche photodiodes in both LPE and VPE GaAs layers. These diodes have low leakage currents and gains of 10-15. The diodes have a peak quantum efficiency of about 75% and an RC-limited risetime of approximately 500 psec.

There are differences in the functional form of the reverse current characteristics of devices in LPE and VPE layers which are not understood. The devices fabricated in LPE material exhibit an ohmic reverse leakage current over almost their entire range. An ohmic component was also observed in VPE diodes in which encapsulants permitting Ga outdiffusion were used; however, this dependence was not observed over the entire range of

reverse voltage. The magnitude of the reverse current is also orders of magnitude lower for the LPE diodes than it was for VPE diodes with poor encapsulation. It therefore seems unlikely that the ohmic character of the reverse current in the LPE photodiodes can be attributed to poor encapsulation and resulting surface leakage paths. It is more likely that other bulk and surface leakage paths not related to Ga outdiffusion are responsible.

Photodiodes fabricated in VPE layers display an exponential reverse leakage over some portion of the reverse voltage characteristics. In early work on diffused GaAs p-n junctions, this type of behavior was attributed to the generation of microplasmas [89]. In this work, however, there is no indication of this process, and there is no indication of local areas of high multiplication in optical scans of these devices. It therefore seems unlikely that microplasmas can explain the shape of the I-V characteristics of these VPE diodes. More work is necessary to determine the nature of the current generation mechanism. Preliminary studies of annealing properties of the VPE material used to fabricate the photodiodes indicate that there is considerable difference in Schottky-barrier diode characteristics formed on the material before and after anneals at 800° and 900°C. This indicates that there may be some problems with the material, and this exponential current behavior may be related to this particular material rather than VPE or implanted material in general. Some DLTS studies have been initiated on these diodes, and early results indicate there is a band of traps which may be related to unannealed implantation damage for these 800°C anneals. It may be that the exponential behavior is related to a voltage dependent emptying of traps.

The spectral response of the avalanche photodiodes drops very rapidly at shorter wavelengths. While the fact that the junctions are deeper

(1.2 μ m) than is desirable for optimum response contributes to this decrease, calculations indicate the primary cause is a very short minority carrier diffusion length in the implanted material. This could be caused by unannealed damage. Since it has been shown that implantation damage from Be continues to anneal at temperatures up to 900°C [82], damage clearly remains after the 800°C anneals used for this photodiode work. Problems with high leakage currents for devices annealed at 900°C prevented comparisons of their spectral response with these devices. Another factor which would influence the spectral response and was not taken into account in the calculations was the possible existence of a "dead" layer at the surface due to the drop in the doping profile near the surface. This would add to the drop in spectral response and make the minority carrier diffusion length seem shorter than it actually is.

Further work should be done to understand the reverse current characteristics and optical properties of these devices more fully. Some possible studies which could lead to a better understanding are:

1. Devices with several different diameters should be fabricated. This would indicate if the majority of the leakage current comes from bulk or edge effects, depending on whether the current changes as the area or circumference of the device.
2. Mesa-etching should be used to fabricate diodes formed by implanting the entire surface, to determine if characteristics are related to the implantation itself or the fact that the implantation was done through a mask.
3. Implantation should be carried out through a Si₃N₄ layer, or alternative alignment procedures should be used so that no Si₃N₄ layer need be deposited and removed before implantation.

This experiment would determine the effect of using Si_3N_4 layers, meeting at the point where the junction reaches the surface.

4. Photodiodes with shallower junctions and uniform doping profiles should be fabricated to investigate the detection properties of devices with a more optimum doping profile.
5. DLTS studies of devices fabricated by various procedures should be used to investigate the effect of the procedures on traps.
6. Further investigations should be carried out on the VPE material to determine its quality and any problems associated with its annealing behavior.

Some work has also been done to study the lateral diffusion of implanted Be, and these results indicate minimal lateral diffusion under nitride masks of the type described here. More work is required, however, to determine the actual extent of lateral diffusion under various processing procedures.

In conclusion, it has been shown that properly deposited Si_3N_4 layers serve as good encapsulants for annealing GaAs at high temperatures, whereas SiO_2 and Si_3N_4 with high levels of oxygen content are unacceptable for this purpose. Also, while work still needs to be done, it is clear that high quality planar p-n junctions can be fabricated in GaAs by ion implantation of Be.

REFERENCES

1. R. C. Eden, "GaAs integrated circuits: MSI status and VLSI prospects," in IEDM Tech. Dig., Dec. 1978, pp. 6-11.
2. B. M. Welch and R. C. Eden, "Planar GaAs integrated circuits fabricated by ion implantation," in IEDM Tech. Dig., Dec. 1977, pp. 205-208.
3. R. Zuleeg, J. K. Notthoff, and K. Lehovec, "Femtojoule high-speed planar GaAs E-JFET logic," IEEE Trans. Electron Devices, vol. ED-25, pp. 628-639, June 1978.
4. C. A. Liechti, "Microwave field effect transistors - 1976," IEEE Trans. Microwave Theory Tech., vol. MTT-24, pp. 279-300, June 1976.
5. J. P. Donnelly, "Ion implantation in GaAs," in GaAs and Related Compounds (St. Louis) 1976, L. F. Eastman, editor, Conf. Ser. 33b, Institute of Physics, Bristol and London, 1977, pp. 166-190.
6. R. L. Van Tuyl, C. A. Liechti, R. E. Lee, and E. Gowan, "GaAs MESFET logic with 4-GHz clock rate," IEEE J. Solid-State Circuits, vol. SC-12, pp. 485-496, Oct. 1977.
7. R. L. Van Tuyl and C. A. Liechti, "High speed integrated logic with GaAs MESFET's," IEEE J. Solid-State Circuits, vol. SC-9, pp. 269-276, Oct. 1974.
8. R. L. Van Tuyl and C. A. Liechti, "Gallium arsenide spawns speed," IEEE Spectrum, vol. 14, pp. 40-47, March 1977.
9. R. C. Eden and B. M. Welch, "Low power depletion mode ion-implanted GaAs FET integrated circuits," IEEE Trans. Electron Devices, vol. ED-24, pp. 1209-1210, Sept. 1977.
10. R. L. Van Tuyl and C. A. Liechti, "High speed GaAs MSI," in 1976 IEEE Int. Solid-State Circuits Conf., Dig. of Tech. Papers, Feb. 1976, pp. 20-21.
11. D. O. Wilson, R. P. Mandal, W. R. Scoble, and H. L. Peterson, "A comparison of high-speed enhancement and depletion mode GaAs MESFET's," in IEDM Tech. Dig., Dec. 1978, pp. 600-602.
12. B. J. Baliga and S. K. Ghandhi, "Lateral diffusion of zinc and tin in GaAs," IEEE Trans. Electron Devices, vol. ED-21, pp. 410-415, July 1974.
13. M. J. Helix, K. V. Vaidyanathan, B. G. Streetman, and P. K. Chatterjee, "Planar GaAs p-n junctions by Be ion implantation," in IEDM Tech. Dig., Dec. 1977, pp. 195-197.
14. P. K. Chatterjee and B. G. Streetman, "Reduced lateral diffusion and reverse leakage in Be-implanted GaAs_{1-x}P_x diodes," Solid-State Electron., vol. 20, pp. 305-306, April 1977.

15. M. J. Helix, K. V. Vaidyanathan, and B. G. Streetman, "Properties of Be-implanted planar GaAs p-n junctions," IEEE J. Solid-State Circuits, vol. SC-13, pp. 426-429, Aug. 1978.
16. R. A. Milano, M. J. Helix, T. H. Windhorn, B. G. Streetman, K. V. Vaidyanathan, and G. E. Stillman, "Planar ion-implanted avalanche photodiodes in GaAs," in GaAs and Related Compounds (St. Louis) 1978, Conf. Ser. 45, Institute of Physics, Bristol and London, 1979, pp. 411-419.
17. F. J. Leonberger, J. P. Donnelly, and C. O. Bozler, "Low-loss GaAs $p^+n^-n^+$ three-dimensional optical waveguides," Appl. Phys. Lett., vol. 28, pp. 616-619, May 15, 1976.
18. A. A. Immorlica, Jr. and F. H. Eisen, "Planar GaAs hyperabrupt varactor diodes," in Sixth Biennial Conf. on Active Microwave Semiconductor Devices and Circuits, Cornell University, Ithaca, N.Y., Aug. 1977.
19. R. K. Ahrenkiel, F. Moser, T. J. Coburn, S. L. Lyu, K. V. Vaidyanathan, P. K. Chatterjee, W. V. McLevige, and B. G. Streetman, "Low dark current photosensors based on GaAs_{0.6}P_{0.4}," in IEDM Tech. Dig., Dec. 1976, pp. 426-428.
20. E. E. Barrowcliff, L. O. Bubulac, D. L. Cheung, W. E. Tennant, and A. M. Andrews, "GaSb metal-insulator-semiconductor field-effect-transistors," in IEDM Tech. Dig., Dec. 1977, pp. 559-562.
21. P. K. Chatterjee, B. G. Streetman, D. L. Keune, and A. H. Herzog, "Be-implanted GaAs_{1-x}P_x light emitting diodes," in IEDM Tech. Dig., Dec. 1975, pp. 187-191.
22. S. T. Picraux, "Vaporization of ion-implanted GaAs," in Ion Implantation in Semiconductors and Other Materials, B. L. Crowder, editor, Plenum Press, New York, 1973, pp. 641-654.
23. J. P. Donnelly, W. T. Lindley, and C. W. Hurwitz, "Silicon- and selenium-ion-implanted GaAs reproducibly annealed at temperatures up to 950°C," Appl. Phys. Lett., vol. 27, pp. 41-43, July 1, 1975.
24. C. O. Bozler, J. P. Donnelly, R. A. Murphy, R. W. Laton, R. W. Sudbury, and W. T. Lindley, "High efficiency ion-implanted lo-hi-lo GaAs IMPATT diodes," Appl. Phys. Lett., vol. 29, pp. 123-125, July 15, 1976.
25. J. L. Tandon, M. A. Nicolet, and F. H. Eisen, "Silicon implantation in GaAs," Appl. Phys. Lett., vol. 34, pp. 165-167, Jan. 15, 1979.
26. J. S. Harris, F. H. Eisen, B. Welch, J. D. Haskell, R. D. Pashley, and J. M. Mayer, "Influence of implantation temperature and surface protection on tellurium implantation in GaAs," Appl. Phys. Lett., vol. 21, pp. 601-603, Dec. 15, 1972.
27. A. G. Foyt, J. P. Donnelly, and W. T. Lindley, "Efficient doping of GaAs by Se⁺ ion implantation," Appl. Phys. Lett., vol. 14, pp. 372-374, June 15, 1969.

28. P. K. Chatterjee, K. V. Vaidyanathan, W. V. McLevige, and B. G. Streetman, "Photoluminescence from Be-implanted GaAs," Appl. Phys. Lett., vol. 27, pp. 567-569, Nov. 15, 1975.
29. K. V. Vaidyanathan, M. J. Helix, D. J. Wolford, B. G. Streetman, R. J. Blattner, and C. A. Evans, Jr., "Study of encapsulants for annealing GaAs," J. Electrochem. Soc., vol. 124, pp. 1781-1784, Nov. 1977.
30. J. Gyulai, J. W. Mayer, I. V. Mitchell, and V. Rodriguez, "Outdiffusion through silicon oxide and silicon nitride layers on gallium arsenide," Appl. Phys. Lett., vol. 17, pp. 332-334, Oct. 15, 1970.
31. K. Gamo, T. Inada, S. Krekeler, J. W. Mayer, F. H. Eisen, and B. M. Welch, "Selenium implantation in GaAs," Solid-State Electron., vol. 20, pp. 213-217, March 1977.
32. R. W. Malbon, D. H. Lee, and J. M. Whelan, "Annealing of ion implanted GaAs in a controlled atmosphere," J. Electrochem. Soc., vol. 123, pp. 1413-1415, Sept. 1976.
33. A. A. Immorlica and F. H. Eisen, "Capless annealing of ion-implanted GaAs," Appl. Phys. Lett., vol. 29, pp. 94-95, July 15, 1976.
34. D. H. Lee, R. M. Malbon, and J. M. Whelan, "Characteristics of implanted n-type profiles in GaAs annealed in a controlled atmosphere," in Ion Implantation in Semiconductors, 1976, F. Chernow, J. A. Borders, and D. K. Brice, eds., Plenum Press, New York, 1977, pp. 115-122.
35. J. Kasahara, M. Arai, and N. Watanabe, "Capless anneal of ion-implanted GaAs in controlled arsenic vapor," J. Appl Phys., vol. 50, pp. 541-543, Jan. 1979.
36. J. F. Gibbons, "Ion implantation in semiconductors part I: range distribution theory and experiments," Proc. IEEE, vol. 56, pp. 295-319, March 1968.
37. J. F. Gibbons, "Ion implantation in semiconductors part II: damage production and annealing," Proc. IEEE, vol. 60, pp. 1062-1096, Sept. 1972.
38. J. W. Mayer, L. Erickson, and J. A. Davies, Ion Implantation in Semiconductors, Academic Press, New York, 1970.
39. P. L. Degen, "Ion implantation doping of compound semiconductors," Phys. Status Solidi A, vol. 16, pp. 9-42, March 16, 1973.
40. D. H. Lee and J. W. Mayer, "Ion-implanted semiconductor devices," Proc. IEEE, vol. 62, pp. 1241-1255, Sept. 1974.
41. J. Lindhard and A. Winther, "Stopping power of electron gas and equipartition rule," Mat. Fys. Medd. Dan. Vid. Selsk., vol. 34, pp. 1-21, 1964.
42. O. B. Firsov, "A qualitative interpretation of the mean electron excitation energy in atomic collisions," J. Exper. Theoret. Phys., vol. 36, pp. 1517-1523, May 1959.

43. S. Lindhard, M. Scharff, and H. Schiott, "Range concepts and heavy ion ranges," Mat. Fys. Medd. Dan. Vid. Selsk., vol. 33, pp. 1-39, 1963.
44. J. F. Gibbons, W. S. Johnson, and S. W. Mylroie, Projected Range Statistics, 2nd edition, Halstead Press, Stroudsburg, Penn., 1975.
45. A. Lidow, J. F. Gibbons, T. Magee, and J. Peng, "Multilayered encapsulation of GaAs," J. Appl. Phys., vol. 49, pp. 5213-5217, Oct. 1978.
46. G. R. Antell, "The effect of the anneal ambient on implanted GaAs and the occurrence of compensated regions in Si implants," Appl. Phys. Lett., vol. 30, pp. 432-434, April 15, 1977.
47. W. A. Pliskin, "Comparison of properties of dielectric films deposited by various methods," J. Vac. Sci. Technol., vol. 14, pp. 1064-1081, Sept./Oct. 1977.
48. M. J. Helix, K. V. Vaidyanathan, B. G. Streetman, H. B. Dietrich, and P. K. Chatterjee, "R.F. plasma deposition of silicon nitride layers," Thin Solid Films, vol. 55, pp. 143-148, Nov. 15, 1978.
49. H. F. Sterling and R. C. G. Swann, "Chemical vapor deposition promoted by r.f. discharge," Solid-State Electron., vol. 8, pp. 653-654, Aug. 1965.
50. Y. Kuwano, "The preparation and properties of silicon nitride produced by a radio frequency glow discharge reaction of silane and nitrogen: preparation and properties of silicon nitride," Jpn. J. Appl. Phys., vol. 7, p. 88, Jan. 1968.
51. Y. Kuwano, "Some properties of silicon nitride films produced by radio frequency glow discharge reaction of silane and nitrogen," Jpn. J. Appl. Phys., vol. 8, pp. 876-882, July 1969.
52. E. A. Taft, "Characterization of silicon nitride films," J. Electrochem. Soc., vol. 118, pp. 1341-1346, Aug. 1971.
53. R. Gereth and W. Scherber, "Properties of ammonia-free nitrogen-Si₃N₄ films produced at low temperatures," J. Electrochem. Soc., vol. 119, pp. 1248-1254, Sept. 1972.
54. O. Meyer and W. Scherber, "Analysis of silicon nitride layers deposited from SiH₄ and N₂ on silicon," J. Phys. Chem. Solids, vol. 32, pp. 1909-1915, Aug. 1971.
55. R. S. Rosler, W. C. Benzing, and J. Baldo, "A production reactor for low-temperature plasma-enhanced silicon nitride deposition," Solid State Technol., vol. 19, pp. 45-50, June 1976.
56. M. Feng, J. D. Oberstar, T. H. Windhorn, L. W. Cook, G. E. Stillman, and B. G. Streetman, "Be-implanted 1.3- μ m InGaAsP avalanche photodetectors," Appl. Phys. Lett., vol. 34, pp. 591-593, May 1, 1979.

57. S. U. Campisano, I. Catalano, G. Foti, E. Rimini, F. Eisen, and M. A. Nicolet, "Laser reordering of implanted amorphous layers in GaAs," Solid-State Electron., vol. 21, pp. 485-488, Feb. 1978.
58. J. A. Golovchenko and T. N. C. Venkatesan, "Annealing of Te-implanted GaAs by ruby laser irradiation," Appl. Phys. Lett., vol. 32, pp. 147-149, Feb. 1, 1978.
59. J. C. C. Fan, R. L. Chapman, J. P. Donnelly, G. W. Turner, and C. O. Bozler, "Ion-implanted laser-annealed GaAs solar cells," Appl. Phys. Lett., vol. 34, pp. 780-782, June 1, 1979.
60. R. E. Anderson, D. J. Wolford, and B. G. Streetman, "Nitrogen implantation in GaAs_{1-x}P_x: annealing properties," J. Appl. Phys., vol. 48, pp. 2453-2463, June 1977.
61. G. T. Marcyk, "Atomic and electrical profile studies of ion-implanted semiconductors," Ph.D. thesis, University of Illinois, 1978. Also Coordinated Science Laboratory Report R-835, UIUC-ENG78-2228.
62. A. S. Grove, O. Leistiko, and C. T. Sah, "Diffusion of gallium through a silicon dioxide layer," J. Phys. Chem. Solids, vol. 25, pp. 985-992, Sept. 1964.
63. P. K. Chatterjee, K. V. Vaidyanathan, M. S. Durschlag, and B. G. Streetman, "Photoluminescence study of native defects in annealed GaAs," Solid State Comm., vol. 17, pp. 1421-1424, Dec. 1, 1975.
64. S. Y. Chiang and G. L. Pearson, "Photoluminescence studies of vacancies and vacancy-impurity complexes in annealed GaAs," J. Lumin., vol. 10, pp. 313-322, June 1975.
65. C. J. Hwang, "Effect of heat treatment on the 1.370 eV photoluminescence emission band in Zn-doped GaAs," J. Appl. Phys., vol. 39, pp. 4307-4312, Aug. 1968.
66. N. Holonyak, Jr. and D. R. Scifres, "Window-heat sink sandwich for optical experiments: diamond- (or sapphire-) semiconductor-indium sandwich," Rev. Sci. Instrum., vol. 42, pp. 1885-1886, Dec. 1971.
67. A. Mooradian and G. B. Wright, "First order Raman effect in III-V compounds," Solid State Comm., vol. 4, pp. 431-434, Sept. 1966.
68. R. J. Blattner, C. A. Evans, Jr., and A. J. Braundmeier, "Mechanism of high-temperature instability of CuO-Ag thin-film solar absorbers," J. Vac. Sci. Technol., vol. 14, pp. 1132-1138, Sept./Oct. 1977.
69. RBS measurements were performed by H. B. Dietrich of NRL.
70. Ellipsometry measurements were performed by P. K. Chatterjee of Texas Instruments.
71. Private communications with P. Peercy and H. J. Stein of Sandia Laboratories.

72. W. A. Lanford and M. J. Rand, "The hydrogen content of plasma-deposited silicon nitride," Extended Abstracts of the 152nd Meeting of the Electrochemical Society, Atlanta, Oct. 1977, paper number 154.
73. T. R. Ohnstein, G. Y. Robinson, M. J. Helix, B. G. Streetman, and K. V. Vaidyanathan, "Electrical properties of plasma-deposited Si-N films on GaAs," presented at 1979 Device Research Conf., Boulder. Abstract to be published in IEEE Trans. Electron Devices.
74. B. Bayraktaroglu, W. M. Theis, and F. L. Schuermeyer, "The use of Si_3N_4 for GaAs surface passivation: electrical characteristics and applications to enhancement type MISFET's," presented at 1979 Device Research Conf., Boulder. Abstract to be published in IEEE Trans. Electron Devices.
75. R. G. Hunsperger, R. C. Wilson, and D. M. Jamba, "Mg and Be ion implanted GaAs," J. Appl. Phys., vol. 43, pp. 1318-1320, March 1972.
76. P. K. Chatterjee, W. V. McLevige, K. V. Vaidyanathan, and B. G. Streetman, "Temperature dependence of photoluminescence from Be-implanted GaAs," Appl. Phys. Lett., vol. 28, pp. 509-512, May 1, 1976.
77. J. P. Donnelly, F. J. Leonberger, and C. O. Bozler, "Uniform-carrier-concentration p-type layers in GaAs produced by beryllium ion implantation," Appl. Phys. Lett., vol. 28, pp. 706-708, June 15, 1976.
78. P. K. Chatterjee, "Acceptor behavior of implanted beryllium in gallium arsenide and gallium arsenide phosphide," Ph.D. thesis, University of Illinois, 1976. Also Coordinated Science Laboratory Report R-721, UILU-ENG76-2209.
79. W. V. McLevige, "Annealing studies of beryllium in gallium arsenide and gallium arsenide phosphide," Ph.D. thesis, University of Illinois, 1977. Also Coordinated Science Laboratory Report R-802, UILU-ENG77-2249.
80. M. Ilegems, "Beryllium doping and diffusion in molecular-beam epitaxy of GaAs and $\text{Al}_{1-x}\text{Ga}_x\text{As}$," J. Appl. Phys., vol. 48, pp. 1278-1287, March 1977.
81. J. A. Hutchby and K. V. Vaidyanathan, "Temperature dependence of electrical properties in Be-implanted semi-insulating GaAs," J. Appl. Phys., vol. 48, pp. 2559-2564, June 1977.
82. W. V. McLevige, M. J. Helix, K. V. Vaidyanathan, and B. G. Streetman, "Electrical profiling and optical activation studies of Be-implanted GaAs," J. Appl. Phys., vol. 48, pp. 3342-3346, Aug. 1977.
83. W. V. McLevige, K. V. Vaidyanathan, B. G. Streetman, J. Comas, and L. Plew, "Diffusion studies of Be-implanted GaAs by SIMS and electrical profiling," Solid State Comm., vol. 25, pp. 1003-1008, March 1978.
84. B. I. Miller and H. C. Casey, "Preparation of GaAs p-n junctions by multiple-layer liquid phase epitaxy," in GaAs and Related Compounds (Boulder) 1972, Conf. Ser. 17, Institute of Physics, Bristol and London, 1973, pp. 231-239.

85. A. G. Foyt, W. T. Lindley, C. M. Wolfe, and J. P. Donnelly, "Isolation of junction devices in GaAs using proton bombardment," Solid-State Electron., vol. 12, pp. 209-214, April 1969.
86. J. Lowen and R. H. Rediker, "Gallium-arsenide diffused diodes," J. Electrochem. Soc., vol. 107, pp. 26-29, Jan. 1960.
87. J. Halpern and R. H. Rediker, "Low reverse leakage gallium arsenide diodes," Proc. IRE, vol. 48, pp. 1780-1781, Oct. 1960.
88. A. S. Grove, Physics and Technology of Semiconductor Devices, Wiley, New York, 1967, pp. 172-180.
89. R. A. Logan, A. G. Chynoweth, and B. C. Cohen, "Avalanche breakdown in gallium arsenide p-n junctions," Phys. Rev., vol. 128, pp. 2518-2523, Dec. 15, 1962.
90. Electron beam lithography was performed by P. K. Chatterjee of Texas Instruments.
91. S. M. Sze and G. Gibbons, "Avalanche breakdown voltages of abrupt and linearly graded p-n junctions in Ge, Si, GaAs, and GaP," Appl. Phys. Lett., vol. 8, pp. 111-113, March 1, 1966.

VITA

Max John Helix was born on March 29, 1953 in Lemont, Illinois. Since September 1971 he has been attending the University of Illinois at Urbana-Champaign. He received a Bachelor of Science degree in Electrical Engineering with highest honors in May 1975. As an undergraduate he received the CRC Outstanding Freshman in Chemistry award. Mr. Helix received a Master of Science degree in Electrical Engineering in May 1976. While in graduate school he held a University of Illinois Fellowship and an IBM Pre-Doctoral Fellowship. Mr. Helix is a member of the Institute of Electrical and Electronics Engineers and the Electrochemical Society as well as Eta Kappa Nu and Tau Beta Pi honor societies.

LND 1280